Identification and Characterization of Candidate Oncogenes and Tumor Suppressor Genes in Hepatocellular Carcinoma and Peripheral Neural Sheath Tumors

A DISSERTATION

SUBMITTED TO THE FACULTY OF THE GRADUATE SCHOOL OF THE

UNIVERSITY OF MINNESOTA

BY

Germán L. Vélez Reyes

IN PARTIAL FULFILLMENT OF THE REQUIREMENTS FOR THE DEGREE OF

DOCTOR OF PHILOSOPHY

Dr. David A. Largaespada

June 2019

Acknowledgements

The following people contributed to the conception and work described in this thesis: Gabriel Kaufmann, Nicholas Koes, Ji Hae Ryu, Mariah Berner, Barbara R. Tschida, Hsiangyu Hu, Juan E. Abrahante, Kyle W. Williams, Bryant Keller, Susan K. Rathe, Wendy Hudson, Sandra Wagner, Aron B. Jaffe, Caitlin Conboy, Nancy Ratner, Timothy K. Starr, Carol Lange, Peter Bitterman, Scott Dehm, Kaylee Schwertfeger, and David A. Largaespada.

Contributions

GLVR, NR, and DAL contributed to the study concept in Chapter 3.

GLVR, BRT, CC, TKS, and DAL contributed to the study concept in Chapter 4.

Data acquisition and analysis contributions by chapter

Chapter 2:

GLVR and DAL contributed to Figures 2.1 to 2.11

NK, JHR, and MB contribute to the data shown in Figures 2.3-2.5, 2.7-2.12, and 2.16

WH also contribute to the data shown in Figures 2.7-2.9 and 2.16

JEA and SKR also contributed to the data shown in Figures 2.1

Chapter 3:

GLVR and DAL contributed to Figures 3.1 to 3.8

CC and BRT contributed to the data in Figure 3.1

HH contributed to the data in Figure 3.2

HH and GK contributed to the data in Figure 3.3

GK and BRT contributed to the data in Figure 3.6

SW contributed to the data in Figures 3.1 and 3.6

Grant Support:

This work was supported by grants to GVR (T32 GM008244, T32 HL007741), DAL (R01 CA134759, R01 CA113636, American Cancer Society Research Professor Award #123939).

This work utilized computing resources at the University of Minnesota Supercomputing Institute. The University of Minnesota Genomics Center provided Sanger sequencing and primer synthesis services. Services from the University of Minnesota Biology Materials Procurements Network, the Research Animal Resources, and the University Imaging Centers that are supported by the National Cancer Institute, were used for the work presented in this thesis.

To my parents and sister,

the only example I need.

Abstract

Cancer is a devastating and intriguing disease. Innovations in screening and treatment have reduced cancer rates and mortality in the last decade. However, we are at a crossroads to better understand the molecular mechanisms and the genetic events that result in malignant transformation of human tumors. Drug resistance is on the rise and malignancies that recur are more difficult to treat. It is our goal to understand the genetic mechanisms and the pathways that drive and promote human tumor malignant transformation.

In order to understand these mechanisms, we have used two different approaches: a mouse *in vivo* liver and a human *in vitro* Schwan cell cancer model. We hypothesized that loss-of-function mutations and/or copy number loss in novel Schwann cell tumor suppressor genes results in the activation of multiple pathways that aid in the malignant transformation of neurofibromas into MPNSTs. In the liver, we hypothesized that RSPO2-driven oncogenic activity occurs via Hippo/YAP signaling.

In the peripheral nerve, we designed a medium-throughput screening methodology using CRISPR/Cas9 technology to validate a previous *in vivo* Sleeping Beauty (*SB)* screen. We were able to confirm the results of the screen and discovered that multiple pathways are activated in Schwann cell tumors. This occurs as a result of copy number alterations and tumor suppressor gene loss. Activation of Wnt, Rho, PI3K/mTOR, Hippo, and Shh appear to be hallmarks of neoplasms of Schwann cell tumors. Interestingly, we also found that loss of normal chromatin folding is a mechanism of aberrant oncogenic expression. In the liver we have made use of the Fah mouse model to show that RSPO2-

induced liver tumors depend on Hippo/YAP signaling. We also discovered that removal of YAP results in reduced tumor burden.

Our studies shed light into the future of cancer treatment and motivate further research. Our data indicates that some liver and peripheral nerve cancers may be vulnerable to targeted therapy. Combination therapy in conjunction with an informed individual's tumor genetic landscape is a reasonable way to treat human cancers. In this thesis we outlined our screening methods, MPNST genes, and the pathways they activate. We also show that RSPO2 works via YAP. Our screening methods show a streamlined way to validate candidate tumor suppressor genes and oncogenes in order to push forward discovery of targeted therapies to alleviate the heavy burden of cancer.

Table of Contents **Page**

List of Tables **Page**

List of Figures **Page**

Chapter 1: Introduction

The genetic landscape and pathways of human peripheral nerve and liver cancers

Neurofibromatosis and Malignant Peripheral Nerve Sheath Tumors:

Peripheral nerve sheath tumors are a feature of Neurofibromatosis Type 1 Syndrome (NF1). About 1 in every 2,800 newborns suffer from NF1, a peripheral nervous system syndrome characterized by the presence of café-au-lait spots, Lisch nodules, and cutaneous neurofibromas. In some cases, NF1 has also being associated with learning disabilities. Other consequences of this syndrome include plexiform neurofibromas, optic nerve gliomas, vasculopathies, and scoliosis[1]. Genetically, NF1 is characterized by the heterozygous loss of neurofibromin 1, a negative regulator of Ras[2]. This loss is a common hallmark of malignant peripheral nerve sheath tumors (MPNSTs), a malignant manifestation of the disease[2]. Other genetic alterations are also common in MPNSTs. Gain-of-function of growth factor receptors, loss of tumor suppressors such as *TP53*, and amplification of *RSPO2* are other examples. NF1 patients are 10,000 times more likely to develop MPNSTs than are people with two wild type copies of *NF1*[3]. NF1 patients have a 30% lifetime risk of developing benign Schwann cell tumors. Plexiform neurofibromas can show as early as birth and are believed to be the initial step in the formation of MPNSTs[4,5]. This transformation happens in about 5%-10% of plexiform neurofibromas[3]. Even though MPNSTs affect about 0.001% percent of the general population, this malignancy poses a huge burden to patients with NF1[4,5,6]. It is estimated that about 10% of all patients with NF1 will suffer from an MPNST in their lifetime[6]. Currently, there are no proven therapies to treat MPNSTs. NF1 patients with MPNSTs also have a poorer response to therapy in comparison to others that develop MPNSTs. They also have a higher risk of recurrence and metastasis (notably to the lung) after treatment[1].

Currently, there are limited targeted therapies available for the treatment of MPNSTs[8].

Physicians rely on standard chemotherapy and radiation with the addition of surgical resection, when possible[4,5,6]. Inhibitors of kinases downstream of NF1, such as PI3K, MEK, and mTOR have been proposed from human and animal models. We have not seen the results of these studies in human clinical trials yet[8, 9]. To increase the burden of NF1 patients, therapies are more limited to them because of the increased carcinogenic risk that radiation poses to them. This has resulted in decreased survival rates in NF1 patients with MPNSTs when compared to the general population with MPNSTs. It is then important to find new pathways that have a role in peripheral neural sheath tumor cell transformation and progression to identify new targets that efficiently treat peripheral neural sheath tumors. It remains necessary and exciting to understand the mechanisms by which oncogene expression activation occurs in these cancers and develop targeted therapies towards this phenomenon.

MPNST progression is likely to involve many unidentified genetic and epigenetic changes. It has been described that Ras hyperactivation is not sufficient to result in malignant transformation of neurofibromas[10]. Neurofibromas are usually composed of a potpourri of cells, from neurons, to fibroblasts and macrophages. Loss of *CDKN2A*, *TP53*, *pRB*, *SUZ12* are hallmarks of progression from neurofibromas to atypical neurofibromas, a precursor of MPNSTs[2, 5, 6]. In fact, MPNSTs have been classified as Type C tumors. MPNSTs are characterized by a high number of copy number alterations (CNA), while harboring a minimal number of recurrent somatic mutations[11]. Recently this has been described by the The Cancer Genome Atlas consortium[12].

The genetic landscape of MPNSTs is rather complicated and several genetic alterations have been described by our lab and others in the las decade. We hypothesize that these

genetics changes at the tumor level, are responsible for the malignant transformation of neurofibromas and plexiform neurofibromas into MPNSTs.

Liver Cancer:

Hepatocellular Carcinomas (HCC) remain one of the deadliest human carcinomas, with over 40,000 diagnoses and over 25,000 deaths each year in the United States alone[1,2]. Long-term liver disease and infection with Hepatitis B or C virus are the most common causes of HCC. High alcohol consumption and obesity are modifiable risk factors known to be common causes of chronic liver disease[15]. The liver is a metabolically active organ that possesses the ability to regenerate in response to injury[16]. This ability is thought to be one of the paths to increased cell division leading to uncontrolled cell division, then resulting in liver cancer. Much research is being performed to understand this process and the mechanisms of long-term liver disease, such as non-alcoholic fatty liver disease. Another known risk factor is the exposure to aflatoxin B1, a fungus commonly found in wheat products and peanuts[15]. In the lab we have focused on better understanding the genes and pathways modulated in liver cancer[17]. Life expectancy of patients suffering from liver cancer is influenced by tumor staging. Diagnosis of advanced stage tumors results in shorter lifespan expectancy, usually months to a year. When diagnosed early, median survival increases to about 5 years, inclusive of treatment and disease management. Staging is determined by percentage of the liver that is affected and the amount of invasion to vasculature and lymphatics. When localized, early-stage liver cancer can be treated with surgical resection or a simple ablation. However, with mid to advance stages, treatment also includes targeted therapies and standard chemotherapy[18].

In 2017, sorafenib a tyrosine kinase inhibitor, was approved for the treatment of unresectable HCC and has helped in increasing the live expectancy of advanced liver cancers[19]. The genetic landscape of HCC is varied, and multiple pathways have been identified to drive liver tumor formation. Activation of Wnt, SHH, Ras, AKT/mTOR, growth factor signaling, and angiogenesis have been identified to drive HCC[17]. It is this varied landscape that calls for further research to target liver cancers based on the pathways activated and genetic changes that drive liver oncogenesis in each case. At advanced stages of HCC systemic therapies improve clinical outcomes, although the median overall survival remains a little over one year. It is, therefore, necessary to better understand the molecular pathways involved in HCC development and invasion in order to find novel strategies to treat such tumors[20]. Moreover, chemotherapy, radiation, and surgery have limited effects in the treatment of HCC.

Sleeping Beauty Transposon Mutagenesis Identifies Human Cancer Genes:

Sleeping Beauty transposon-transposase mutagenesis system is based on the principle of transposition. Transposition is the way in which a DNA element is movable and can be inserted anywhere in the genome[21]. Two kinds of transposable elements exist. Class 1 relies on an RNA intermediary, requiring a retro-transcriptase in a later step. Hence retrotransposon. After the transposable DNA element is integrated in the genome its only way of replication is via the host's transcription machinery. Once the transposon has been transcribed and the retro-transcriptase translated, the retro-transcriptase uses RNA as a template for DNA synthesis. This dsDNA element is then integrated in the genome, aided by a transposase. On the other hand, Class 2 retrotransposons are DNA transposons and

are mobilized in a “cut and paste mechanism”. This class requires a transposase to cut the DNA element, which is then replicated during the S-phase of the cell cycle. Once copies are made, this DNA element can integrate into a site in the genome. Usually, transposon integration sites do not share many characteristics and the enzymes necessary for their activity are encoded by the transposon itself.

Exploiting the application of transposition technology *in vivo*, in 2013 we published work done using *Sleeping Beauty* in mice with the goal to identify novel driver genes of MPNSTs[22]. The need for such a screen was brought up by the fact that only a handful of driver genes had been identified to drive MPNSTs at the time. Moreover, current therapies have shown limited success. It is known that loss of the tumor suppressor *TRP53* and *EGFR* overexpression occur in over 50% MPNSTs[23]. Therefore, we genetically engineered mouse animal models with *Trp53* dominant negative background and *EGFR* overexpression exclusive to the Schwann cell lineage. In this screen, Schwann cell precursors were targeted by using the *CNP-Cre* transgene. In this manner, *SB* mutagenesis would be conditionally and temporally relegated to the Schwann cell lineage.

The first discovery was that overexpression of *EFGR* alone was enough to induce tumor formation[23]. This was potentiated with transposition and furthermore, at about 80% penetrance with the combination of the three, including dominant negative *Trp53*. The transposition vector contained T2/Onc, composed of a splice acceptor, a poly-A tail, a promoter (murine stem cell virus), and an early termination codon. Using next generation sequencing (NGS) and the software TAPDANCE we were able to identify common insertions sites (CIS). CIS are sites were the *SB* transposon was found to land/integrate

with a high frequency. Using both methods, we were able to identify 87 grade 3 PNST and 695, with 37 genes common to both tumor types. A list of genes can be found in Figure 2.1. Known driver mutations relevant in human models were observed. *Nf1* and *Pten* were the most common tumor suppressors found. Moreover, we found that the Wnt, PI3K, and Ras pathways were involved in Schwann cell tumor formation. These findings are the foundation to my thesis work on MPNSTs described in Chapter 2.

The Role of the Wnt Pathway in MPNSTs and Hepatocellular Carcinoma:

The Wnt pathway was first described in drosophila. It emerged as developmental pathway and a determinant of cell fate decisions. In humans it has an active role in multiple organs, most classically, the intestinal epithelium[24]. Wnt was first identified as a human cancer pathway in MMTV screens and later loss of the Wnt negative regulator *APC* was identified as the cause of familial adenomatous polyposis[25, 26]. Further research has resulted in the description of the Wnt canonical and non-canonical pathways in cancer and tissue regeneration, specially of the liver and the epithelial intestinal lining. Mutations in other Wnt pathway components, such as AXIN1/2, CTNNB1, and amplification of R-spondins have been described in human cancers[27, 28, 29]. Wnt activation occurs via the binding of a Wnt ligand to the transmembrane receptors Frizzled and lipoprotein-receptor related protein(s) (LRP). This causes recruitment of the β-catenin destruction complex, composed of AXIN1/2, APC, GSK3β and CK1. Recruiting of the destruction complex results in the phosphorylation of β-catenin by GSK3β and CK, tagging it for ubiquitination by β-TrCP and destroyed by the proteasome. In the presence of a Wnt ligand, the destruction complex remains inactive and the levels of β-catenin

increase in the cytoplasm. β-catenin then translocates to the nucleus and binds to the TCF/LEF transcription factors to promote the transcription of genes necessary for cell cycle progression and stem cell maintenance[30].

Wnt pathway activation is a feature of some MPNSTs[3]. We have identified in our lab that a large fraction of human MPNSTs possess alteration in one or more Wnt pathway components. Multiple mechanisms have been proposed based on gene expression data of human tumors. Downregulation of Wnt negative regulators, such as *APC* and *GSK3β* has been observed. Overexpression of *CTNNB1* is enough to transform immortalized human Schwann cells *in vitro*. However, expression of activated β-catenin was not sufficient to induce tumor formation in a Neurofibromatosis animal model.

Over a third of human HCCs exhibit gene expression profiles consistent with Wnt signaling activation. β-catenin -activating mutations occur in approximately one third of these cases[12]. However, multiple strategies targeting β-catenin and Wnt pathway components have had limited success in clinical trials because of toxicity caused by systemic off-target effects[18, 28]. It remains possible that some alterations in Wnt-pathway regulators are better drug targets, as well as other downstream Wnt effectors.

R-spondins are secreted Wnt modulatory factors that have been identified to act as oncogenes in human cancers of the peripheral nerve and liver[31]. We and others have described that a subset of cancers show overexpression of *RSPO2.* The mechanism(s) by which *RSPO2* overexpression occurs is not well understood. Is one of our goals to understand this mechanism in the context of MPNSTs.

In mammals, the R-spondin protein family contains four secreted proteins that modulate the Wnt pathway. R-spondins were first identified as an important growth factor for gut

organoids in vitro[32]. They exert their function by activating the Wnt pathway upon binding to the family of leucine-rich repeat-containing G-protein coupled receptors (LGR) and/or LRPs in the presence of a Wnt ligand. Wnt-ligands, such as Wnt3a, are necessary for the activation or modulation of the Wnt pathway by RSPO2. R-spondins are crucial in normal development of limbs, bone and the intestinal epithelia. R-spondins are thought to exert their oncogenic function by the transcriptional activation of Wnt responsive genes that regulate cell proliferation and survival[33]. Understanding the pathways activated by R-spondins will inform the search for new therapies against Wnt-driven cancers that contain mutations in *APC*, *AXIN2*, and/or *CTNNB1*. Understanding RSPO2 signaling will enhance our knowledge of the Wnt pathway, and further enhance the approach against Wnt-driven tumors. The development of therapies against pathways parallel or that synergize with the Wnt-canonical pathway may reduce tumor burden when used in combination with standard chemotherapy.

The Hippo/YAP Pathway Role in Cancer:

Recent studies have found that Hippo/Yap activation occurs in many human cancers[34]. This finding is important, as its activation results in increased survival and invasion. The main node of the Hippo pathway is YAP, a transcriptional regulator that influences cell proliferation and survival by controlling the expression of survival genes, such as *BIRC5* and *BCL2L1*, via binding to TEAD transcription factors. YAP is negatively regulated by Hippo activation of LATS1/2 that further phosphorylates YAP and target it for cytoplasmic sequestration by 14-3-3 and/or destruction via the proteasome after

ubiquitination by β-TRcP[35]. Control of YAP-mediated signaling has also been found to occur via Wnt, Rho, Shh, and Notch pathways[34].

A sole receptor for the activation of Hippo has not been found yet. Many have shown that the Hippo/YAP axis acts downstream of mechanoreceptors. Also, many alternative pathways of activation exist[36]. Wu et al recently found that loss of *Lats1/2* led to TAZ/YAP activation in Schwann cells in a NF1 mouse model resulting in tumor formation in mice. It is not clear if these tumors were composed of Schwann cells, fibroblast, or a mixture of both[37]. However, pathways of YAP activation relevant to human MPNSTs have not been described yet. No known mutations or gene expression alterations in *LATS1/2* occur in human tumors. Sleeping Beauty screen in mice that we performed for the discovery of novel genes involved in MPNST progression found components of the Hippo signaling pathway. *TAOK1*, for example, encodes a serine/threonine kinase that acts as a tumor suppressor via the inhibitions of YAP nuclear translocation by direct YAP phosphorylation that results in its cytoplasmic arrest and degradation[38]. We also found *Taok1* to be a *SB*-CIS gene in the context of loss of *NF1*[22]. It is then imperative to continue investigating the role of the Hippo/YAP pathway in human peripheral nerve sheath tumors and understand its role in the initiation, progression, and transformation of MPNSTs.

On the other hand, the knowledge of the role of the Hippo/YAP pathway in liver regeneration and hepatocyte transformation is more advanced. Interestingly, YAP has been found to inhibit hepatocyte differentiation in the mouse liver and to maintain a proliferative status[39]. This is similar to the phenomena observed in the intestinal epithelium, where β-catenin signaling maintains a stem cell-like status in LGR5-positive

cells in the intestinal crypt. Removal of β-catenin results in the exit of this cell stage and differentiation into goblet cells and enterocytes[40]. These two examples are only two of many in which signaling pathways maintain cancer cells in an undifferentiated status. The ultimate differentiation of these cells can be a novel avenue to cancer treatment, as terminally differentiated cells are usually short-lived, vulnerable, and easier to target based on surface markers.

The Hippo/YAP pathway has also emerged as a regulator of the micro-RNA processing machinery[41]. This was found to occur via a novel mechanism, in which at low densities nuclear YAP sequesters p72, a protein that aids in the scaffolding of the microprocessing machinery and identification of target miRNA sequences. During high cell density, YAP activity remains low and, in the cytoplasm, allowing for proper function of miRNA processing. In cancer, although tumors live in a high cell density state, many alterations occur and YAP remains sequestered by p72, altering miRNA processing. In cancer YAP nuclear translocation is increased via multiple mechanisms, such as Wnt signaling, resulting in further sequestration of p72. The miRNA repertoire influenced by Hippo/YAP signaling is thought to influence cell proliferation and survival and to modulate *MYC*, a known human oncogene. The latter can occur even in the presence of a defective YAP that does not bind to TEAD, the necessary co-transcription factor necessary for canonical Hippo pathway to occur. Hippo has also been found to influence inflammatory cell recruitment to the liver and influence tumor formation. Hence, Hippo/YAP signaling has become a mainstay human cancer pathway and the specific targeting of YAP will likely open new promising avenues for successful cancer treatment.

The Rho/GDI2 Axis:

The Rho signaling pathway is known to regulate cell polarity, adhesion, motility, the cell cycle, and survival[42]. Activation of Rho signaling can occur through 3 small GTPases: CDC42, Rho, and Rac. Downstream we can find the effectors: FAK, PAK, ROCK, LIMK, amongst others. The main effects of these effectors are to influence actin polymerization and entrance into the cell cycle. GDI2 is part of the family of GDP-dissociation inhibitors. Its main function is to control the access of Rho GTPases to guanine exchange factors (GEFs) and GTPase activating proteins (GAPs). GDI2 offers another level of regulation in the Rho pathway[43]. As with the Ras pathway, Rho exists in two forms: Rho-GDP, its inactive form and Rho-GTP, its active form. GDIs have been shown to have a role in modulating both stages. The loss of Rho negative regulators is known to occur in a variety of human cancers. Its effects are context-dependent and poorly understood today. Rho biology is better known for its role in cell invasion and migration, which is pivotal in cancer. Little is known about Rho signaling in MPNSTs and the role of GDIs in human cancer is still not clear. GDI2, specifically, has been identified only once in literature to acts as a tumor suppressor gene in human lung cancer[44]. Further, the role of Rho signaling in cancer may have a regulatory function in Hippo/YAP signaling via altering cell stiffness and migration, modulating Hippo via F-actin remodeling. A small subset of human MPNSTs have loss-of-function mutations according to TCGA data. We hypothesize that GDI2 is a MPNST tumor suppressor gene. Loss of *GDI2* therefore results in activation of Rho signaling. Targeting the Rho pathway is an attractive strategy to treat such tumors.

RSPO2 Aberrant Expression and Chromatin Dynamics:

Novel RSPO2 overexpression has been found to occur in little over 10% of all colorectal cancers (CRC), exclusive of *APC* mutations[45, 46]. Moreover, in an effort to find novel tumor suppressors and promoters of cancer, our lab conducted multiple forward genetic Sleeping Beauty screens in mice. Our lab found that overexpression of *RSPO2* in mice had an important role in the development of cancers of the intestine and peripheral nerve tissue[47-50]. We also demonstrated that RSPO2 expression is upregulated in a subset of Schwann cell tumors and serves as a driver of Wnt signaling in MPNSTs. In the liver, *RSPO2* overexpression occurs via copy number gain. It is important to understand the role of RSPO2 in carcinogenesis and tumor maintenance, as it has been implicated in a subset of breast, colon, liver, plexiform neurofibromas, and MPNSTS[51, 52].

A common characteristic of RSPO2-driven cancers is the presence of an *RSPO2* fusion transcript that results in its overexpression. The *EIF3E-RSPO2* fusion transcript is an example, in which 2-5% of the total *RSPO2* mRNA in a cell is expressed under the hypothesized influence of the *EIF3E* promoter[3]. In *APC* intact colorectal tumors, the *EIF3E-RSPO2* fusion transcript has been found to be associated with recurrent genomic deletions and/or inversions[45]. This fusion is one of the many possible mechanisms in which *RSPO2* gains its oncogenic function. In other words, normal expression of *RSPO2* is not oncogenic, but when overexpressed it becomes tumor promoting via a gain-of-function mechanism. This fusion transcript is found in tumor tissue, but not in the normal surrounding tissue. Interestingly, tumors that harbor *RSPO2* fusions also contain *BRAF* or *KRAS* activating mutations. On the other hand, most *APC*-mutant tumors have low to no expression of *RSPO2*, possibly via promoter hypermethylation[53]. It remains to be

understood how *RSPO2* overexpression occurs in tumors that do not harbor inversions and/or deletions. As a transcription-induced chimera (TIC) is possible in the absence of deletions, inversions, and/or insertions, we believe that the mechanism in which this happens is via the loss of a border element (such as CTCF) that further affects chromatin conformation leading to the generation of an *EIF3E-RSPO2* TIC.

CTCF is a border element that controls proper chromatin looping[54]. Loss of CTCF function results in promoter hijacking. That happens when a promoter goes under the control of a distal enhancer and/or promoter, thereby regulating in aberrant expression. Examples of such phenomena scarcely exist in the scientific literature[59,60]. One example is the expression of *Igf2* in mice[57]. Also, CTCF has been found to interact with SUZ12, a structural component of the polycomb receptor complex 2 (PRC2)[55]. Rescue of *SUZ12* re-establishes the interaction of the PRC2 complex with CTCF, leading the rescue of normal chromosomal looping and tri-methylation of H3K27 to suppress *IGF2* expression. This H3K27me3 is important in basic processes such as development in *C. elegans* to maintain proper control of gene expression[56]. In this manner, proper function of PRC2 requires CTCF, playing a role in proper placement of gene silencing marker H3K27me3, keeping proper gene regulation and isolation[57, 58]. It is yet to be determined whether chromatin conformation and loss of border element function is one of the many mechanisms in which RSPO2 overexpression occurs in RSPO2-driven tumors in the absence of genetic alterations.

Even though many studies have shown the oncogenic role of RSPO2, others have shown a protective role of RSPO2 in colorectal cancer[53]. Wu and colleagues hypothesized that RSPO2 stabilizes ZNRF3 upon binding to LGR5. ZNRF3 is a well-described negative

regulator of the Wnt/β-catenin pathway that is often mutated in pancreatic cancer. However, it has also been shown that RSPO2 potentiate the Wnt pathway by inducing the uptake of LGR5 along with ZNRF3 and RNF43, which are negative regulators (via ubiquitination of the Wnt receptors Frizzled)[61, 62, 63]. This conflict is yet to be resolved. It has also been established in the literature that Wnt activation is a common feature of HCC. Currently, targeted therapies against RSPO2 using immunotherapy are being developed to target in R-spondin-driven cancers[64]. However, a better understanding of R-spondin oncogenic activation will help us better understand the role of chromatin dynamics in cancer.

Hypotheses

1. Multiple pathways result in the malignant transformation of neurofibromas into MPNSTs.
2. The Hippo/YAP pathway is activated by the loss of the tumor suppressor genes *TAOK1*, *APC*, or *GDI2* in a subset human MPNSTS.
3. Altered chromatin dynamics result in the aberrant activation of oncogenic expression of *RSPO2* via the loss-of-function of the border element CTCF.
4. *RSPO2* is a liver cancer oncogene that activates Hippo/YAP signaling.

Objectives

1. To develop a streamlined screening methodology for the validation of candidate tumor suppressor genes and oncogenes.
2. To identify novel peripheral nerve sheath tumor suppressor genes and pathways.
3. To better understand regulation of oncogenic expression.
4. To understand the pathways activated by RSPO2 in liver cancer.

Chapter 2: Transposon Mutagenesis Guided CRISPR/Cas9 Screening Reveals Pathways Driving Malignant Peripheral Nerve Sheath Tumor Development and Maintenance

Overview

Malignant Peripheral Nerve Sheath tumors (MPNSTs) are highly aggressive, soft tissue, Schwann cell sarcomas. Half of these tumors occur sporadically, while the rest occur in the context of Neurofibromatosis Type 1 Syndrome (NF1), usually developing from pre-existing plexiform neurofibromas. NF1 is characterized by loss-of-function mutations in the gene encoding neurofibromin, a negative regulator of the Ras pathway. Patients who suffer from NF1 syndrome have a limited number of therapies available to them. Therapies are more limited to them because of the increased carcinogenic risk that radiation therapy poses to them. Inhibitors of kinases downstream of NF1, such as PI3K, MEK, and mTOR have been proposed from human and animal models, but we have not seen results in human clinical trials yet. This has resulted in low survival rates of NF1 patients with MPNSTs when compared to the general population with MPNSTs. It is important to find new pathways that have a role in peripheral neural sheath tumor cell transformation and progression to find new targets that efficiently treat peripheral neural sheath tumors. It remains necessary and exciting to understand the mechanisms by which oncogene expression activation occurs in these cancers and develop targeted therapies towards this phenomenon.

To better understand genetic factors that give rise to MPNSTs, we performed a Sleeping Beauty (SB) transposon screen in mice. The results implicated Wnt/β-catenin, PI3K-AKT-mTOR, and many other pathways. We next sought to validate SB screen gene hits in a human cellular model using CRISPR/Cas9 technology as a tool to induce loss-of-function mutations in tumor suppressor gene (TSG) and oncogene candidates. A total 103 genes were independently targeted with multiple single guide RNAs (sgRNA) in

immortalized human Schwann and MPNST cell lines and effects on transformation assessed. Transformation was assessed by anchorage-independent colony formation in soft agar, transwell migration, and xenograft tumor formation in NRG mice. In these assays, more than 30 genes scored as TSG candidates. Our results revealed a role for the Wnt/β-catenin, Hippo/Yap, RhoA, growth factor receptor signaling, and gene expression regulation pathways in human neurofibroma and MPNST development and maintenance. Specifically, we found that *TAOK1* and *GDI2* loss of function led to very potent transformation of immortalized human Schwann cells and tumor formation in a xenograft model. *TAOK1*, deleted in up to 8% of MPNSTs, encodes a ser/thr kinase that negatively regulates the Hippo/Yap pathway, which has been implicated in the genesis and progression of MPNST. We have found that expression of *TAOK1* is also reduced in human neurofibromas, MPNSTs, and MPNST cell lines. On the other hand, *GDI2* is a regulator of the RhoA pathway that has been found to act as a suppressor of lung cancer metastasis. We have found reduced *GDI2* copy number, expression and promoter hypermethylation in MPNST. Interestingly, we have found that the PRC2 components SUZ12 and CTCF regulate oncogenic expression, specifically that of *RSPO2*. Our screening methods have found novel pathways involved in the development of human MPNSTs. These have generated hypothesis-driven pre-clinical studies that we are pursuing at the moment. We are devising methods to target the pathways implicated by our studies and that are represented in human MPNSTs. We show that multiple mechanisms suppress Hippo/YAP activation relevant to human MPNSTs. This new knowledge will impact the search for therapies against plexiform neurofibromas and MPNSTs.

Methods

Tissue culture reagents and cell lines:

HSC1λ and S462s were a kind gift in collaboration with Dr. Margaret Wallace[65]. Clonal cell lines N5 and N10 are derived from HSC1λ and underwent CRISPR/Cas9 targeting against *NF1*. The N5 cell line was derived from clone found to have a deletion, resulting in loss-of-function of *NF1*. The N10 cell line was derived from a single clone in which *NF1* remained intact. Cells were cultured in DMEM supplemented with 10% FBS, 1% penicillin/streptomycin. All cells were grown on tissue culture-treated plates at 37°C and 5% CO2. Gene knockdown via siRNA was done with commercially available SmartPools (Dharmacon) against CTCF, CTNNB1, or RSPO2 and a siNon-targeting pool was used as a negative control.

In vitro Drug Studies:

Small molecule inhibitors of SMO, TNKS, PORCN, FAK, and/or YAP were used to asses cell viability after treatment with vismodegib, LGK-979 and ETC-159, IWR-1 and JW-55, Defactinib, Verteporfin respectively. Drugs were solubilized to the desired concentration in DMSO independently. A total of 4,000 cells per well in a 96-well plate were seeded and drug diluted in media was then added in triplicates with a DMSO control included. Cell viability was determined in an AlamarBlue assay (Invitrogen).

CRISPR/Cas9 Knockout of Candidate Tumor Suppressor Genes and Oncogenes:

CRISPR/Cas9 modified cell lines were generated using lentiviral vectors expressing Cas9

and a guide RNA directed against each candidate gene (Table 1). Lentiviral vectors were generated by transfecting 293T cells with two viral packaging plasmids and CC9 v2 Cas9/guide RNA-containing plasmid from Zhang lab at MIT (crispr.mit.edu). Guide RNA sequences were cloned into a stuffer region of the plasmid using Bsmb1 restriction sites. Guide RNA sequences to the gRNA used in the screen and this chapter can be found in Table 1. Sequences were designed to target downstream of the translational start site.

Quantitative reverse transcriptase PCR (qRT-PCR):

RNA was isolated from cell lines using the trizol method and treated with DNase to remove contaminating genomic DNA (Turbo DNA-free Kit, Ambion). A total of 1ug of RNA was used as a template to synthesize using the SuperScript III First-Strand Synthesis System (Invitrogen). qRT-PCR reactions were conducted with FastStart Universal SYBR Green Master mix (Roche), using 0.5 ul of cDNA template per 25 ul reaction. Primer sequences for qRT-PCR reactions are listed in Table 2. Data were normalized to the housekeeping control ACTB and the delta delta CT was calculated to determine fold-change value.

Oncogenic potential in vitro and in vivo studies:

Soft-agar assays were performed using 0.48% low melting point agarose in sterile water. 7,500 cells were plated per well in a 6-well plate. Pictures were taken in dissecting microscope at 1.5X and analyzed using ImageJ. Xenograft models were performed in NRG mice and 3 million cells were injected in the flank subcutaneously in media

containing matrigel (1:1). Tumors were harvested 4 months post-injection. IACUC protocol #1509-33035A.

Western Blot Analysis:

A total of 2 million cells were lysed using RIPA buffer, supplemented with a cocktail phosphatase inhibitor and a cocktail protease inhibitor. For nuclear fractions, a hypotonic solution supplemented with NP-40 was used to lyse the cells. Nuclear fractions were isolated via centrifugation and then lysed with complete RIPA buffer. Whole-cell lysates and cell fractions were sonicated and prepared in solution composed of SDS and a reducing agent, then boiled prior size separation in either a 10% or a gradient (4%-12%) polyacrylamide gel (Invitrogen). Gels were transferred to a PVDF membrane overnight. Membranes were then blocked in 5% non-fat milk TBST for 1 hour at room temperature. Primary antibodies were diluted to manufacturers recommendation in 5% TBST milk or 5% BSA milk and incubated overnight at 4 degrees C. A list of antibodies and concentrations used in this chapter is available in Table 4. After wash in TBST, HRP-conjugated secondary antibodies were then added and incubated at room temperature for 45 minutes and developed using HRP chemiluminescence and visualized in a LICOR machine.

Chromatin Conformation Capture Assay:

In order to perform a 3C assay, we first generated a 3C library, composed of fragmented cellular DNA. Ten million cells per samples were harvested, fixed in 1% formaldehyde, and lysed in a cold hypotonic solution. Nuclear fragments were isolated via

centrifugation and digested using EcoR1 overnight at 37C. SDS was then added and samples were heated to 65 degrees C to inactivate the restriction enzyme. Ligation was performed after, overnight at 16 degrees C. DNA was then isolated and cleaned using a 1:1 solution of Phenol:Chloroform and precipitated with NaAcetate. DNA was then used in a PCR assay with multiple primers designed to span regions to be thought to be involved in TIC of *EIF3E* and *RSPO2.* List of primer sequences can be found in Table 5. Bands were isolated and DNA purified and sent for sequencing. Results were then aligned using nBlast.

ChIP-qPCR:

The ChIP-qPCR assay described in this chapter was performed by employing the ChIP-IT kit form Active Motif. In summary, cells of interest were fixed on tissue culture plates using paraformaldehyde and harvested by scraping. The cells were then lysed on ice using a dounce homogenizer, then sheared using sonication. Immunoprecipitation was performed using an antibody against CTCF (Cell Signaling Technologies) at a concentration of 1:50. CTCF was then pulldown using magnetic beads that attached to the biotinylated secondary antibody. DNA-CTCF crosslinked chromatin was then eluted, reverse crosslinked and treated with Proteinase K to isolate pulled-down DNA. Primers designed to span the regions identified to be CTCF binding sites between the *EIF3E* and *RSPO2* sited were then used in a qPCR reaction to identify the amount of binding. Samples were normalized to an IgG control. List of primers can be found in Table 5

Results

A streamlined approach to assess Tumor Suppressor Gene Candidates and oncogene function in human MPNST Cell lines:

In the past we have implemented Sleeping Beauty mutagenesis in a mouse screen that successfully identified about 100 MPNST genes, most of this list is composed of candidate tumor suppressor genes (Figure 2.1). To a lesser extent it identified candidate oncogenes. We then sought to understand the relevance of these candidate genes in human Schwann cell tumors. We took a biased medium-throughput approach in order to evaluate the role of genes found to have a role in MPNST development in our previous murine Sleeping Beauty screen. We used CRISPR/Cas9 technology to evaluate loss of function of candidate oncogenes and tumor suppressor genes in human Schwann cell and MPNST cell lines (Figure 2.2). We designed 2-3 guides per candidate genes and cloned gRNA sequences into an all-on-one lentiviral vector (Zhang Lab). We also included a gRNA against GFP, to serve as a negative control. Viral pools were transduced, and cells were selected in puromycin. Each generated cell line expressed 2-3 gRNAs targeting one single candidate gene. Cell lines transduced were HSC1λ, N5s and N10 (immortalized human Schwann cells) and S462, an MPNST cell line from a lung metastasis. The selection of these cell lines was based on the need to have a normal human Schwann cell line, a *NF1* null cell line, and an aggressive MPNST cell line that lacks *NF1* and contains multiple mutations commonly found in MPNST. S462 cell line has loss-of-function mutations in *CDKN2A*, *SUZ12*, and *PTCH1*. We first evaluated the effects on anchorage-independent proliferation in a soft agar colony formation assay. We cultured the cells for

14 days, fixed, stained, and counted colonies per quadrant in duplicates. We found that most of the SB-CIS genes scored in the soft agar screen (Figure 2.3, 2.4). Although, several genes were found to have an effect when knocked out in a $NF1^{-/-}$ background. We were also able to identify candidate oncogenes in the MPNST cell line S462(Figure 2.3).

Tumor Suppressor Gene Candidates that score suggest multiple important pathways and control systems that are operative in the Schwann Cell Lineage: Genes like *CDKN2A*, *NF2*, *NF1*, and *SUZ12* are known MPNST tumor suppressor genes that served as positive controls in our screen. We then narrowed down our results to include genes that validated as candidate tumor suppressor genes and oncogenes in the soft agar screen. These genes were evaluated for migration and tumor formation. Transwell migration assay revealed that only some genes had a modest effect in migration in a transwell-migration assay. We found that tumor formation was easily predicted by migration as seen in the rest of Chapter 2 (Figure 2.4B). Multiple pathways were represented such as Wnt, Chromatin Dynamics, Ras, and cell cycle regulation pathways, with a new focus on Hippo/Yap and RhoA signaling. Wu and colleagues[37] have previously developed a mouse model, in which the total loss of *Lats1* and *Lats2* in mice results on Schwann cell tumor formation. LATS1/2 phosphorylate YAP, resulting in YAP cytoplasmic sequestration. We have also identified downregulation in the expression of *TAOK1* in human MPNSTs (Figure 2.6C). On the other hand, *GDI2*, a negative regulator of Rho signaling, is hypermethylated at its promoter, as found in MPNST human tumor samples. This results in the downregulation of *GDI2* expression, leading to Rho activation.

Loss of *APC* results in Wnt pathway activation and tumor formation:

We have previously described a role for the Wnt pathway in MPNSTs and it is now a known feature of MPNSTs[3]. However, it remains unclear what relevant genetic changes in Wnt pathway components are relevant to Wnt activation in MPNSTs. We have found that in vitro β-catenin activation results in increased Schwann cell proliferation and survival. In this study we found that loss of β-catenin destruction complex components, such as APC and GSK3β results in Schwann cell transformation (Figure 2.5, Table 1). Other forms of Wnt pathway activation may also result from overexpression of Wnt ligands and RSPO2. Knockout of APC (Figure 2.5A) in immortalized Schwann cells resulted in increased colony formation in an anchorage-independent assay (Figure 2.5C-E). Moreover, we found that loss of *APC* also results in increased migration in a transwell assay (Figure 2.5 C) and tumor formation in a xenograft model (Figure 2.5D). We also found that loss of *APC* resulted in increased levels of *CTNNB1*(Figure 2.5C).

Knockout of *TAOK1* results in Hippo/YAP pathway activation:

Previous studies have found a role for the Hippo/YAP pathway in MPNST development[53]. However, a common cause describing the mechanism of Yap activation in human MPNSTs has not been described. We also found this gene to be a SB-CIS that co-occurred with the concomitant loss of NF1 (Figure 2.6A). In our screen we found a similar result, but only limited to tumor formation in the xenograft model. One out of fifteen MPNTS have loss of *TAOK1* according to TCGA data (Figure 2.6B). Moreover, loss of *TAOK1* results in increased YAP levels (Figure 2.7A), as highlighted in the

literature describing the Hippo pathway. Loss of *TAOK1* was sufficient to result in anchorage-independent growth (Figure 2.7B), but not in tumor formation. Concomitant loss of *NF1* and *TAOK1* was necessary to form tumors in a xenograft model (Figure 2.7C). We also found that loss of YAP1 in S462 cells (Figure 2.8A) resulted in loss of tumor formation in a xenograft model (Figure 2.8B). S462 cells are a highly utilized MPNST metastatic cell line known for its ability to form colony in soft agar assay, its highly migratory phenotype, and the ability to form tumors in xenograft models. We also used the small molecule verteporfin that inhibits YAP/TAZ binding. We found that this also had a deleterious effect in colony formation in soft agar, suggesting a direct role for YAP signaling in tumor formation (Figure 2.8 C, D). The kinase inhibitor, dasatinib was used in combination as it inhibits the pathways activated by loss of *NF1*.

Loss of *GDI2* results in Rho pathway activation via Fak and Hippo/Yap activation: GDI2 is a master regulator of the Rho signaling pathway. It stabilizes the Rho-GDP bound form, which is the inactive form. Because of its function, we hypothesize that it acts as a tumor suppressor gene via actin remodeling and further inhibition of motility. Promoter hypermethylation has been found to occur in MPNSTs, resulting in low copy number of *GDI2* (Figure 2.9A). Loss of *GDI2* was one of the most robust (Table 1) tumor suppressor gene candidates to score in anchorage-independent growth. Loss of GDI2 led to tumor formation in a xenograft model and increased migration in a transwell assay (Figure 2.9B-D). We then wanted to understand which Rho pathway effector was active upon loss of GDI2. We found that FAK (Figure 2.10A, B) and ROCK (data not shown) were both active upon loss of GDI2. We found that FAK of ROCK were both active upon

loss of GDI2. Drug studies revealed that Rho inhibitors, specially inhibitors of FAK, decreased viability of MPNST cell lines and colony formation in soft agar (Figure 2.10A). In a nuclear fractionation Western blot assay, in which we blotted for YAP, and found that loss of GDI2 results in nuclear accumulation of YAP, resulting in further activation of the pathway (Figure 2.10C). This likely occurs via F-actin remodeling, which is a known pathway enhanced by Rho activation, here resulting as a consequence of *GDI2* loss. So far, we have shown that the loss of tumor suppressor gene in human Schwann cell leads to the transformation and activation of the Hippo/Yap pathway.

Loss of PTCH1 in human Schwann cells results in activation of the Sonic Hedgehog pathway:

The Shh is an emergent pathway in MPNSTs. Although much is known about Shh role in glial cell development, Shh pathway component mutations have been obscured, likely to old methods of RNA-seq analysis. New whole exome sequences in work yet to be published by our collaborators show that *PTCH1* inactivating mutations is a feature of up to 1/3 of MPNSTs (data not shown, manuscript in preparation with collaborators). Also, loss of PTCH1 is a feature of about 10% of MPNSTs available in TCGA (Figure 2.11A). *PTCH*1 is a MPNST *SB*-CIS gene and we found that its loss results in cell transformation as assessed in anchorage-independent soft agar and transwell migration assays (Figure 2.11B, C). Also, we found, via RNA sequencing and western blotting, that *PTCH*1 is differentially expressed in MPNST cells lines when compared to levels in HSC1λ cells. The Shh pathway is similarly active according to levels of GLI1. Of the 5 available MPNST cell lines, S462-TYs have the highest amount of *GLI1* expression, a marker of

Shh activity (Figure 2.12A, B). SHH activation is a known feature of basal carcinoma. Smoothened is a SHH component that acts as a receptor for Shh ligands. Vismodegib was developed as a small molecule inhibitor of smoothened and has been successful at treatment basal carcinoma. To test the sensitivity of cells to smoothened inhibition, we found that MPNSTs cell lines and human immortalized cell lines that lack *PTCH1* via CRISPR/Cas9 knockout were the most sensitive to treatment with vismodegib (Figure 2.12C). This is exciting as it opens a new avenue for the treatment of human MPNSTs.

Loss of the border element *CTCF* results in activation of oncogene expression:

Previously, we have found that the Wnt pathway modulator, *RSPO2* is overexpressed in a small subset of human MPNSTs[3]. We found the then novel *EIF3e-RSPO2* transcript overexpressed, yet 90% of the *RSPO2* transcript did not show genetic alterations. This conundrum drove us to hypothesize that changes in chromatin dynamics/architecture is responsible for the changes in expression of *RSPO2*. One of the mechanisms by which this could happen is via loss of insulator function of the polycomb repressor complex (Figure 2.13). SUZ12, for example, is known to be mutated in MPNSTs. Other examples have emerged in the field, such as CTCF. In fact, CTCF was found[76] to play a role in the expression regulation of *PDGFR,* a known oncogene in glioblastomas. In order to understand the role of CTCF in the regulation of *RSPO2* expression, we decided to knockdown *CTCF* using a smartPool siRNA (Thermo). Here, we found that the knockdown of *CTCF* leads to an increase in the expression *of RSPO2* mRNA. Interestingly, the effect of *CTCF* knockdown is the greatest at day 3 of siRNA transfection in HSC1λ cells that normally do not express *RSPO2* (Figure 2.14). These

results in both cell lines suggest that CTCF has a role in the regulation of *RSPO2* expression. Knockout of *CTCF* led to increased colony formation in soft agar and migration. Moreover, it results in tumor formation in mice (Figure 2.15C-E). As we have previously shown, *RSPO2* activates both Wnt and Hippo signaling pathways (see chapter 3), which explains transformation in these cells. We also aimed to understand the effect of knockdown *RSPO2* and *CTNNB1* in the S462 MPNST cell line. This cell line has high levels of RSPO2 and a Wnt active transcription signature. We found that knockdown of *RSPO2* resulted in decreased cell viability, but not knockdown of *CTNNB1*(Figure 2.16). Interestingly, knockdown of RSPO2 did not result in decreased levels of CTNNB1. Also, knockdown of *CTNNB1* did not significantly altered levels of RSPO2.

The MPNST cell line S462 is sensitive to Tankyrase but not to Porcupine inhibition:

RSPO2 activation of canonical Wnt pathway is dependent on Wnt ligand binding to Frizzled and LRPs. Because of this we tested the use of porcupine inhibitors, a class of small molecule that impedes the acylation on Wnt ligands in the endoplasmic reticulum and inhibits their secretion[67]. On the other hand, tankyrase is known to destabilize Axin1/2 resulting in decreased CTNNB1 destruction and in increased Wnt signaling[68]. We used 3 different tankyrase and 2 porcupine inhibitors (data not shown) to examine the effects on cell viability (Figure 2.17). We found that porcupine inhibitors had little to no effect on cell viability, however, tankyrase inhibitors are successful at decreasing cell viability. Although these 2 kinds of molecules have not been tried in clinic yet, they present a new avenue for the treatment of *RSPO2*-high tumors.

CTCF is a border element that binds between the *EIF3E* and *RSPO2* loci:

It is intriguing how RSPO2 overexpression occurs in a subset of human MPNSTs. Since we described this phenomenon in Watson et al[3], we have been fascinated by the idea that aberrant chromatin folding can result in oncogenic expression and transcriptional induced chimeras. The loss of *CTCF*, mutation of the binding motif, and/or hypermethylation of such can result in the loss of the border element and RNAPII runoff, leading to *RSPO2* overexpression. Using ENCODE, we found 3 different regions that contain the CTCF binding motif "CCCTC" (Figure 2.18). Prediction of CTCF binding sites can illustrate genes that are isolated, likely to maintain regulatory elements distant from a downstream gene promoter[68, 69]. In order to verify the predicted CTCF binding sit, we performed a ChIP-qPCR for CTCF. We designed 10 sets of primers that would span the three different regions and quantified the amount of binding in a high RSPO2 (S462) cell line and a low RSPO2 cell line (HSC1λ). Although, we couldn't find any specific patterns, we found that CTCF binding differs between each cell line and that specific CTCF binding might influence CTCF isolating function (Figure 2.19). In order to understand this phenomenon, we can employ CRISPR/Cas9 technology to mutate CTCF binding sites in different combinations to find the loci combination necessary to isolate *EIF3E* and *RSPO2*.

Chromatin Conformation Capture reveals interaction of an upstream active promoter with the RSPO2 promoter:

A hallmark of RSPO2-driven cancers is the presence of the *EIF3E-RSPO2* fusion transcript that results in *RSPO2* overexpression. In *APC* wild-type colorectal tumors the *EIF3E-RSPO2* fusion transcript has been found to be associated with recurrent genomic

deletions. However, this is not the case of MPNSTs primary tumors and cell lines. We hypothesize that *RSPO2* overexpression occurs via a novel epigenetic mechanism, such as loss of insulator activity that brings its promoter under the influence of distant enhancers, promoters, and simultaneous generation of transcription-induced chimeras (TICs). In this scenario, TIC generation may be a signature of loss of proper insulator function and proper epigenetic control of gene expression. Using Chromosome Conformation Capture (3C) technology[70], we aimed to determine if there exists an interaction of the *EIF3E* promoter with the *RSPO2* promoter. This data will help us understand if the proximity of the two gene loci play a role in the fusion of *EIF3E-RSPO2* and the overexpression of *RSPO2*.

Using 41 primer pairs designed to span 3DP predicted 3C DNA, we were able to identify particular regions of interaction between the *EIF3E* and *RSPO2* promoters (Figure 2.20). These regions are highlighted by the unique bands observed in S462 3C DNA but not in HSC1λ 3C DNA. These regions were then sequenced and found to align with both promoter regions. Because *EIF3E* is a constitutively expressed gene, we hypothesize that this found interaction with the less active *RSPO2* promoter enhances *RSPO2* overexpression in an aberrant manner (see model in Figure 2.21). Limitations of this 3C assay ensue the need for more technologically advanced assays, such as HiC to analyze and better understand whole genome chromatin interactions that influence oncogenic expression.

Discussion

In this study we were able to validate the *SB*-CIS genes from our previous work in mice performed in our laboratory as previously referenced. We found a role for many pathways previously represented in MPNST genetic screens. We also found novel pathways, such as Rho signaling and Chromatin Dynamics. Interestingly these pathways converge downstream in YAP signaling (Figure 2.22). The mechanisms that we uncovered include copy number variations and loss-of-function mutations in known tumor suppressor genes, such as *TAOK1*, *APC*, *NF2*, and others (see Table 3). Moreover, oncogenic expression of genes such as *YAP* or *RSPO2* also result in Hippo activation. Our results indicate that the dysregulation of the Hippo pathway can occur via 3 different mechanisms: the loss of Hippo negative regulators, Wnt activation, and Rho modulation. Loss of *TAOK1* and *NF2* are frequent events in MPNSTs. Examination of human RNA-seq data, CNA, and methylation, reveal that *TAOK1* is down-regulated, in some cases deleted, that the *GDI2* promoter is hypermethylated, *RSPO2* is overexpressed, and that *APC* is lost a subset of human cancers. We have also shown that *RSPO2* signaling results in activation of both Wnt and YAP signaling, via bypass of LATS1/2 negative regulation of YAP.

TAOK1 encodes a serine/threonine-protein kinase that enhances LATS1/2 function via phosphorylation. This results in further YAP phosphorylation and its cytoplasmic sequestration. *NF2*, another tumor suppressor and *SB*-CIS gene, is known to negatively regulate the Hippo pathway via activation of LATS1/2. The tumor suppressor gene *TAOK1* is linked to *NF1*. It is located 1000Mb away. *SUZ12* is also linked to *NF1*. It is

possible that in a subset of cases loss of *TAOK1* occurs concomitantly with the loss of *NF1* and/or *SUZ12* (Figure 2.6A). Also, Wu and colleagues have described loss in the expression of *LATS1* and *LATS2* in human MPNSTs, known Hippo/YAP pathway negative regulators. They found that loss *Lats1/2* and *Mts* deletion in mice resulted in significant tumor penetrance in a murine model. However, this model did not take into consideration loss of *NF1* and changes that are relevant in humans. Moreover, careful examination of the specimen pathology revealed that these tumors were mainly composed of fibroblast and not Schwann cells. Verteporfin has been used as a model small molecule to study YAP activity. Its use in humans is limited, but our studies show an increased need for development of a targeted Hippo/Yap inhibitor. More relevant would be a drug that acts at the nuclear level, as we have discovered here that many roads led to YAP nuclear activation and subsequent signaling, resulting in increased cell survival and proliferation. It is our hypothesis that YAP oncogenic activity occurs via both YAP co-transcriptional and micro-RNA processing functions. In order to analyze the effects of YAP in micro-RNA function we would have to perform loss-of-function assays of TAZ, the main regulator of micro-RNA processing downstream of YAP.

We have also found a role for chromatin dynamics via CTCF, in the regulation of *RSPO2* expression. The role of CTCF has been previously described in *IDH*-mutant gliomas, where the resultant DNA hypermethylation causes loss of binding of CTCF[76]. We have also reported that PRC2 complex elements, such as *SUZ12* are often mutated in MPNSTs with the concomitant loss of *NF1*. In fact, both genes are in the same arm of chromosome 17 in humans and they might be lost in one single event. CTCF is a border element that keeps distal enhancers from downstream promoters. Our results indicate that loss of

CTCF leads to aberrant overexpression of *RSPO2*, which activates both Hippo and Wnt pathways. We have also observed that *RSPO2* overexpression in the liver leads to both Wnt and Hippo pathway activation, and that RSPO2-driven liver tumors are abolished by loss of *Yap1* in the mouse liver (see Chapter 3). Moreover, we found that the MPNST cell line, S462, which expresses high levels of *RSPO2*, has a unique interaction between the constitutively expressed *EIF3E* and the *RSPO2* promoter. This finding gives us more insights into the effects of aberrant chromatin folding resulting in oncogenic expression. Further analysis of chromatin interactions, using technologies such as HiC and ChIP-Seq are needed to further understand the cellular effects of aberrant chromatin folding in oncogenic expression.

On the other hand, multiple mechanisms exist that contribute to the activation of the Wnt pathway. Here, we describe a role for the loss of *APC*, the main negative regulator of Wnt signaling by acting as a scaffold for the β-catenin destruction complex. In fact, *APC* was found to be lost in a subset of MPNSTs in the most recent TCGA Research Consortium Analysis of soft tissue sarcomas. YAP has also been found to bind to APC and phosphorylated by GSK3β. Therefore, the loss of APC results in the release of both β-catenin and YAP and subsequent translocation to the nucleus. We hypothesize that this results in increased proliferation and survival of Schwann tumor cells. This event can result in further mutational events.

The Rho pathway appears to also regulate Hippo signaling according to previously published work[42, 44]. Rho pathway activation ultimately has an eminent role in actin cytoskeleton and cellular tension. Hippo is known to be regulated in a mechanosensory fashion. Hippo controls organ size, and when lost this can go out of proportion. So, when

tumors are growing in cell number, Hippo acts as an escape mechanism to normal control of cell proliferation and organ size. Also, Hippo may also have a role in the regulation of cell survival and proliferation in circulating cancer cells and metastatic events. Hippo is activated in low pressure situations, so the as soon as cells are released from a tumor these pathways can activate and aid in the survival of cells that if not cancerous would be otherwise poised to undergo anoikis. In fact, loss of *GDI2* results in Rho activation via FAK and Hippo activation via increased YAP1 stabilization.

The Shh pathway is an emergent MPNST signaling pathway. We have confirmed in our studies, that loss of *PTCH1*, a receptor that acts as a negative regulator of the Shh pathway, results in Schwann cell transformation. This has not been described before. However, Shh has been shown to play a major role in glial cell differentiation[71].

Based on our data, many mechanisms exist that result in oncogenic activation of the Hippo, Wnt, and Shh pathways in neurofibromas. MPNSTs harbor variegated mutations and a high number of CNVs. This makes a case for combination therapy. Double or even triple targeting is a strategy that is being slowly implemented in the clinic against aggressive tumors. Rho, Hippo, Wnt, and Shh pathways are targetable. We show that Hippo, Wnt, and Shh inhibition halts cell transformation and proliferation *in vitro*, making attractive targets for the treatment of MPNSTs. Verteporfin has been used as a model small molecule to study YAP activity. Its use in humans is limited due to systemic non-specific targeting. Our studies show an increased need for development of a targeted Hippo/Yap inhibitor. We propose that MPNST should be targeted with MEK inhibitor in combination with YAP, Rho, and/or Wnt inhibitors. Knowing the specific landscape of

individual MPNSTs will shed light into the right combination of targeted therapies to use in patients.

Figure 2.1: A Sleeping Beauty Transposon Screen Reveals Novel Genes and Pathways Implicated in Schwann Cell Tumorigenesis and Maintenance

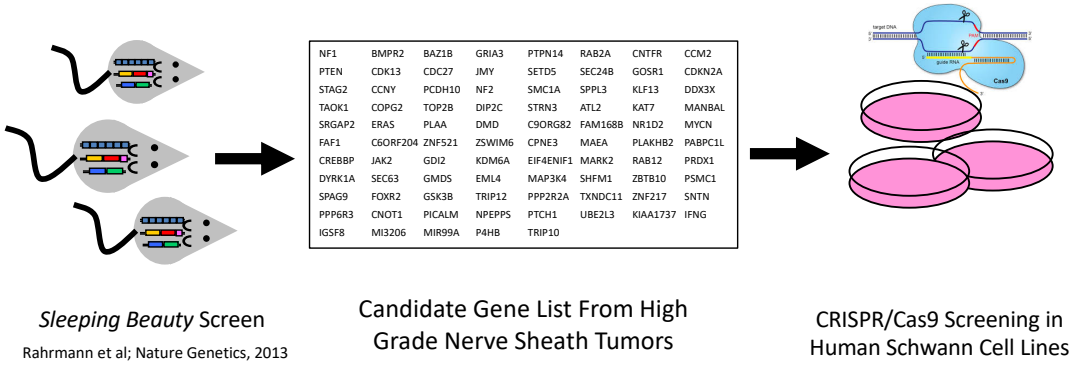

Figure 2:1: Figure depicting the foundational work for the investigation and findings in this dissertation. The list of genes shows the *SB*-CIS genes that were examined in human Schwann and MPNST cell lines.

Figure 2.2: A Medium-Throughput Screening Method to Identify Novel Human MPNST Genes

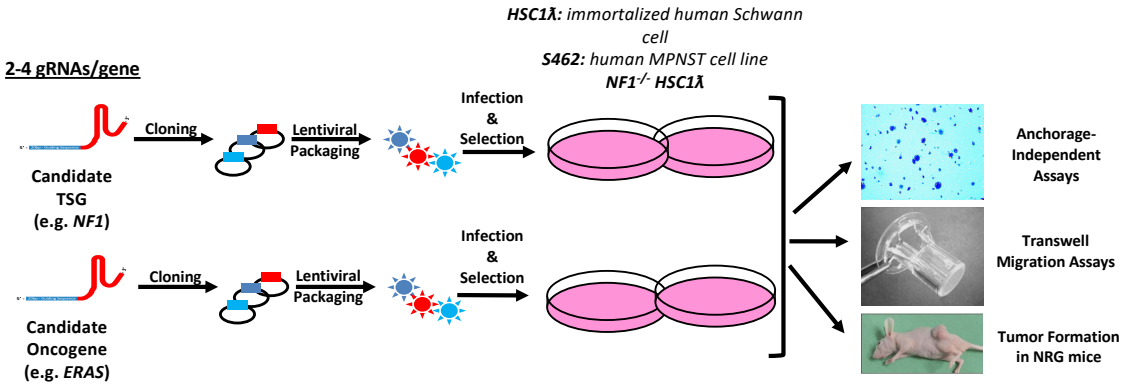

Figure 2.2: Diagram depicting screening method. First, gRNAs were designed to target genes selected and then stable cell lines, established via puromycin selection, and assessed for transformation upon genetic knockout.

Figure 2.3: Screening in MPNST Cell Lines Reveal Candidate Oncogenes

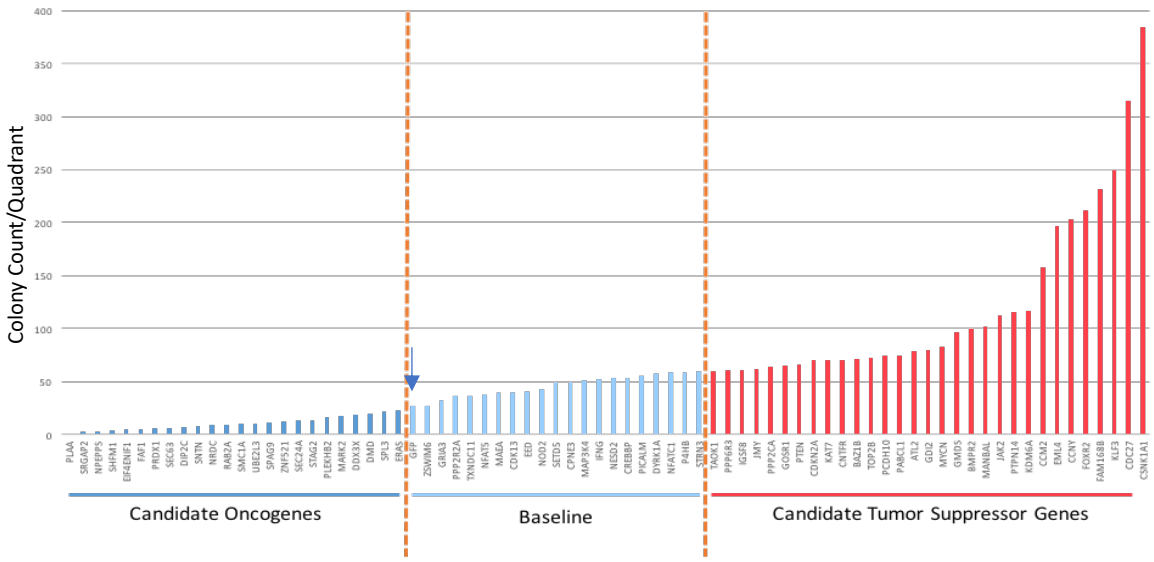

Figure 2.3: Graph depicting average colony count in soft agar assay in the MPNST cell line S462.

Figure 2.4: Screen Results Summary

A

TSG Candidates

Gene	HSC1L	N10	N5
APC	51	15	63
AXIN2	87	0	48
BAZ1B	28	0	24
CDC27	18	35	34
CDK13	14	41	27
CDKN2A	16	23	27
CPNE3	53	55	18
CREBBP	0	65	24
CSNK1A1	83	0	33
CTCF	32	0	20
EIF4ENIF1	100	26	24
FAM168B	90	17	0
IFNG	14	45	0
PPP2CA	13	21	7
PPP6R3	20	9	4
RNF43	19	0	46
SHFM1	22	0	11
SMC1A	76	0	12
SNTN	53	1	10
TOP2B	15	1	22

NF1 Mutant TSG candidates

Gene	N5	S462
APC	63	36
BAZ1B	24	18
CCM2	100	41
CCNY	32	53
CDC27	34	82
CDK13	27	10
CDKN2A	27	18
CREBBP	24	14
CSNK1A1	33	100
GDI2	56	21
JAK2	32	29
JMY	28	16
KLF3	25	65
LGR6	55	23
TOP2B	22	19

Candidate Oncogenes

Gene	S462
AXIN2	2
DDX3X	5
DIP2C	2
DMD	5
EIF4ENIF1	1
ERAS	6
FAF1	1
LGR5	7
LRP5	3
MARK2	4
NPEPPS	1
NRDC	2
PLAA	0
PLEKHB2	4
PRDX1	1
RAB12	2
RAB2A	0
RNF43	3
SEC63	2
SHFM1	1
SMC1A	3
SNTN	2
SPAG9	3
SPPL3	6
SRGAP2	1
STAG2	4
UBE2L3	3
WNT5a	1
ZNF521	3
ZNRF3	4
ZSWIM6	7

Percentile

0
10
30
50
70
100

B

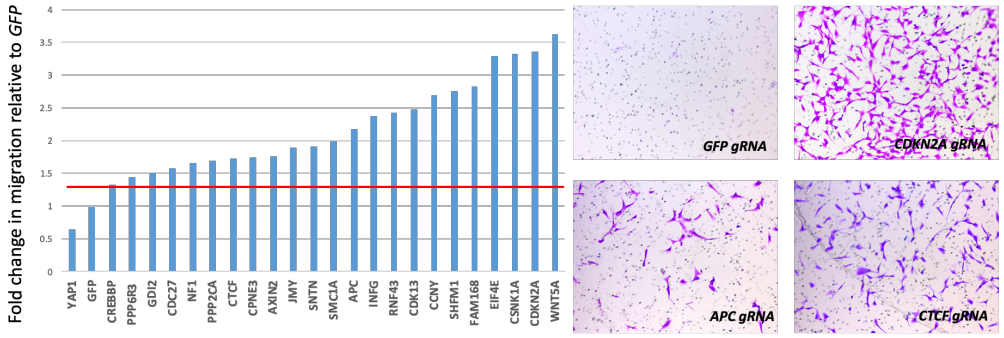

C

Gene Name	Tumor formation (animals with tumors/total animals injected)
APC	4/4
TAOK1	0/4 (4/4 with loss of *NF1*)
YAP1	0/4 (S462 cell lines)
GDI2	4/4
PTCH1	2/4 (3/4 with loss of *NF1*)

Figure 2.4: (A) Shows percentile scores of individual genetic knockouts in different human Schwann cell lines and the MPNST cell line S462. The N10 cell line is a clone derived from HSC1λ and the N5 cell line is a HSC1λ clone that is *NF1* deficient via CRISPR/Cas9 modification. (B) Table depicting scores of cell migration of CRISPR/Cas9 cell in a transwell assay. (C) Table depicting tumor formation in xenograft model of selected validated genes in HSC1λ cells.

Figure 2.5: APC KO Results in Anchorage-Independent Growth, Transwell Migration and Tumor Formation in Normal Immortalized Human Schwann Cells

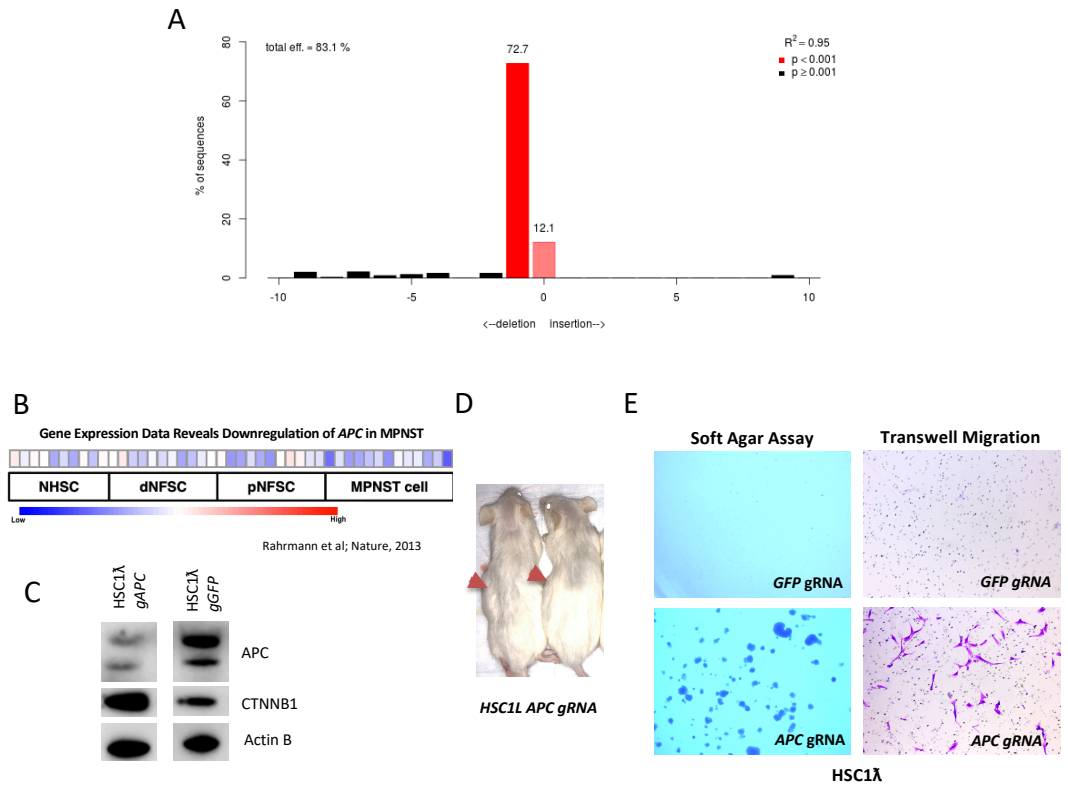

Figure 2.5: (A) InDel analysis using the online software TIDE showing that our gRNA design approach is effective at causing genomic deletions in gene of interest. (B) MicroArray data showing expression levels of *APC* in different tissue types and cell lines. Each bar represents a unique tissue or cell line sample. NHSC: non-human Schwann cells; dNFSC: dermal neurofibroma; pNFSC: peripheral neurofibroma. (C) Western blot showing loss of APC via CRISPR/Cas9 and increased CTNNB1 levels. (D) Loss of *APC* results is tumor formation in NRG xenograft model. (E) Loss of *APC* results in anchorage-independent growth and cell migration.

Figure 2.6: *TAOK1* is Linked to *NF1* and Co-Deletion is Likely to Occur in Some MPNSTs

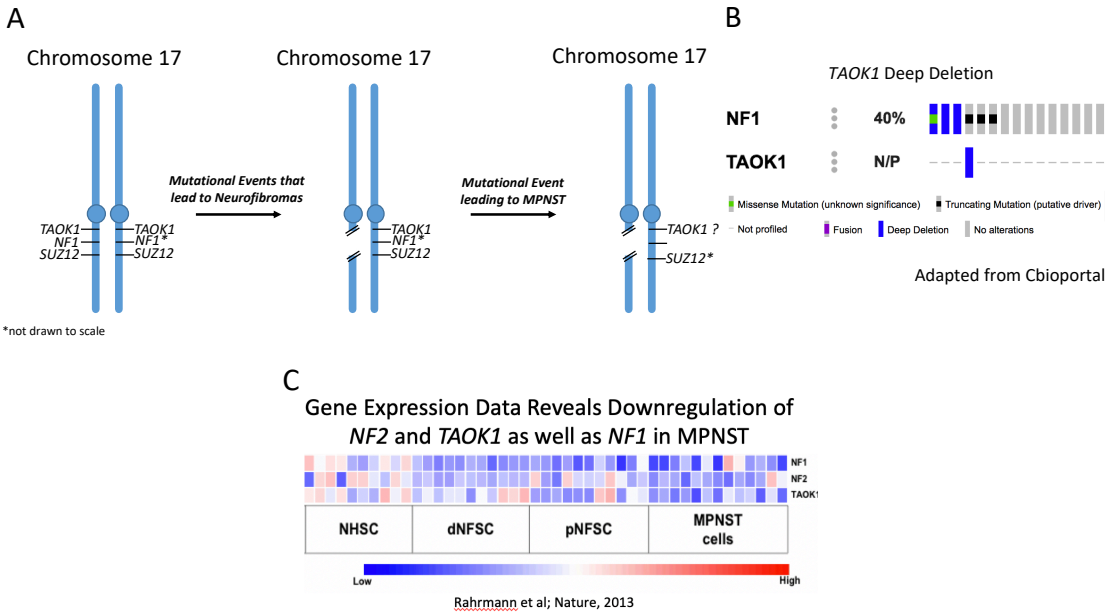

Figure 2.6: (A) Figure depicting the hypothesized mechanism of concomitant loss of *TAOK1* with *NF1* and/or *SUZ12*. (B) TCGA data showing mutations in *NF1* and *TAOK1* in a set of 15 human MPNSTs. (C) MicroArray data showing expression levels of *NF1, NF2,* and *TAOK1* in different tissue types and cell lines. NHSC: non-human Schwann cells; dNFSC: dermal neurofibroma; pNFSC: peripheral neurofibroma.

Figure 2.7: Loss of the *TAOK1* Gene Results in Schwann Cell Transformation *in vitro*, but Co-deletion of *NF1* is Necessary for Xenograft Tumor Formation

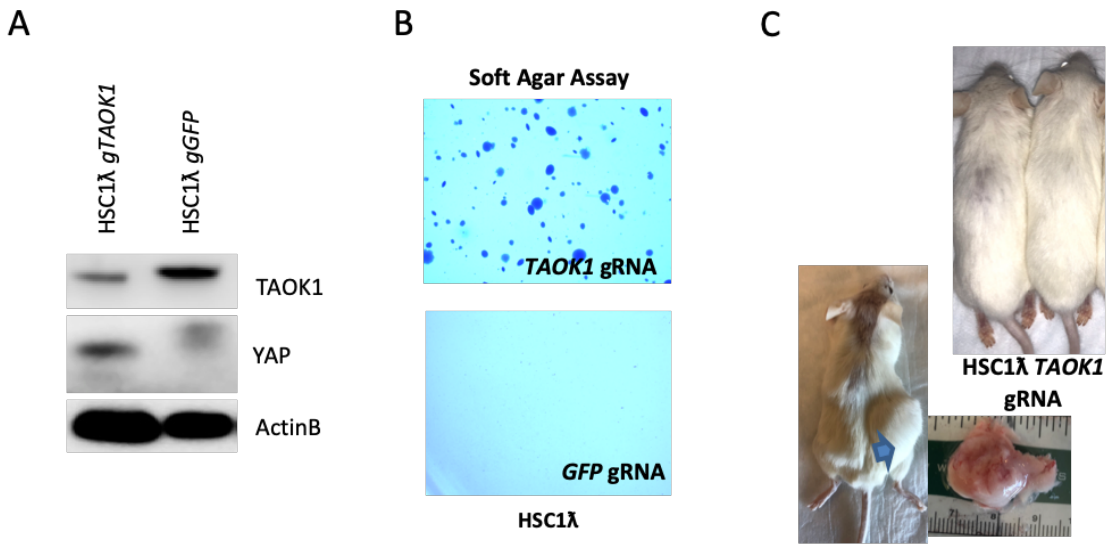

Figure 2.7: (A) Western blot showing TAOK1 decreased levels and increased YAP levels upon gRNA against *TAOK1* in a human immortalized Schwann cell line . (B) Anchorage-independent assay showing cell transformation upon *TAOK1* knockout. (C) Tumor formation in NRG mice. Picture on the left show tumor formation of HSC1λ *NF1*$^{-/-}$, *TAOK1*$^{-/-}$ cells. Picture on the right shows that HSC1λ *TAOK1*$^{-/-}$ cells do not form tumors on a xenograft model.

Figure 2.8: *YAP1* KO or Inhibition Results in Decreased Anchorage-Independent Growth in Soft Agar and Xenograft Tumor Formation in Human MPNSTs

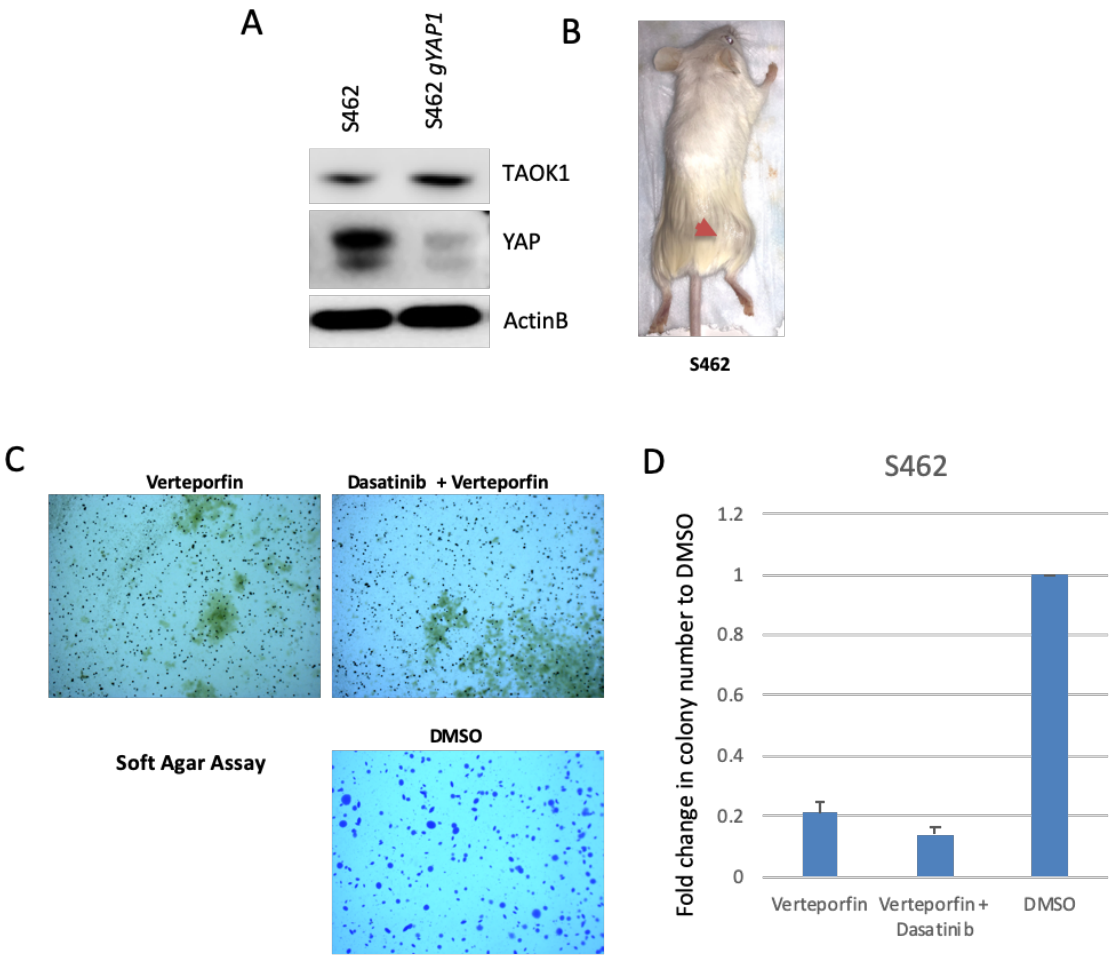

Figure 2.8: (A) Western blot showing knockout of *YAP*. (B) Tumor formation is abrogated upon *YAP* knockout on the S462 MPNST cell line. S462 cell lacking YAP1 were injected on the left flank, while wild type S462 were injected on the right flank. (C) Inhibition of YAP/TAZ activity and tyrosine kinase inhibition results in loss of anchorage-independent growth. Treatment with verteporfin and/or dasatinib results in decreased colony formation in soft agar. (D) Quantification of (C).

Figure 2.9: Loss of *GDI2* Results in Anchorage-Independent Growth, Migratory Phenotype, and Xenograft Tumor Formation

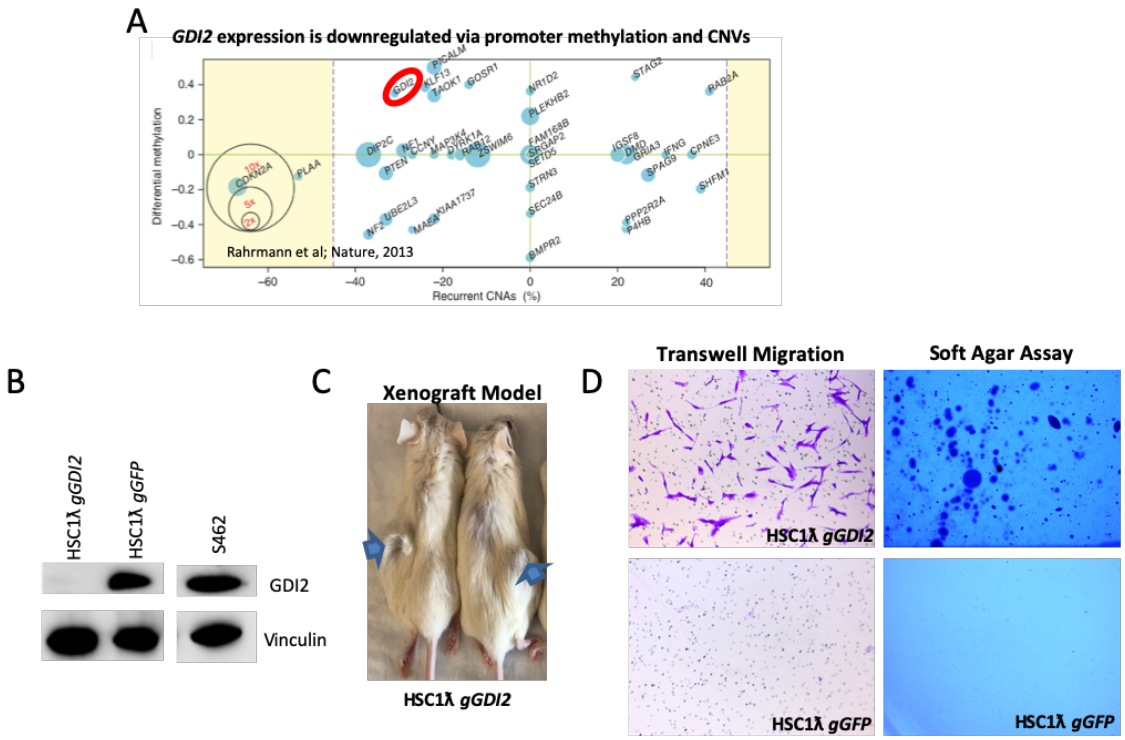

Figure 2.9: Figure from Rahrmann et al showing that *GDI2* promoter is hypermethylated in human MPNSTs. Each dot size represents sample coverage where the change was found. (B) Western blot showing knockout of *GDI2* in an immortalized Schwann cell line and levels in S462 MPNST cells. (C and D) Loss of *GDI2* results in transformation as seen by increased anchorage-independent growth cell migration, and tumor formation in NRGs. Arrows on figure C show tumor formation of *GDI2* knockout cells in a xenograft model.

Figure 2.10: Defactinib is FAK inhibitor that inhibits anchorage-independent growth of Rho active cells

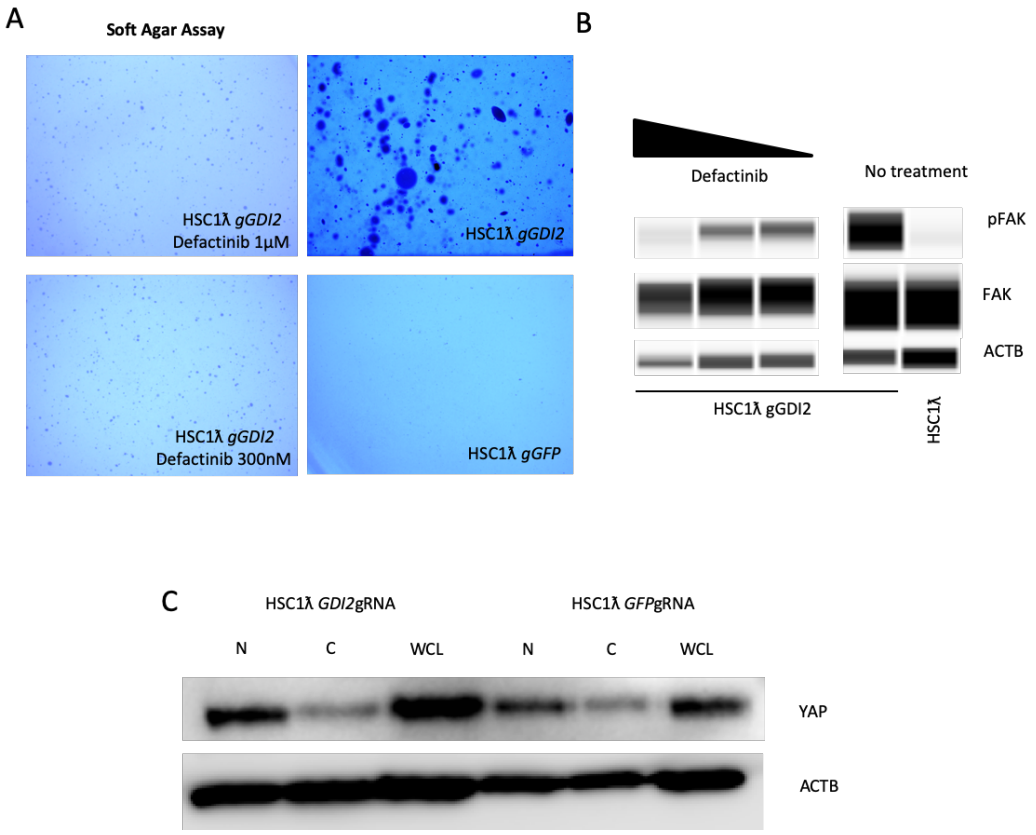

Figure 2.10: (A and B) Loss of *GDI2* results in FAK activation and treatment with defactinib, a Rho inhibitor, results in decreased anchorage-independent growth. (C) Loss of *GDI2* results in increased YAP levels and nuclear localization.

Figure 2.11: Loss of Shh Regulator *PTCH1* Results in Anchorage-Independent Growth and Migration in Human Schwann Cells

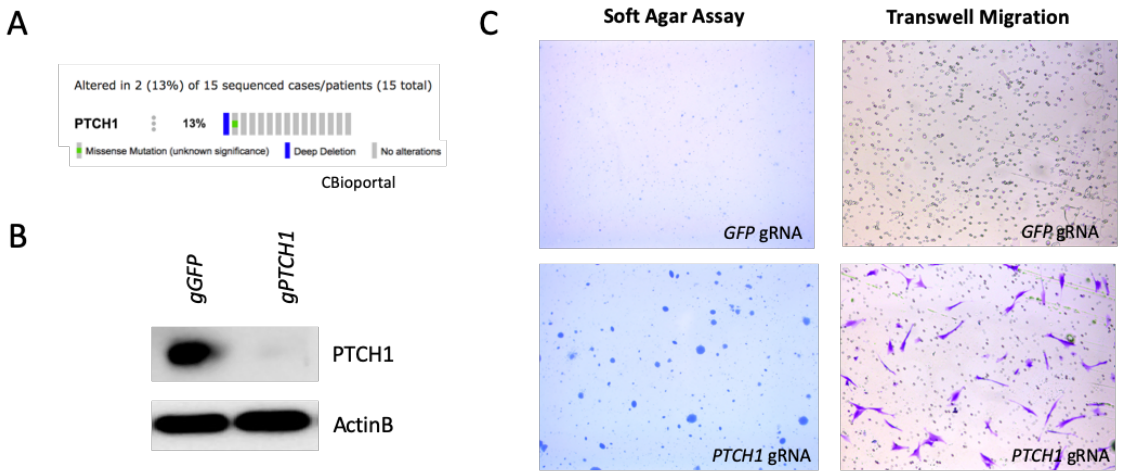

Figure 2.11: (A) TCGA data shows that *PTCH1* is deleted in 1 out of 15 human MPNSTs. (B) Western Blot showing knockout of *PTCH1*. (C) Loss of *PTCH1* results in anchorage-independent growth and increased migration in a transwell migration assay.

Figure 2.12: Knockout of *PTCH1* in Human Schwann Cells Results in Increased Sensitivity to Vismodegib, a Smoothened Inhibitor

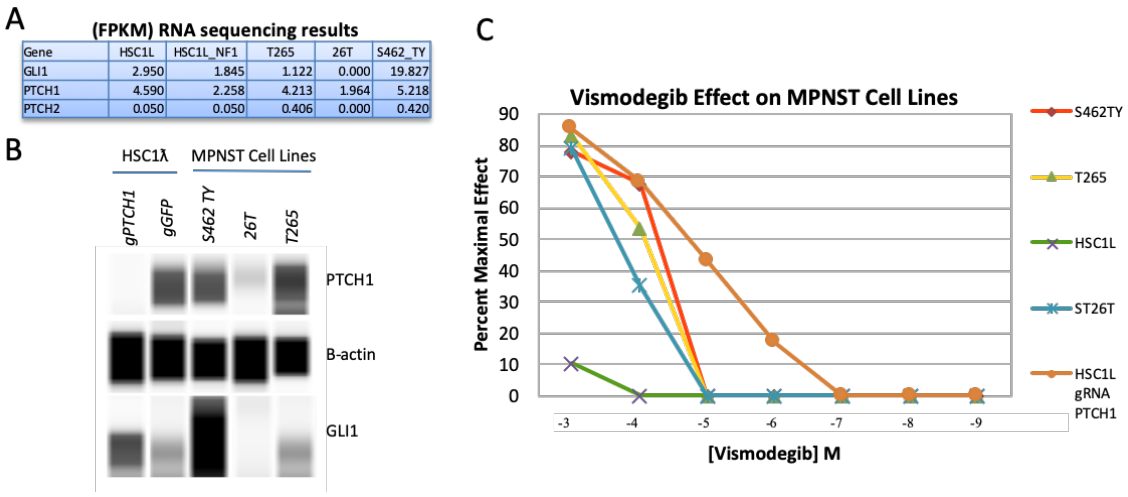

Figure 2.12: (A) Table showing raw FPKM values of gene expression in different human Schwann cell lines and MPNST cell lines. (B) Western blot using Wes technology (Protein Simple) indicating levels of PTCH1, ACTB, and GLI1 in human Schwann cell lines and MPNST cell lines. (C) *PTCH1* knockout cell lines are sensitive to smoothened inhibition via vismodegib treatment. Notice that MPNST cell lines are more sensitive than immortalized Schwann cell line HSC1λ.

Figure 2.13: Genetic Mechanism of Transcription-Induced Chimeras and Oncogenic Overexpression

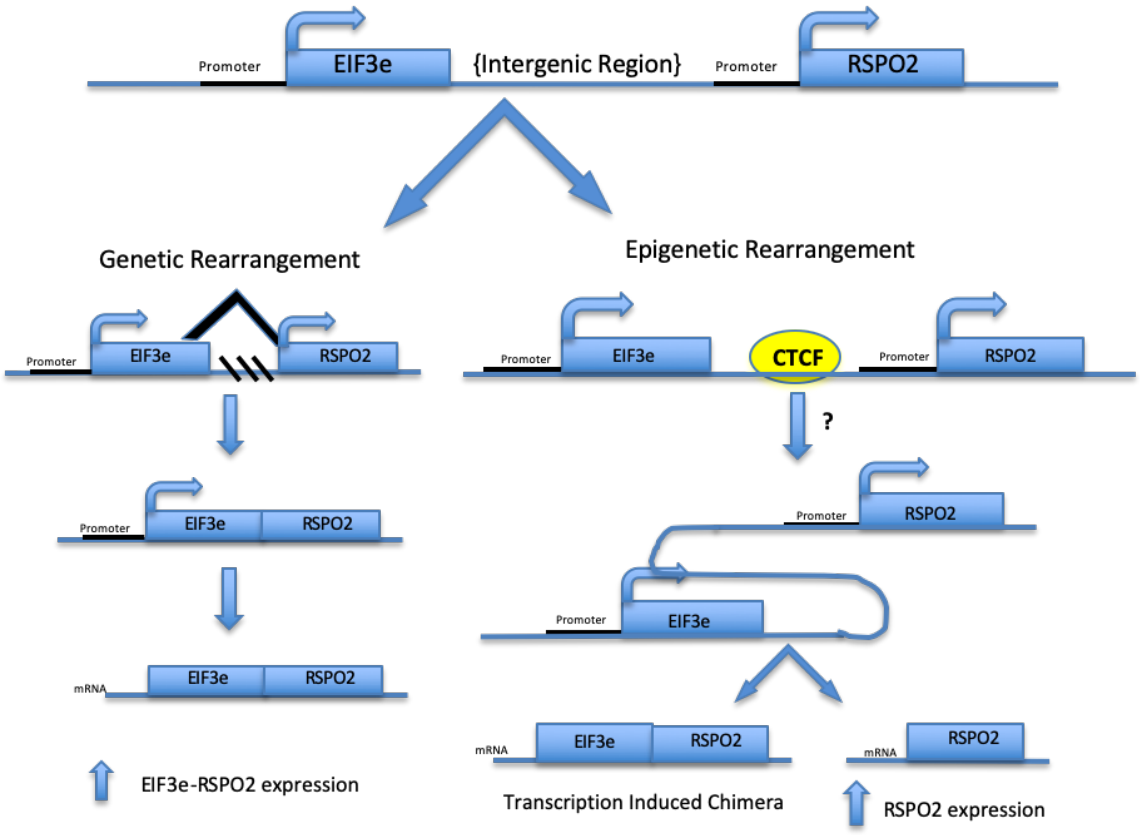

Figure 2.13: Model depicting our hypothesis of the different mechanisms in which *RSPO2* overexpression occurs in a subset of human MPNSTs. Both mechanisms are possible, depending on the cellular context, genome instability, and mutational landscape.

Figure 2.14: Border Element *CTCF* Keeps *RSPO2* Expression in Check

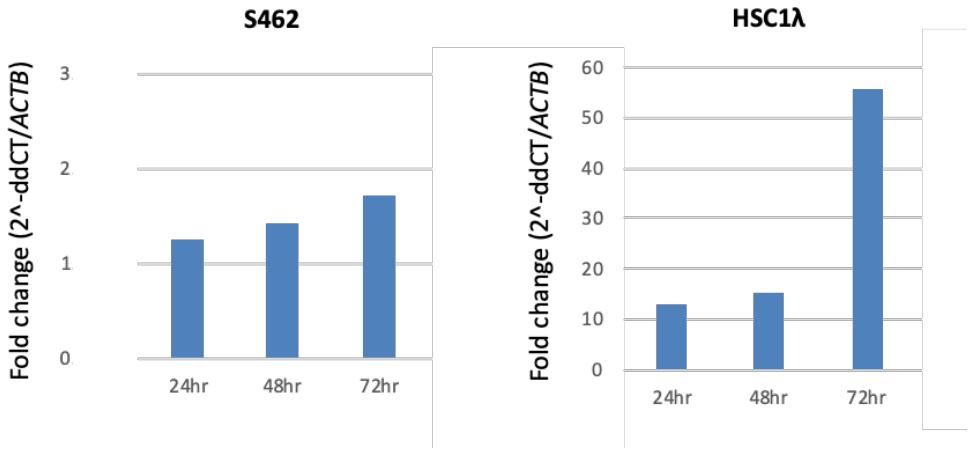

Figure 2.14: CTCF knockdown results in *RSPO2* overexpression as measured via RT-qPCR over 3 days in the human MPNST cell line S462 and the human immortalized Schwann cell line HSC1λ. Fold change values shown for RSPO2 mRNA abundance, using a scrambled siRNA as control.

Figure 2.15: *RSPO2* is Overexpressed in a Subset of Human MPNSTs and Loss of the Border Element *CTCF* Results in Schwann Cell Transformation

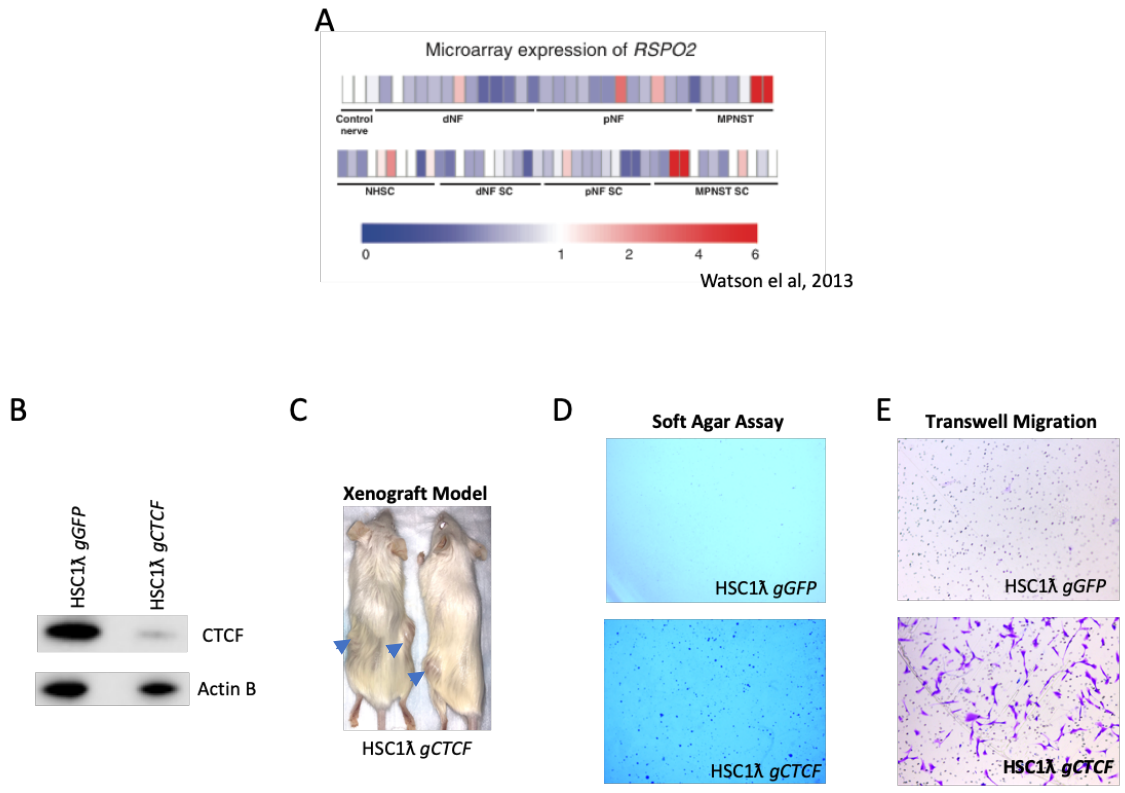

Figure 2.15: (A) MicroArray expression data showing *RSPO2* expression levels in different tissues. dNF: dermal neurofibroma; pNF: peripheral neurofibroma, MPNST: malignant peripheral nerve sheath tumor samples, NHSC: non-human Schwann cells, dNF SC: dermal neurofibroma cell line, pNF SC: peripheral neurofibroma cell line, MPNST SC: malignant peripheral nerve sheath tumor cell line. (B) Western blot showing *CTCF* knockout. (C) *CTCF* knockout HSC1λ cells for tumors in a xenograft model. (D), (E) Shows human Schwann cell transformation after *CTCF* knockout. (D) anchorage-independent assay in show agar showing increased colony formation upon *CTCF* knockout and € shows increased migration upon loss of *CTCF*.

Figure 2.16: Knockdown of *RSPO2* Has a Modest Effect on The Survival of MPNST Cell Lines

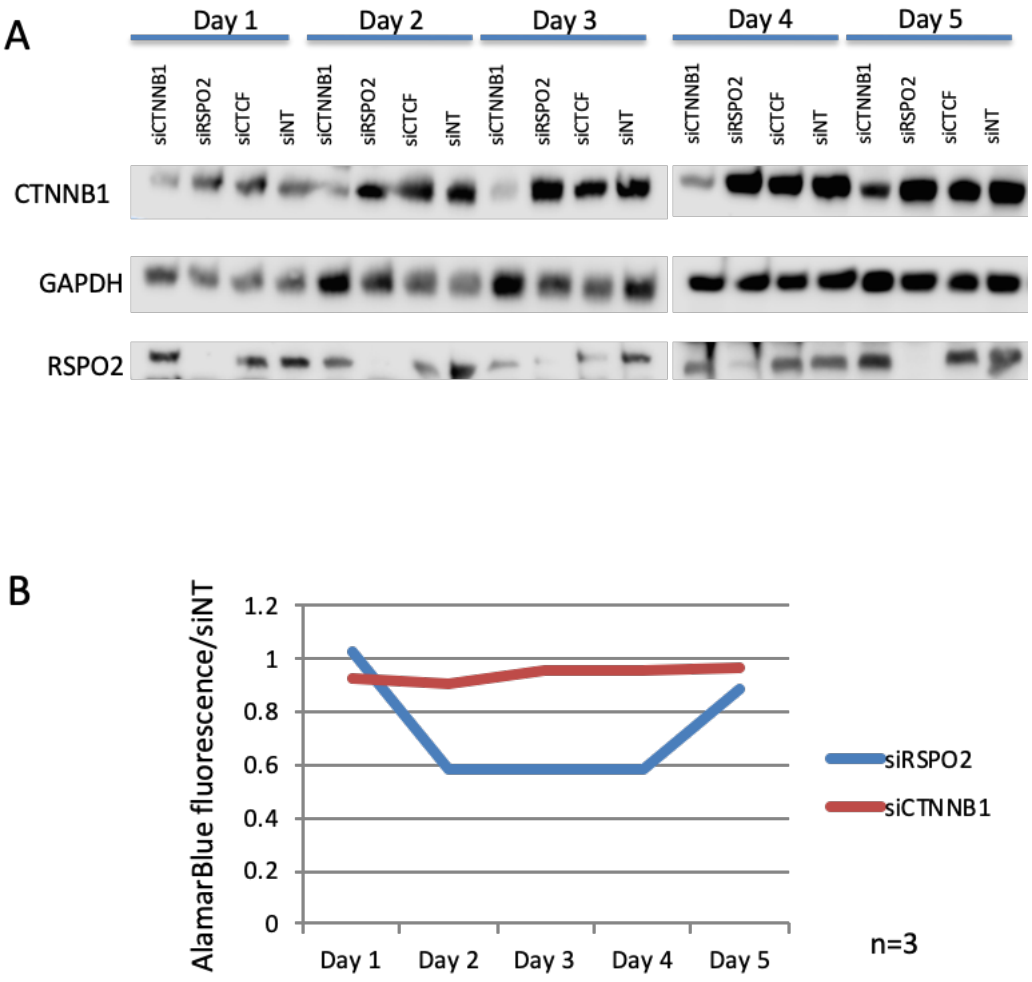

Figure 2.16: (A) Western blot showing knockdown of *RSPO2* and *CTNNB1* using siRNA. siNT is the scrambled control. siRNA efficiency is dramatically reduced across at day 5, except for *RSPO2*. (B) AlamarBlue assay assessing cell viability after knockdown. *RSPO2* knockdown is more effective than *CTNNB1* both at the protein level and at affecting cell viability.

Figure 2.17: Tankyrase Inhibition Reduces Cell Viability in The MPNST Cell Line S462

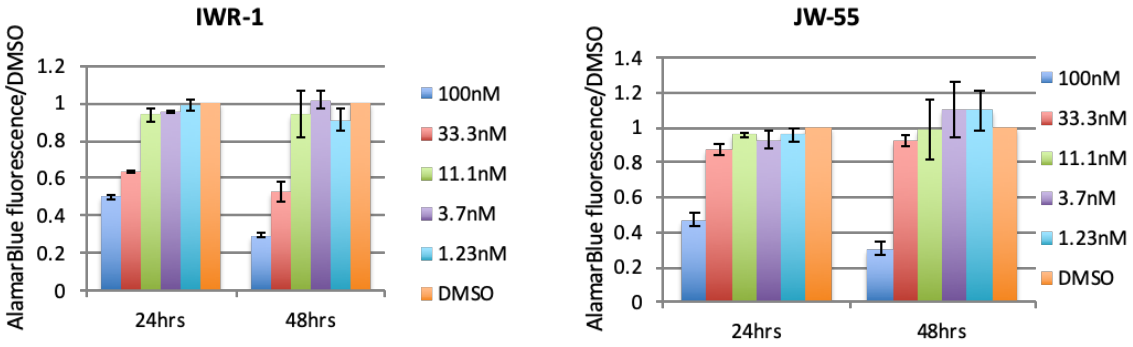

Figure 2.17: Bar graph showing the effects on cell viability of tankyrase inhibitors IWR-1 and JW-55 in S462 cells.

Figure 2.18: ENCODE Predicts 3 Binding Sites for CTCF In the Intergenic Region Between *EIF3E* and *RSPO2*

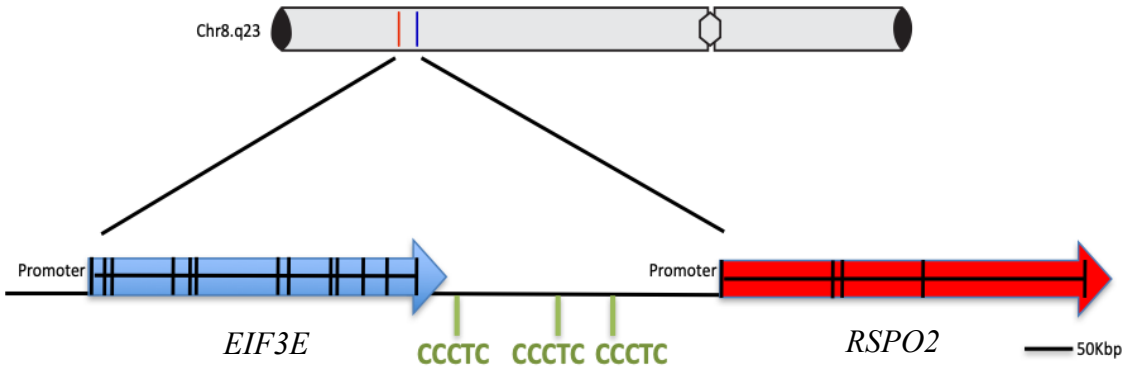

Figure 2.18: CCCTC is the binding motif of CTCF, a transcriptional repressor involved in insulation, transcriptional regulation, and chromatin architecture. We hypothesize that loss of *CTCF* and/or binding motif leads to *RSPO2* overexpression.

Figure 2.19: CTCF Binds To 7 Different Sites in The *EIF3E-RSPO2* Intergenic Region

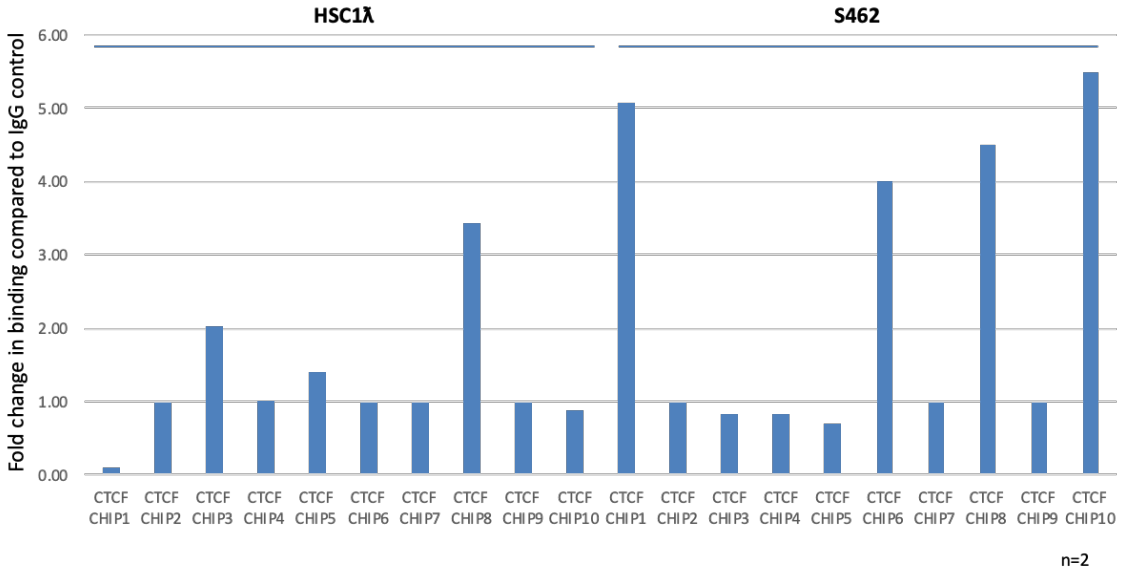

Figure 2.19: Chart depicting fold change in binding of CTCF when compared to IgG control. Ten primer sets were used to amplify 10 CTCF binding sites predicted between *EIF3E and RSPO2*. Each site represents a CCCTC sequence. Fold changed was determined using qPCR in genomic DNA isolated from chromatin immunoprecipitation assay via pulldown of CTCF-bound DNA.

Figure 2.20: 3C DNA Can Be Isolated, PCR Amplified, And Identifies Aberrant Promoter Interactions

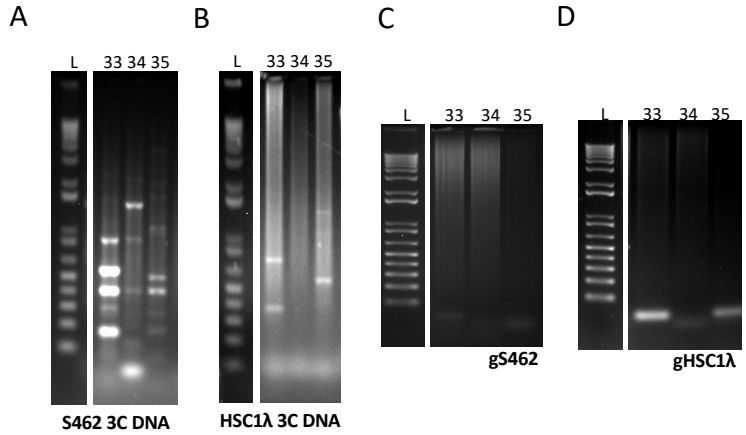

Figure 2.20: 2% agarose gels showing amplified 3C DNA. L: MWM, 33, 34, 35: Primer set used in the reaction (Table 5). (A) Gel showing amplification of S462-derived 3C DNA (B) Gel showing amplification of HSC1λ -derived 3C DNA (C), (D): Gels showing amplification of gDNA used as a negative control.

Figure 2.21: Boundaries: Keeping the Oncogenome in Check

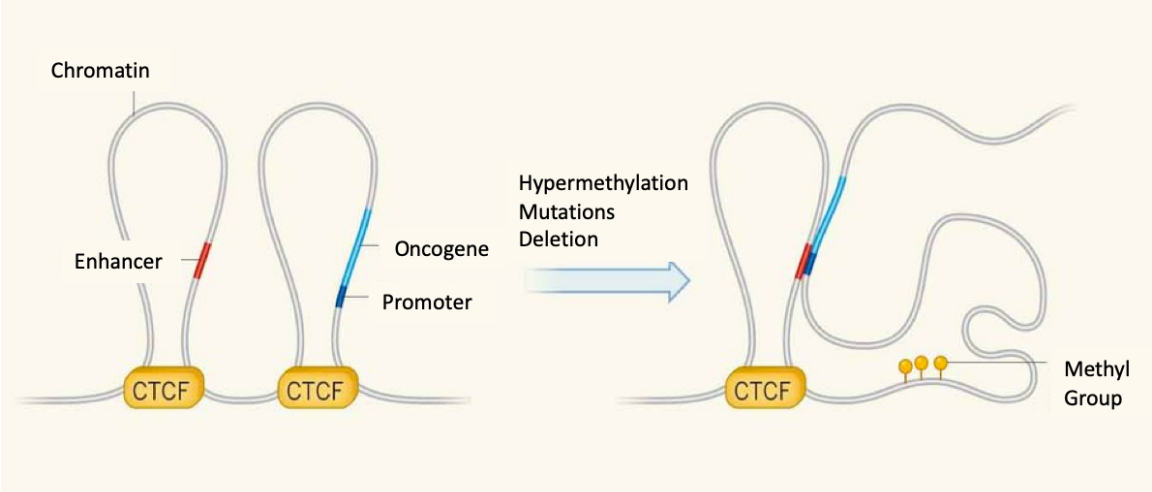

Adapted from Grimmer and Costello, *Nature 2016*

Figure 2.21: Figure depicting model we hypothesize is the mechanism of aberrant *RSPO2* overexpression in MPNSTs.

Figure 2.22: Hiippo/YAP Pathway is Activated Via Different Mechanisms in MPNSTs

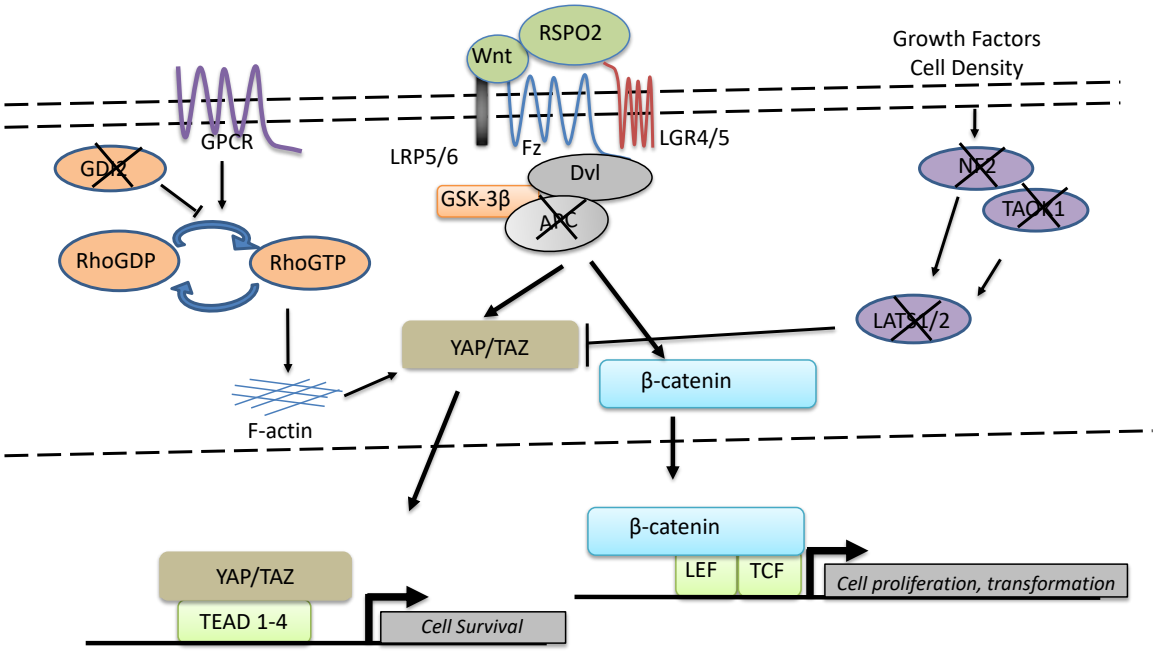

Figure 2.22: Diagram summarizing results showing overall Hippo/YAP activation via the loss of multiple tumor suppressor genes that occur in MPNSTs.

Chapter 3: RSPO2 Activates the Hippo/Yap Pathway in the Mouse Liver and is Required for Liver Tumor Formation

Overview

Each year, more than 30,000 people succumb to liver cancer in the United States. Hepatocellular carcinoma represents the second cause of cancer-related death globally. R-spondins are secreted regulators of Wnt signaling that function in development and promote tissue stem cell renewal. R-spondin 2 (RSPO2) has been reported to be activated by chromosomal rearrangements in colorectal cancer (CRC) and over-expressed in a subset of hepatocellular carcinomas. Previous work in our laboratory by Caitlin Conboy and colleagues revealed that a subset of liver cancers was characterized by high levels of *RSPO2* (Figure 3.1). Using the Fah mouse model, we were able to determine that *RPSO2* is a liver oncogene and that it activates the Wnt pathway. Moreover, the Hippo/YAP pathway has been implicated in many human cancers, influencing cell survival. We asked what other pathways are activated by RSPO2 in the liver. Histological and gene expression studies showed activation of Wnt/β-catenin and Hippo/YAP pathways upon *RSPO2* overexpression. Using the Fah mouse model, we demonstrate that knockdown of *Yap1* results in reduced tumor penetrance upon *RSPO2* overexpression in the context of loss of *Trp53*, suggesting that *RSPO2* overexpression leads to tumor formation in the mouse liver in a Hippo/Yap dependent manner. Overall, our results suggest a role for YAP in the initiation and progression of liver tumors and uncovers a novel pathway activated in RSPO2-induced malignancies. In this chapter we show that RSPO2's oncogenic activity requires Hippo/Yap activation in hepatocytes. These results suggest that both RSPO2 and YAP1 are novel druggable targets in Wnt-driven tumors of the liver.

Methods

Tissue culture reagents and cell lines:

HH7 cell line was kindly donated[72]. HH7 cells were cultured in DMEM supplemented with 10% FBS, 5% non-essential amino acids, glutamine, and 1% penicillin/streptomycin. All cells were grown on tissue culture-treated plates at 37°C and 5% CO_2.

In vitro gene knockdown and overexpression and proliferation assays:

For overexpression experiments, lentiviral particles used to transduce target cells were produced in 293T cells by co-transfection with capsid and help constructs. Lentiviral particles were collected from the supernatant of 293T cells and later added to target cells in media supplemented with 6ug/ml of polybrene. Lentiviral expression vectors were cloned with RSPO2 or dsRed regulated by a CAGGS promoter and followed by an IRES-RFP to monitor transduction efficiency. Infected cells were selected via Fluorescent Assisted Cell Sorting (FACS). Overexpression levels were monitored via western blotting.

Mouse strains, hydrodynamic injection, and liver analysis:

All animal work was conducted according to an institutionally approved animal welfare protocol (IACUC protocol #1509-33035A). Mouse strains and hydrodynamic injection protocols were performed as described (Bell et al., 2007; Keng et al., 2011). The Fah mice used in this study received 20 ug plasmid DNA per plasmid by hydrodynamic tail

vein injection. Plasmid DNA encoded transposon-based sequences expressing *Fah*, *GFP*, luciferase, and either *RSPO2*, *GFP* control, *Trp53* shRNA, *Yap1* shRNA or no plasmid control. Mice were maintained on 2-(2-nitro-4-trifluoromethylbenzoyl)-1,3-cyclohexanedione (NTBC) drinking water until after injections. NTBC is a hepatoprotective drug used to compensate for the lack of the Fah gene. At day 150, mice were euthanized in CO2 and lungs, hearts, spleens, pancreases, livers, and all tumor tissue was removed and either fixed in 10% formaldehyde or frozen in RNA later. and visually inspected for macroscopic tumors. Macroscopic hyperplastic nodules were counted. Fixed tissue was paraffin-embedded, mounted, and sectioned at 5μm. Slides were then processed and stained with hematoxylin and eosin (H&E). YAP staining was performed in the same way (HH and GK), using YAP (D8H1X) Rabbit mAB #1074 (Cell Signaling) at 1:400.

Quantitative reverse transcriptase PCR (qRT-PCR):

RNA was isolated from cell lines and mouse liver tissues using the PureLink RNA Mini Kit (Ambion). RNA samples were treatted with DNase to remove remaining genomic DNA (Turbo DNA-free Kit, Ambion). Complementary DNA was synthesized from 1 ug template RNA per sample using the SuperScript III First-Strand Synthesis System (Invitrogen). qRT-PCR reactions were conducted with FastStart Universal SYBR Green Master mix (Roche), using 0.5 ul of cDNA template in a 25 ul reaction. Primer sequences for qRT-PCR reactions are listed in Table 2. Data were normalized to ACTB using the following equation: relative quantification (RQ) = ((2^(CT_ACTB))/((2^(CT_GOI)).

Oncogenic potential in vitro studies of RSPO2 in HH7 cells:

Soft-agar assays were performed using 0.48% low melting point agarose in sterile water. 7,500 cells were plated per well in a 6-well plate. Pictures were taken in dissecting microscope at 1.5X and analyzed using ImageJ. Xenograft models were performed in NRG mice and 3 million cells were injected subcutaneously in media containing matrigel (1:1). Tumors were harvested 4 months post-injection. Cells were lysed with a hypotonic solution and nuclear fractions were isolated using NP-40 followed by centrifugation. Pellets were resuspended in RIPA buffer, supplemented with protease and phosphatase inhibitors.

CRISPR/Cas9 Knockout of Yap1:

CRISPR/Cas9 HH7-*RSPO2 YAP1* modified cell lines were generated using lentiviral vectors expressing Cas9 and a guide RNA directed against *YAP1*. Lentiviral vectors were generated by transfecting 293T cells with two viral packaging plasmids and CC9 v2 Cas9/guide RNA-containing plasmid from Zhang lab at MIT (crispr.mit.edu). Guide RNA sequences were cloned into a stuffer region of the plasmid using Bsmb1 restriction sites. Guide RNA sequences were 5'-GGCGTAGCCCTCGCTCGC-3'and 5'-CGGCGCTGTCCTCGCTCT-3' and targeted the translational start site.

Results

The Hippo/Yap pathway is activated upon RSPO2 signaling in the mouse liver:

Recent studies have shown the Hippo pathway to interact with Wnt signaling via YAP binding to the β-catenin destruction complex and it is required for CRC cell survival[73, 74]. Based on the pronounced phenotype of hepatomegaly in liver overexpressing *RSPO2*, we tested the effect of *RSPO2* overexpression on YAP nuclear localization, as a measurement of Hippo activation. We stained liver tissue and scored each section for Yap nuclear and cytoplasmic localization. We assessed Yap staining qualitatively and scored each field of view using 0 (no staining), 1 (low), 2 (medium) and 3 (high) (Figure 5A). We found that upon *RSPO2* overexpression Yap nuclear localization and overall levels were increased (Figure 3.2). Further, RNA was isolated from normal and tumor liver tissue from the Fah/RSPO2/shp53 mice described above and quantified via qRT-PCR. We saw a significant overexpression of the Yap target gene *Birc5* in RSPO2 tumor tissue (Figure 3.3A). On the other hand, we found *RSPO2* overexpression in the mouse liver results in overexpression of the Yap target gene *Bcl2l1* in *RSPO2*-high and tumor tissue (Figure 3.3B). We also tested the expression levels of Ctgf, Wisp, and Wrch1, genes that are activated upon non-canonical Wnt activation (Figure 3.3). We found that non-canonical Wnt was active in RSPO2-induced tumors. Interesting, the Wnt activation marker, *Axin2* was not high in RSPO2-drive tumors. Likely, due to tumor cell exhaustion or activation of Hippo and non-canonical Wnt taking over canonical Wnt pathway.

RSPO2 overexpression in immortalized human hepatocytes results in anchorage-independent growth and xenograft tumor formation:

Next, we overexpressed *RSPO2* in HH7, an immortalized human hepatocyte cell line. We first tested the oncogenic effects of *RSPO2* in HH7 cells by measuring anchorage-independent growth in soft agar, migration in a transwell assay, and tumor formation in a xenograft model. We found that *RSPO2* overexpression led to cellular transformation including both anchorage-independent growth and tumor formation in contrast to an *RFP* control (Figure 3.4). These effects were abrogated by a gRNA targeting *YAP1*. However, *RSPO2* overexpression did not have a significant effect in the migration of hepatocytes in a transwell assay. We then evaluated the effects of *RSPO2* overexpression in YAP nuclear localization in human hepatocytes. We observed in a western blot that levels of total and nuclear YAP protein were increased, accompanied by levels of β-catenin in *RSPO2*-high HH7 cells and post-translational stabilization of both YAP and β-catenin in both cytoplasmic and whole cell fractions (Figure 3.5).

Knockdown of *Yap1* inhibits *RSPO2*-induced tumor formation in mouse liver:

In order to determine if *RSPO2*-driven liver tumors depend on YAP for development and maintenance, we hydrodynamically injected an expression vector encoding a shRNA versus Yap1 in the presence or absence of RSPO2 and/or shTrp53 (Figure 3.6A). Control mice were injected with a transposon vector expressing *Fah*, with *GFP* and luciferase to track liver repopulation. Experimental mice were injected with a transposon vector expressing *Fah*, *GFP*, luciferase, and *RSPO2*, and additional *GFP* and *RSPO2* cohorts were injected with a second transposon vector expressing *Trp53* shRNA, all containing a

second and/or third vector expressing an shRNA against *Yap1*. Necropsies were performed to assess tumor formation 150 days PHI. *Yap1* knockdown was confirmed via IHC (Figures 3.6B, C), with both cytoplasmic and nuclear stains showing reduced staining for Yap when the shRNA vectors were co-injected. Knockdown of *Yap1* resulted in a dramatic decrease in tumor penetrance, suggesting a direct role of *Yap1* in RSPO2-mediated tumorigenesis. Only 1 of 9 (11%) experimental animals hydrodynamically injected with *RPSO2*, sh*Trp53*, and sh*Yap1* expression vectors formed tumors, while RSPO2/shp53-injected mice again had 68% tumor penetrance (Figures 3.6D, E).

Discussion

Several groups have reported that Wnt and Hippo signaling pathways interact[73, 74]. We found that *RSPO2* overexpression led to accumulation of cytoplasmic and nuclear YAP in the mouse liver. Yap target genes involved in the regulations of apoptosis, *Bcl2l1* and *Birc5*, were upregulated in some *RSPO2*-driven liver tumors. Hippo/YAP activation mechanisms are varied. As demonstrated by Azollin and colleagues, we hypothesized that Hippo signaling occurs via a Wnt activation mechanism. Also, that Hippo signaling is enhanced by further inactivation of APC, stabilizing YAP post-translationally. We also demonstrated YAP activation downstream of RSPO2 in immortalized human hepatocytes and found that ectopic *RSPO2* expression led to anchorage-independent growth and tumor formation in NRG mice. These transformation events were abrogated after the loss of *YAP1*.

Moreover, we have shown that knockdown of *Yap1* in the mouse liver results in direct abrogation of RSPO2-driven tumor development and maintenance. This is a novel finding that opens new routes for the development of therapies against RSPO2-driven cancer. The Hippo/Yap pathway is activated upon lower density/size in the liver and its inhibition has been shown to restore hepatocyte differentiations in HCC[75]. Activation of the pathway gives rise to cell proliferation and survival. Although YAP1 is necessary for liver regeneration and regulation of organ size, we demonstrate that YAP1 is stabilized at the post-transcriptional level upon *RSPO2* overexpression. Targeting of YAP would be a reasonable approach versus RSPO2-driven HCC, to promote apoptosis of tumor cells. Verteporfin and statins are being tested as inhibitors of the Hippo pathway, where

Verteporfin inhibits the Yap-TEAD interaction, whilst statins through inhibition of RhoA signaling[76, 77]. Inhibiting YAP may selectively target HCC tumor cells that depend on it for survival. Porcupine and tankyrase inhibitors are candidate drugs to target RSPO-high tumors that have yet to be tried in clinic to treat this subset of tumors.

Future studies are required to determine whether *RSPO2* expression and downstream activation of canonical Wnt and Hippo pathways is required for tumor maintenance in RSPO2-high cancers. Although unclear, is the role of non-canonical Wnt signaling in RSPO2-high cancers. In summary, we show that *RSPO2* overexpression activates both canonical Wnt and Hippo signaling and promotes tumor formation in the liver. This raises the enticing possibility that both R-spondins and/or YAP could be used as biomarkers and/or therapeutic targets. Indeed, initial studies attempting therapeutic targeting of R-spondins are showing promise[78]. We have developed useful *in vitro* and *in vivo* model systems for the testing of targeting R-spondins or combination therapies with Wnt and/or Hippo/YAP inhibitors.

Figure 3.1: *RSPO2* overexpression in the mouse liver results in formation of hepatic tumors in the presence of an shRNA against *Trp53*

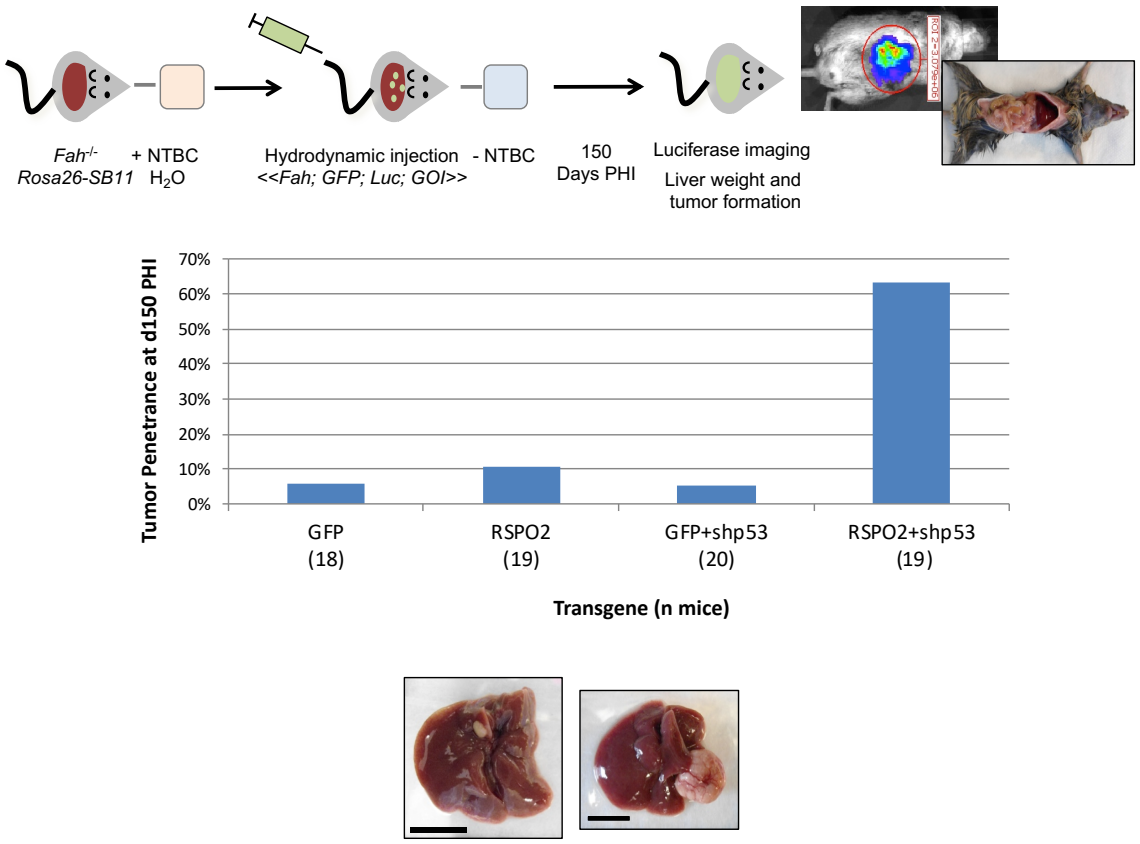

Figure 3.1: Top: Fah experimental mouse model that shows that *RSPO2* overexpression leads to hyperplastic growth of the mouse liver. NTBC is a hepatoprotective drug in the Fah$^{-/-}$ background. Middle: *RSPO2* overexpression in the mouse liver leads to a dramatic increase in tumor penetrance in the absence of *Trp53*. Bottom: Gross pathology of liver specimen 150-day PHI, showing normal and tumor tissue.

Results in Figure 3.1 are part of the work performed as part of Caitlin Conboy's thesis work and to be published in a manuscript co-author with me.

Figure 3.2: *RSPO2* activates the Hippo/Yap pathway in the mouse liver

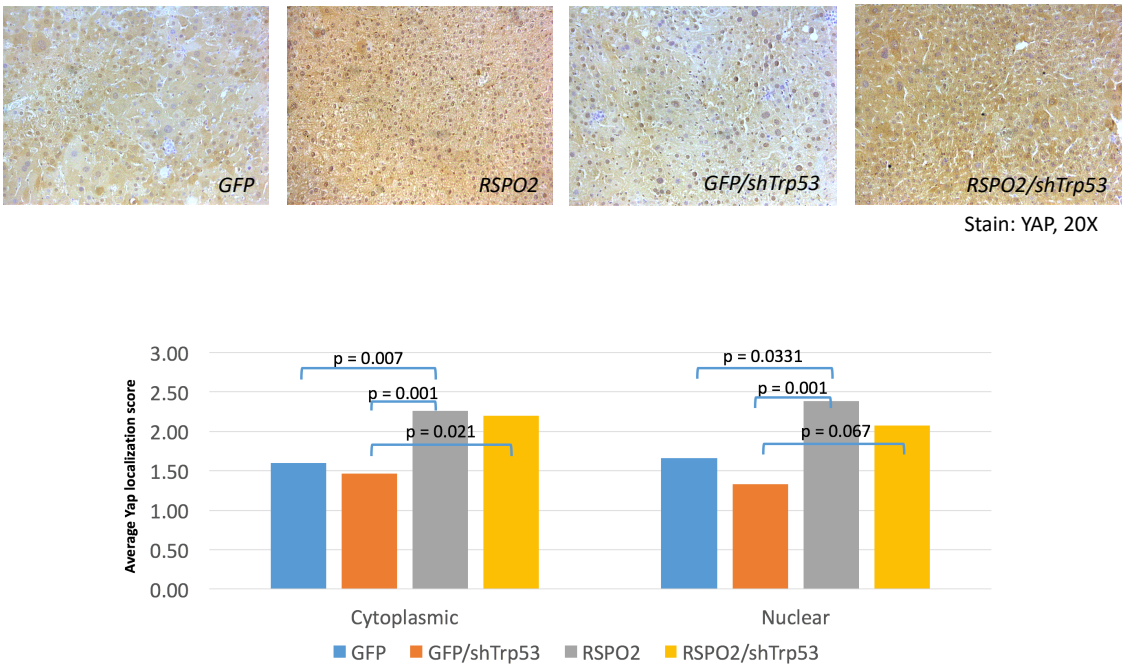

Figure 3.2: Top: IHC Yap staining of mouse liver tissue. Bottom: Y-axis shows intensity of stain (0: no stain; 1: low; 2: medium; 3: high) in either the cytoplasm (left) or nucleus (right). Samples in the *RSPO2*-overexpressing cohorts showed increased staining, and therefore increased Yap localization, in both the cytoplasm and the nucleus. P-values shown between cohorts; all except between nuclear *GFP/shTrp53* and *RSPO2/shTrp53* were found to be significant.

Figure 3.3: *RSPO2* modulates the expression of Hippo/Yap target genes in mouse liver

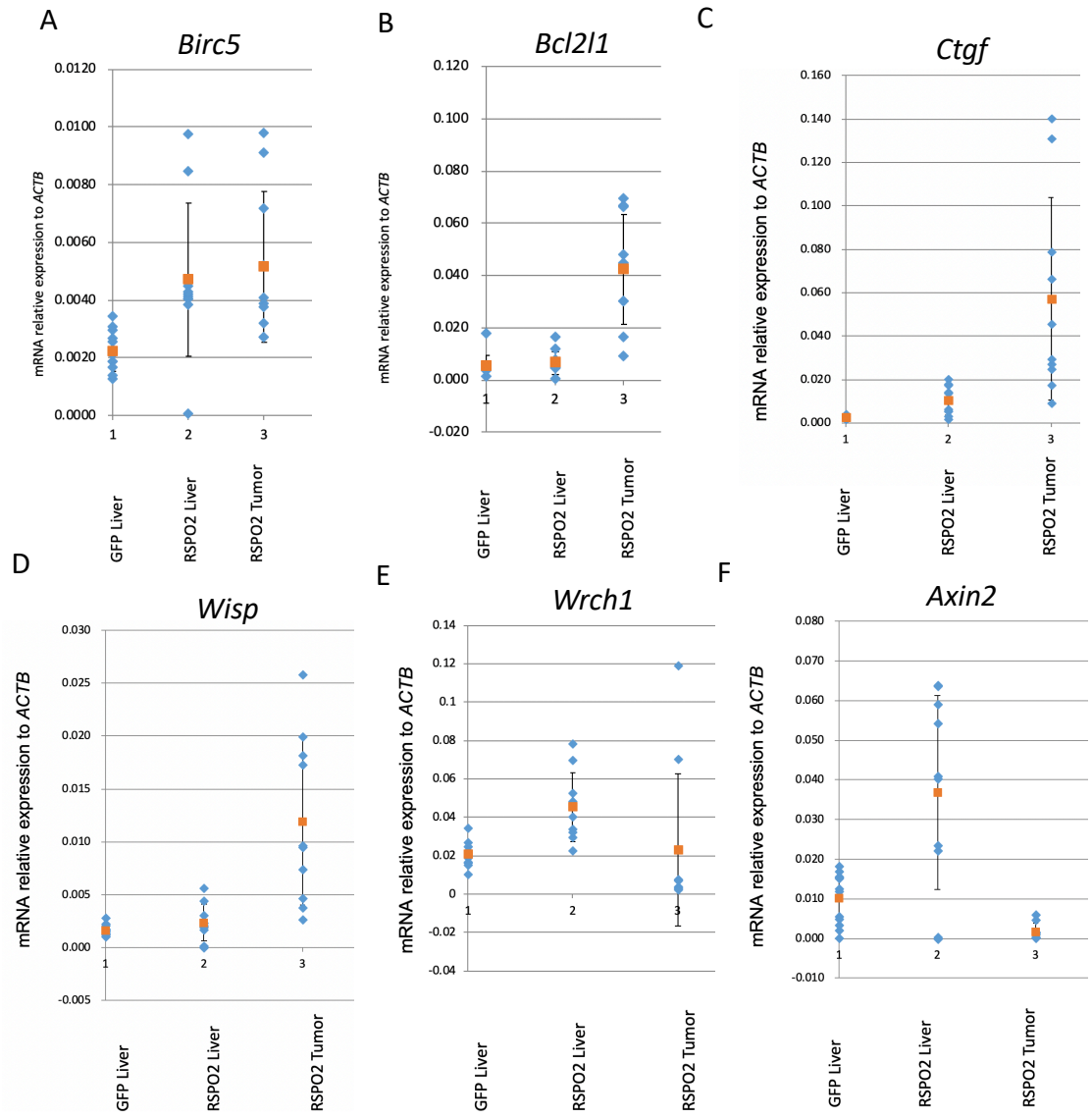

Figure 3.3: (A) *Birc5* expression levels. (B) *Bcl2l1* expression levels. (C) *Ctgf* expression levels. (D) *Wisp* expression levels. (E) *Wrch1* expression levels. (F) *Axin2* expression levels. *Birc5* and *Bcl2l1* are anti-apoptotic, characteristic Hippo pathway responsive genes. *Wisp* and *Wrch1* are non-canonical Wnt responsive genes. *Axin2* is a Wnt responsive gene. Relative quantification via RT-qPCR was normalized to *Gapdh* expression. Each dot represents an independent sample analyzed.

Figure 3.4: *RSPO2* overexpression results in immortalized hepatocyte cell transformation in a YAP dependent manner

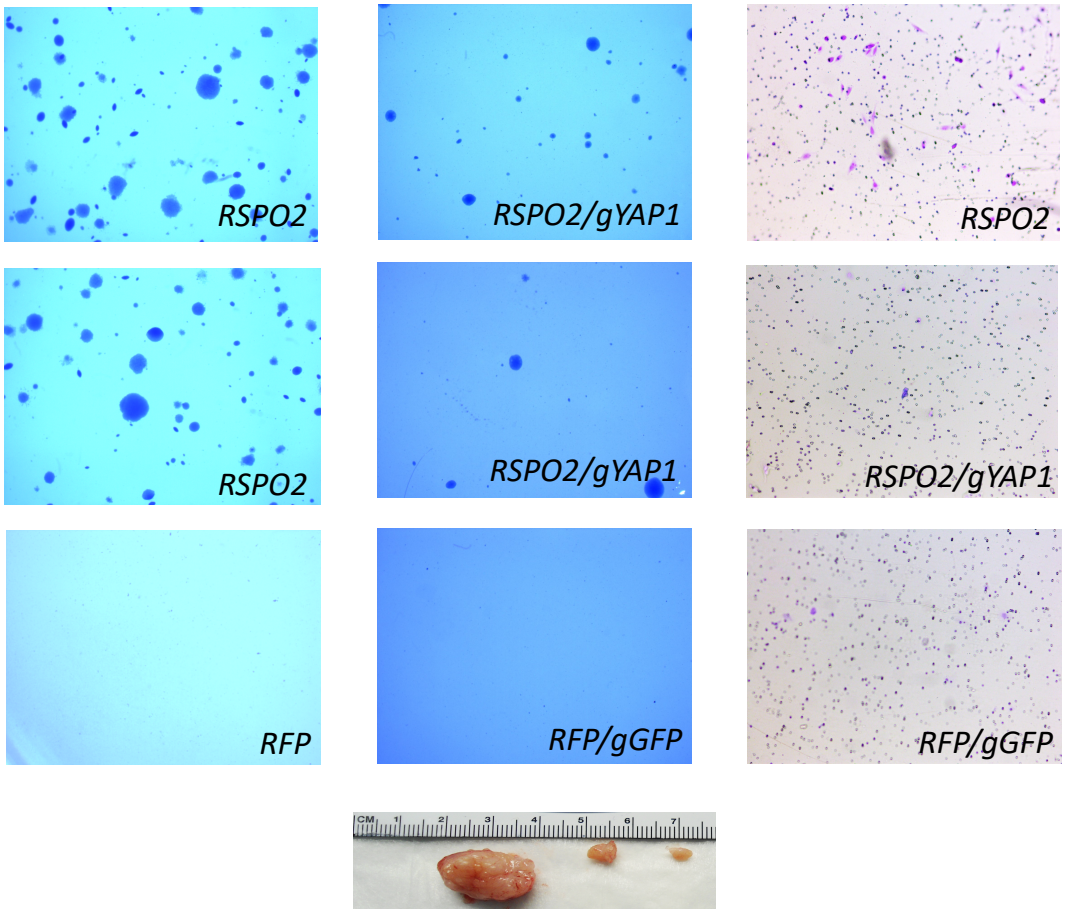

Figure 3.4: Left: soft agar assays showing anchorage-independent growth in RSPO2 and RSPO2-flag-overexpressing HH7 cells. Center: CRISPR/Cas9 KO of *YAP1* results in reduced colony formation in soft agar (duplicate of two independent experiments). R1 and gRNA HH7 cells show no anchorage-independent growth. Left: Transwell migration assays show increased migration upon *RSPO2* overexpression. HH7 phenotype is rescued upon *YAP1* KO. Bottom Center: Representation of HH7_RSPO2 tumors in NRG mice.

Figure 3.5: *RSPO2* overexpression in immortalized human hepatocytes results in YAP activation

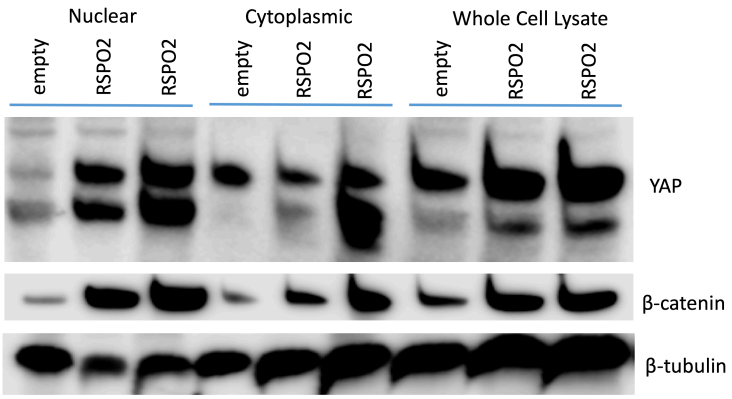

Figure 3.5: Western blot showing overexpression of *RSPO2* results in increased levels of YAP in the nucleus of HH7 cells, immortalize human hepatocytes. Two independently-generated cell lines with *RSPO2* overexpression were blotted here for comparison.

Figure 3.6: *Yap1* knockdown results in decreased tumor penetrance in the presence of *RSPO2* overexpression

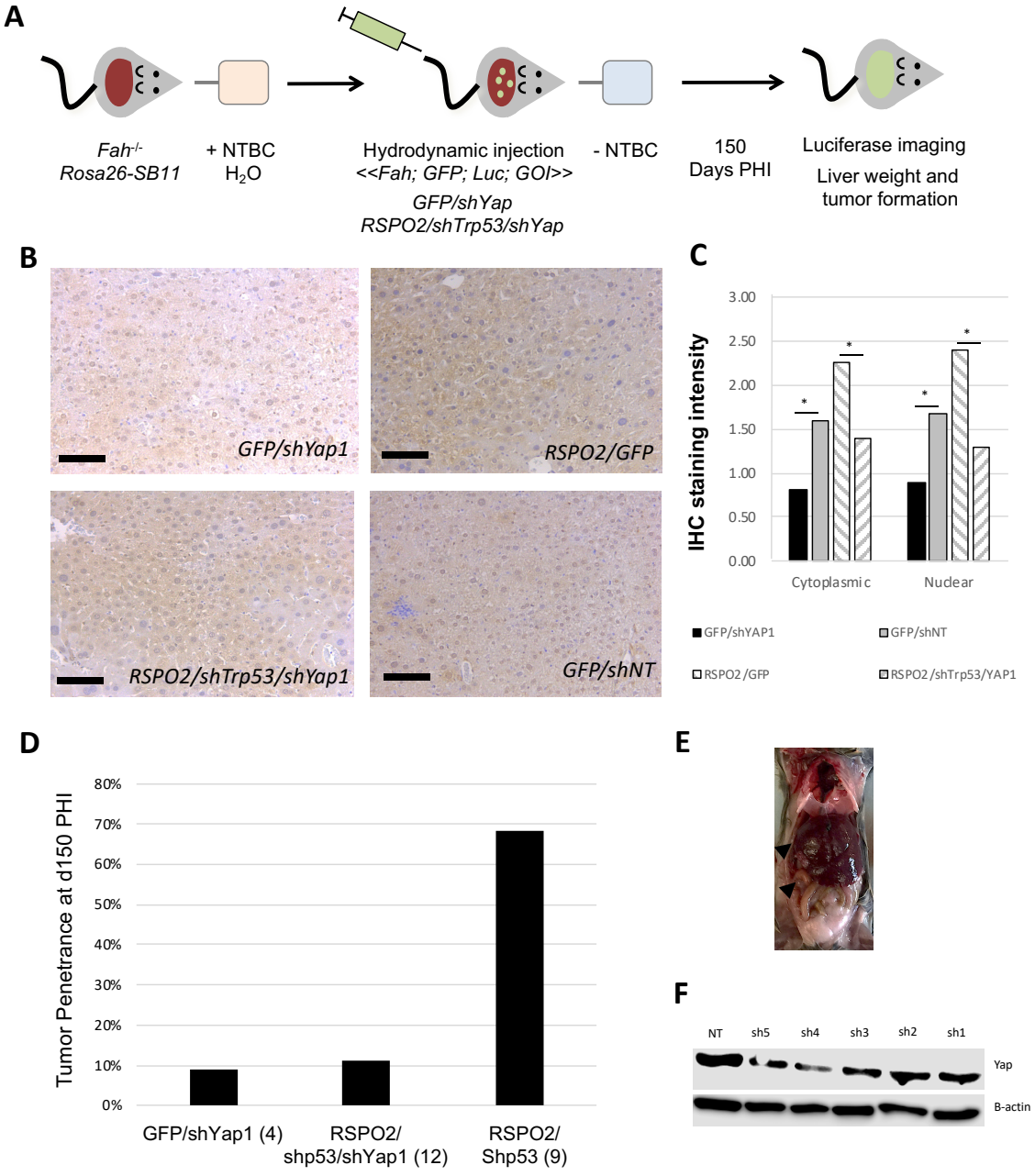

Figure 3.6: (A) Experimental diagram. (B) IHC showing in vivo knockdown of *Yap1*in the mouse liver. Scale bars represent 100µm. (C) Quantification of (B). (D) Tumor penetrance in Fah-null mice injected with *GFP/shYap1* (10 animals),

RSPO2/shp53/shYap1 (9), or *RSPO2/shp53* (19) at 150 days PHI ($p<0.05$). (E) Figure depicting 2 nodules found in the RSPO2/shp53/shYap1 only animal to show tumor penetrance. (F) Western blot showing shRNA efficiency against *Yap1* in mice hepatocytes. shRNA #4 was selected since it was found to be the best knockdown. Note that YAP is necessary for liver regeneration, reason why we did not want an shRNA that completely knocked down *Yap1*. The Fah mouse model depends on liver cell regeneration (see methods for further details).

Figure 3.7: The Hippo/YAP pathway is activated by RSPO2

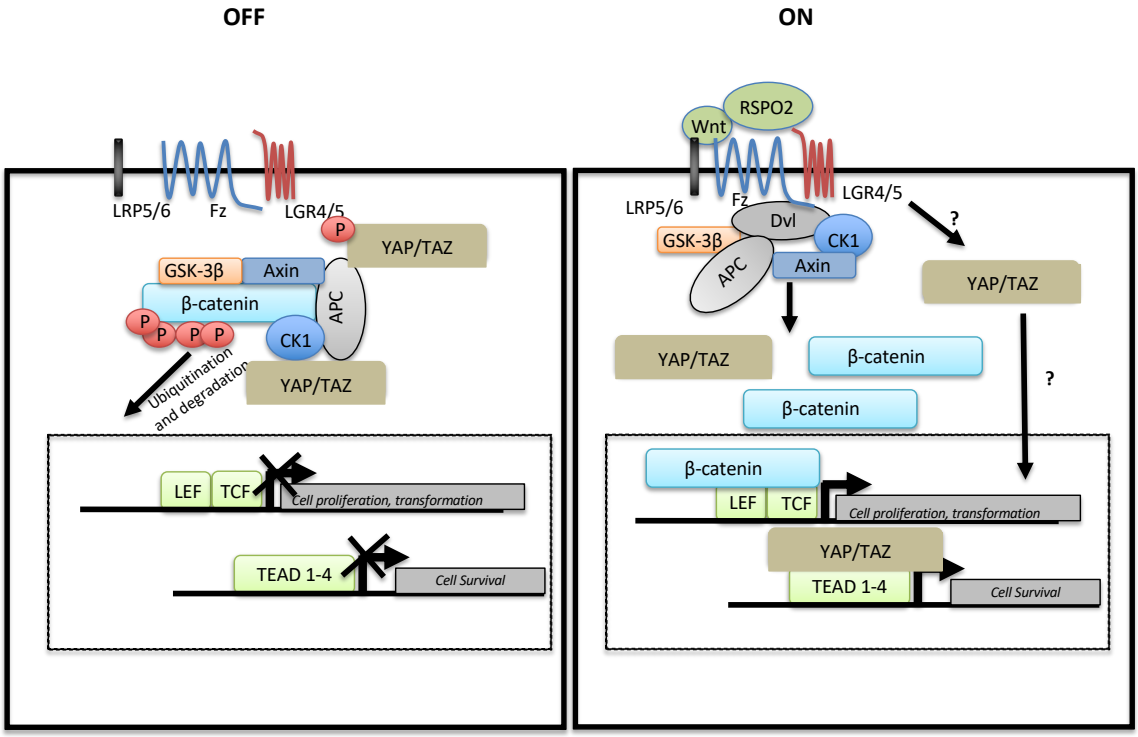

Figure 3.7: A schematic diagram depicting the mechanism of Yap activation upon autocrine/paracrine Wnt and RSPO2 signaling. Binding of RSPO2 in the present of Wnt leads to the expression of genes necessary for cell proliferation, survival, and invasion. YAP nuclear localization is negatively regulated by the β-catenin destruction complex upon phosphorylation.

Table 1: List of guideRNA Sequences

Name/Gene	Primers	Name/Gene	Primers	Name/Gene	Primers	Name/Gene	Primers
GFP	CACCGAGCTGGACGGCGACGTAAAG	hsDMD gRNA #1 FW	CACCGATTCTATTACTGCCGACTGC	hsNESD2 gRNA #1 FW	CACCGATGGGGGATTTCTACGACC	hsSPPL3 gRNA #1FW	CACCGGGCGGGCGAACGGCAAGAC
hsAPC gRNA #1FW	CACCGAACAGCATCGAGCCAACCT	hsDMD gRNA #1 RV	AAACGCAGTCGGCAGTAATAGAATC	hsNESD2 gRNA #1 RV	AAACGGTCGTAGAAATCCCCCATC	hsSPPL3 gRNA #1RV	AAACGTCTTGCCGTTCGCCCTGCCC
hsAPC gRNA #1RV	AAACAGGTTGGCTCGATGCTGTTC	hsDMD gRNA #2 FW	CACCGTTCTATTACTGCCGACTGCT	hsNESD2 gRNA #2 FW	CACCGTAGAAATCCCCCATCTTCGG	hsSPPL3 gRNA #3FW	CACCGCGCCGCCGCCATGTTGGGTT
hsAPC gRNA #2 FW	CACCGCCGAGCAGCGGCTAGGCTTC	hsDMD gRNA #2 RV	AAACAGCAGTCGGCAGTAATAGAAC	hsNESD2 gRNA #2 RV	AAACCGAAGATGGGGGATTTCTAC	hsSPPL3 gRNA #3RV	AAACAACCCAACATGGCGGCGGCGC
hsAPC gRNA #2 RV	AAACGAAGCCTAGCCGCTGCTCGG	hsDMD gRNA #3 FW	CACCGACTCCATCATGCCAATAAGT	hsNFAT5 gRNA #1FW	CACCGATGTCCCACTCCGAATAACC	hsSRGAP2 gRNA #1FW	CACCGAAGGTCACACGGCTAGATGG
hsAPC gRNA #3 FW	CACCGAAGCCTAGCCGCTGCTCGG	hsDMD gRNA #3 RV	AAACTTATTGGCATGATGGAGTC	hsNFAT5 gRNA #1RV	AAACGGTTATTCGGAGTGGGACATC	hsSRGAP2 gRNA #1RV	AAACCCATCTAGCCGTGTGACCTTC
hsAPC gRNA #3 RV	AAACCCGAGCAGCGGCTAGGCTTC	hsDVL1 gRNA #1FW	CACCGTCGGCCAGCGTGACGCGCTC	hsNFAT5 gRNA #2FW	CACCGTGTTTGGAAGAGTAGCGTTG	hsSRGAP2 gRNA #2FW	CACCGACCATCTAGCCGTGTGACCT
hsAPC gRNA #5 FW	CACCGCCGGAAGCCTAGCCGCTGCT	hsDVL1 gRNA #1RV	AAACGAGCGCGTCACGCTGGCCGAC	hsNFAT5 gRNA #2RV	AAACCAACGCTACTCTTCCAAACAC	hsSRGAP2 gRNA #2RV	AAACAGGTCACACGGCTAGATGGTC
hsAPC gRNA #5 RV	AAACAGCAGCGGCTAGGCTTCCGGC	hsDVL1 gRNA #2FW	CACCGATTTGTAGGCGTGCACGGGC	hsNFATC1 gRNA #1FW	CACCGTTCATGGTGCCGCCGGCGCG	hsSTAG2 gRNA #1FW	CACCGAGAAGAACCGCGGCTCGATC
hsATL2 gRNA #1FW	CACCGTGGTTAACCGCGGCGCTT	hsDVL1 gRNA #2RV	AAACGCCCGTGCACGCCTACAAATC	hsNFATC1 gRNA #1RV	AAACCGCGCCGGCGGCACCATGAAC	hsSTAG2 gRNA #1RV	AAACGATCGAGCCGCGGTTCTTCTC
hsATL2 gRNA #1RV	AAACAAGCGCCGCGGTTAACCACGC	hsDVL2 gRNA #1FW	CACCGGGGCTTTGAGTCGCACCCCG	hsNFATC1 gRNA #5FW	CACCGGCTGGTGCTTGGCATCCGCG	hsSTAG2 gRNA #3FW	CACCGTTTGGCCGCGCTTCCGCCG
hsATL2 gRNA #2FW	CACCGTTGGGTCGCTGGTCCGTCGC	hsDVL2 gRNA #1RV	AAACCGGGGTGCGACTCAAAGCCCC	hsNFATC1 gRNA #5RV	AAACCGCGGATGCCAAGCACCAGCC	hsSTAG2 gRNA #3RV	AAACCGGCGGAAGCGCGGCCAAACC
hsATL2 gRNA #2RV	AAACGCGACGGACCAGCGACCCAAC	hsDVL2 gRNA #2FW	CACCGGAAAAAGCACGGATCTGCGA	hsNOD2 gRNA #1 FW	CACCGCTGACAGATTTCGCCTGAAG	hsSTRN3 gRNA #1FW	CACCGACAATGGACGAGCTTGCCGG
hsAXIN1 gRNA #1FW	CACCGCTTCGGTGAAACTTGCTCCG	hsDVL2 gRNA #2RV	AAACTCGCAGATCCGTGCTTTTTCC	hsNOD2 gRNA #1 RV	AAACTTCAGGCGAAATCTGTCAGC	hsSTRN3 gRNA #1RV	AAACCCGGCAAGCTCGTCCATTGTC
hsAXIN1 gRNA #1RV	AAACCGGAGCAAGTTTCACCGAAGC	hsdyrk1a gRNA #1 FW	CACCGACCCACTTGTAGCACCACT	hsNOD2 gRNA #2 FW	CACCGACAGATTTCGCCTGAAGAG	hsSTRN3 gRNA #2FW	CACCGAGGGCGAGACGCCGACAGCT
hsAXIN1 gRNA #3FW	CACCGCATTTTGGGACTCTGCGTCA	hsdyrk1a gRNA #1 RV	AAACAGTGGTGCTACAAGTGGGTC	hsNOD2 gRNA #2 RV	AAACTCTTCAGGCGAAATCTGTC	hsSTRN3 gRNA #2RV	AAACAGCTGTCGGCGTCTCGCCCTC
hsAXIN1 gRNA #3RV	AAACTGACGCAGAGTCCCAAAATGC	hsdyrk1a gRNA #2 FW	CACCGGGCAAACTATAATGGTTGT	hsNOD2 gRNA #3 FW	CACCGCTCTACATGGGCCTCACCTT	hsSUZ12 gRNA #1 FW	CACCGACGGCTTCGGGCGGCAAATC
hsBAZ1B gRNA #1 FW	CACCGCAGGAGCGGCGCCATCGCGG	hsdyrk1a gRNA #2 RV	AAACAACCATTATAGTTGCCC	hsNOD2 gRNA #3 RV	AAACAAGGTGAGGCCCATGTAGAGC	hsSUZ12 gRNA #1 RV	AAACGATTTGCCGCCCGAAGCCGTC
hsBAZ1B gRNA #1 RV	AAACCGCGATGGCGCCGCTCCTGC	hsEED gRNA #1FW	CACCGGAATAGTTCCGTGAATAGTC	hsNPEPPS gRNA #1FW	CACCGAGGAGCGGCTGAAGACGAGA	hsSUZ12 gRNA #2 FW	CACCGTCGGGCGGCAAATCCGGCGG
hsBAZ1B gRNA #2 FW	CACCGAACGGCTTCACCAGCGGAA	hsEED gRNA #1RV	AAACGACTATTCACGGAACTATTCC	hsNPEPPS gRNA #1RV	AAACTCTCGTCTTCAGCCGCTCCTC	hsSUZ12 gRNA #2 RV	AAACCGCCGGATTTGCCGCCCGAC
hsBAZ1B gRNA #2 RV	AAACTTCCCGCTGGTGAAGCCGTTC	hsEED gRNA #2FW	CACCGAGACTTTCGCTCCCTAGCAG	hsNPEPPS gRNA #2FW	CACCGGAAGAGCAGGCGGGCGAGCG	hsTAOK1 gRNA #1FW	CACCGTATACTGCTATCCCGATCCT
hsBMPR2 gRNA #1 FW	CACCGAGCCGCGGGCGATGCGACTA	hsEED gRNA #2RV	AAACCTGCTAGGGAGCGAAAGTCTC	hsNPEPPS gRNA #2RV	AAACCGCTCGCCGCCTGCTCTTCCC	hsTAOK1 gRNA #1RV	AAACAGGATCGGGATAGCAGTATAC
hsBMPR2 gRNA #1 RV	AAACTAGTCGCATCGCCCGCGGCTC	hsEIF4ENIF1 gRNA #1 FW	CACCGAGTATGACCCGCCCATGCG	hsP53 gRNA FW	CACCGCCCCTTGCCGTCCCAAGCAA	hsTAOK1 gRNA #3FW	CACCGCTGCTTGCTTTAGTTGA
hsBMPR2 gRNA #2 FW	CACCGAGCCCTAGTCGCATCGCCCG	hsEIF4ENIF1 gRNA #1 RV	AAACGCATGGGCGGGTCATACTC	hsP53 gRNA RV	AAACTTGCTTGGGACGGCAAGGGGC	hsTAOK1 gRNA #3RV	AAACTCAACTAACAGAGCAGGCAGC
hsBMPR2 gRNA #2 RV	AAACGGGCGATGCACTAGGGCTC	hsEIF4ENIF1 gRNA #2 FW	CACCGATGGGCGGGTCATACTCCAC	hsPPP2CA gRNA #1FW	CACCGGGCCGTTATGCCGGAGCAAG	hsTOP2B gRNA #1FW	CACCGCGGTGTTATGCCGGAGCAAG
hsCCM2 gRNA #1 FW	CACCGAAGTCGGCCGCCGTAAAGA	hsEIF4ENIF1 gRNA #2 RV	AAACGTGGAGTATGACCGGCCCATC	hsPPP2CA gRNA #1RV	AAACAGGAGTCGAGTGAACGGCGCC	hsTOP2B gRNA #1RV	AAACCTTGTCCGGCATAACACCGC
hsCCM2 gRNA #1 RV	AAACTCTTTACGGCGGCCGACTTC	hsEML4 gRNA #1 FW	CACCGCGAAACCGTCCATCTTGCG	hsPPP2CA gRNA #3FW	CACCGAGACCCTGTGGGTCATCGTC	hsTOP2B gRNA #5FW	CACCGCATTTGCACACCGGGGAGAG
hsCCM2 gRNA #2 FW	CACCGCTCCCGCGGCGGCTGAGT	hsEML4 gRNA #1 RV	AAACGCAAGATGGACGGTTTCGC	hsPPP2CA gRNA #3RV	AAACGACGATGACCCACAGGGTCTC	hsTOP2B gRNA #5RV	AAACCTCTCCCCGGTGTGCAAATGC
hsCCM2 gRNA #2 RV	AAACACTCAGCGCGCGCGGGAGCG	hsEML4 gRNA #2 FW	CACCGCAAGATGGACGGTTTCGC	hsPPP2R2A gRNA #1FW	CACCGTCACCATTTGCAGCGCAACA	hsTRIP10 gRNA #10FW	CACCGTCAGGTTAAAGTTTGACCCT
hsCCNY gRNA #1 FW	CACCGACATTCAAGGAGAGGACGC	hsEML4 gRNA #2 RV	AAACGCGAAACCGTCCATCTTGCGC	hsPPP2R2A gRNA #1RV	AAACTGTTGCGCTGCAAATGGTGAC	hsTRIP10 gRNA #10RV	AAACAGGGTCAAACTTTAACCTGAC
hsCCNY gRNA #1 RV	AAACGCGTCCTCTCCTTGAATGTC	hsEML4 gRNA #3 FW	CACCGTCGTCCGTCCGTTCGCCCT	hsPPP2R2A gRNA #2FW	CACCGCTGCCATGTTGCGCTGCAAA	hsTRIP10 gRNA #1FW	CACCGAAGTCCGTCCTTGGGGATAC
hsCCNY gRNA #2 FW	CACCGTCTGTGTCATAAATGTACTA	hsEML4 gRNA #3 RV	AAACAGGGCGAACGGACGGACGAC	hsPPP2R2A gRNA #2RV	AAACTTTGCAGCGCAACATGGCAGC	hsTRIP10 gRNA #1RV	AAACGTATCCCCAAGGACGGACTTC
hsCCNY gRNA #2 RV	AAACTAGTACATTTATGACACAGAC	hsERAS gRNA #1 FW	CACCGACAACAGGGGATACGTTAG	hsPPP6R3 gRNA #1 FW	CACCGCCTGAGCGCAACTAGCGG	hsTRIP12 gRNA #1FW	CACCGACACCCCGCACACTTTCAAT
hsCDC27 gRNA #1 FW	CACCGACGGTAGGGCAAGTTTACGG	hsERAS gRNA #1 RV	AAACTAACGTATCCCCTGTTGTC	hsPPP6R3 gRNA #1 RV	AAACCGCTAGTTGCGCTCAGGCGC	hsTRIP12 gRNA #2FW	CACCGCTATCCCATTGAAAGTGTGC
hsCDC27 gRNA #1 RV	AAACCGTAAACTTGCCCTACCGTC	hsERAS gRNA #2 FW	CACCGAGACAACAGGGGATACGTTA	hsPPP6R3 gRNA #2 RV	AAACGAGCGCAACTAGCGGCGGGTC	hsTRIP12 gRNA #2RV	AAACGCACACTTTCAATGGGATAGC
hsCDC27 gRNA #3 FW	CACCGTTCCCGTCCGAGCCAACGTC	hsERAS gRNA #2 RV	AAACTAACGTATCCCCTGTTGTCTC	hsPPP6R3 gRNA #2FW	CACCGACCCGCCGCTAGTTGCGCTC	hsTRIP12gRNA #1RV	AAACATTGAAAGTGTGCGGGTGGTC
hsCDC27 gRNA #3 RV	AAACGACGTTGGCTCGGACGGGAAC	hsFAF1 gRNA #1 FW	CACCGCGCTAGGCGCTCATGCACT	hsPRDX1 gRNA #1 FW	CACCGCCTCACCTCCGGAGTGTC	hsTXNDC11 gRNA #1FW	CACCGCATGTAATGTCGGAATGCGG
hsCDK13 gRNA #2 FW	CACCGTCGGCTCGGGCAGCGCAACG	hsFAF1 gRNA #1 RV	AAACAGTGCATGAGCGCCTAGCGC	hsPRDX1 gRNA #1 RV	AAACGACACTCCGGAGGTGAGGCGC	hsTXNDC11 gRNA #1RV	AAACCGCATTCCGACATTACATGC
hsCDK13 gRNA #2 RV	AAACGTTGCGCTGCCCGAGCCGAC	hsFAF1 gRNA #2 FW	CACCGTCGGTAACCTTCAGGCGCCC	hsPRDX1 gRNA #2 FW	CACCGTGTAGTCCCAGACACTCCGG	hsTXNDC11 gRNA #3FW	CACCGTCGGCGGGCCGGCTCCGTCG
hsCDK13 gRNA #3 FW	CACCGCACCCAACGTCAGGGCGCGA	hsFAF1 gRNA #2 RV	AAACGGGCGCCTGAAGGTTACCGAC	hsPRDX1 gRNA #2 RV	AAACCGGAGTGTCTGGGACTACAC	hsTXNDC11 gRNA #3RV	AAACCGACGGAGCCGGCCCGCCGAC
hsCDK13 gRNA #3 RV	AAACTCGCGCCCTGACGTTGGGTGC	hsFAF1 gRNA #3 FW	CACCGGGAGCGAAGCGCGCACCT	hsPTEN gRNA #1 FW	CACCGCGGGACTCTTTATGCGCTG	hsUB2L3 gRNA #1FW	CACCGCGGCCGGCCGCGATGCATTC
hsCDKN2A gRNA #1 FW	CACCGCACGCCTCTGACGCGACATC	hsFAF1 gRNA #3 RV	AAACAGGTGCGCGCTTCGCTCCCGC	hsPTEN gRNA #1 RV	AAACAGCGCATAAAGAGTCCCGC	hsUB2L3 gRNA #1RV	AAACGAATGCATCGCGGCCGGCCGC
hsCDKN2A gRNA #1 RV	AAACGATGTCGCGTCAGAGGCGTGC	hsFAM168B gRNA #1 FW	CACCGATGAATCCTGTTTATAGTCC	hsPTEN gRNA #2 FW	CACCGACTCTTTATGCGCTGCGGC	hsUB2L3 gRNA #2FW	CACCGCTCTGGCAGCGGCCGGGCGT
hsCDKN2A gRNA #2 FW	CACCGTGTCCAGATGTCGCGTCAG	hsFAM168B gRNA #1 RV	AAACGGACTATAAACAGGATTCATC	hsPTEN gRNA #2 RV	AAACGCCGCAGCGCATAAAGAGTC	hsUB2L3 gRNA #2RV	AAACACGCCCGGCCGCTGCCAGAGC
hsCDKN2A gRNA #2 RV	AAACTGACGCGACATCTGGACAC	hsFAM168B gRNA #3 FW	CACCGAAGATCCAGGACTATAAAC	hsPTEN gRNA #3 FW	CACCGGGCGCCTCGGAAGACCGA	hsWNT3a gRNA #1FW	CACCGCTCTGGGCAGCTACCCGATC
hsCNOT1 gRNA #1 FW	CACCGAGGTCGCGCGCTCACGTCG	hsFAM168B gRNA #3 RV	AAACGTTTATAGTCCTGGATCTTC	hsPTEN gRNA #3 RV	AAACTCGGTCTTCCGAGGGCCCGC	hsWNT3a gRNA #1RV	AAACGATCGGGGTAGCTGCCCAGAGC
hsCNOT1 gRNA #1 RV	AAACGACGTGAGCGCGCGACCTC	hsFOXR2 gRNA #1 FW	CACCGATCTAGGGAGCTTATCAGT	hsPTPN14 gRNA #12FW	CACCGACATGGCCCCCGTGGCGCCC	hsWNT3a gRNA #2FW	CACCGACGCTCTCGGGGCGGACTCC
hsCNOT1 gRNA #2 FW	CACCGACGTGAGCGCGCGACCTC	hsFOXR2 gRNA #1 RV	AAACACTGATAAGCTCCCTAGATGC	hsPTPN14 gRNA #12RV	AAACGGGCGCCACGGGGGGCCATGTC	hsWNT3a gRNA #2RV	AAACGGAGTCCGCCCCGAGAGCGTC
hsCNOT1 gRNA #2 RV	AAACGAGGTCGCGCGCTCACGTCGC	hsFOXR2 gRNA #2 FW	CACCGCACTGATTAGTGGTCAGACC	hsPTPN14 gRNA #1FW	CACCGAAGGACAGCCTTTCCGCGC	hsWNT5a gRNA #1FW	CACCGGTCCAAGGCAGTTCGTGTAG
hsCNTFR gRNA #1 FW	CACCGCTCAGTCCAGGGGTAGCGT	hsFOXR2 gRNA #2 RV	AAACGGTCTGACCACTAATCAGTGC	hsPTPN14 gRNA #1RV	AAACGGCGCGAAAGGCTGTCCTTCC	hsWNT5a gRNA #1RV	AAACCTACACGAACTGCCTTGGACC
hsCNTFR gRNA #1 RV	AAACGCTACGCCCTGGACTGAGC	hsGDI2 gRNA #1 FW	caccgCTGTACAGGTCGCATAGCAC	hsRAB12 gRNA #1FW	CACCGATTATCGGCTCCCGCGGCGT	hsWNT5a gRNA #2FW	CACCGATCCTCTACACGAACTGCCT
hsCNTFR gRNA #2 FW	CACCGAATGTACTCCTTCCCGGCGT	hsGDI2 gRNA #1 RV	aaacGTGCTATGCGACCTGTACAGc	hsRAB12 gRNA #1RV	AAACACGCCGCGGGAGCCGATAATC	hsWNT5a gRNA #2RV	AAACAGGCAGTTCGTGTAGAGGATC
hsCNTFR gRNA #2 RV	AAACGCCGGGAAGGAGTACATTC	hsGDI2 gRNA #2 FW	CACCGATAGCACCGGCAACAGCTTC	hsRAB12 gRNA #4FW	CACCGCCGCATGCGTGTATGGATCC	hsWNT5b gRNA #1FW	CACCGTGCATGTCCCGCCGCGTGTC
hsCOPG2 gRNA #1 FW	CACCGAAACATCTTCTTGGATTGAT	hsGDI2 gRNA #2 RV	AAACGAAGCTGTTGCCGGTGCTATC	hsRAB12 gRNA #4RV	AAACGGATCCATACACGCATGCGGC	hsWNT5b gRNA #1RV	AAACAGACACGCGGCGGGACATGCAC
hsCOPG2 gRNA #1 RV	AAACATCAATCCAAGAAGATGTTTC	hsGMDS gRNA # 1FW	CACCGCGTGTGCCATGTCCCGCGG	hsRAB2A gRNA #1FW	CACCGAAGAGATAGGCGTACGCCA	hsWNT5b gRNA #5FW	CACCGCCGCGGGCCTGACACGCGGC
hsCOPG2 gRNA #2 FW	CACCGAGAATATGCAAACATCTTCT	hsGMDS gRNA #1 RV	AAACCGCGGGACATGGCACACGC	hsRAB2A gRNA #1RV	AAACTGGCGTACGCCTATCTCTTC	hsWNT5b gRNA #5RV	AAACGCCGCGTGTCAGGCCCGCGGC
hsCOPG2 gRNA #2 RV	AAACAGAAGATGTTTGCATATTCTC	hsGMDS gRNA #4 FW	CACCGTGATGAGCGCCACGTTCCT	hsRAB2A gRNA #3FW	CACCGCACTGAGCGGCCGCGGCCAC	hsYAP1 gRNA #1FW	CACCGGGCGTAGCCCTCGCTCGCC
hsCPNE3 gRNA #1 FW	CACCGTAGTAAACCGTTTGATGCTA	hsGMDS gRNA #4 RV	AAACAGGAACGTGGCGCTCATCAC	hsRAB2A gRNA #3RV	AAACTGGCCGCGGCCGCTCAGTGC	hsYAP1 gRNA #1RV	AAACGGCGAGCGAGGGCTACGCCC
hsCPNE3 gRNA #1 RV	AAACTAGCATCAAACGGTTTACTAC	hsGOSR1 gRNA # 1FW	CACCGCGTCCAACGTCAGCCGGGAT	hsSEC24A gRNA #3FW	CACCGAGAGTGCGGCGCCATGCCTC	hsYAP1 gRNA #7FW	CACCGCGGCGCTGTCCTCGCTCTC
hsCPNE3 gRNA #2 FW	CACCGAGTAAACCGTTTGATGCTAT	hsGOSr1 gRNA #1 RV	AAACATCCCGGCTGACGTTGGAGCGC	hsSEC24A gRNA #3RV	AAACGAGGCATGGCGCCGCACTCTC	hsYAP1 gRNA #7RV	AAACGAGAGCGAGGACAGCGCCGCC
hsCPNE3 gRNA #2 RV	AAACATAGCATCAAACGGTTTACTC	hsGOSr1 gRNA #2 FW	CACCGTTTGTCGTCCAACGTCAGCC	hsSEC24A gRNA #5FW	CACCGAGACCACTGCTGAAAGCGGA	hsYBX1 gRNA#1 FW	CACCGCCCGGGGTGTGATGGTAACT
hsCPNE3 gRNA #3 FW	CACCGTAACTTACAGGTGAGCTTC	hsGOSr1 gRNA #2 RV	AAACGGCTGACGTTGGACGACAAAC	hsSEC24A gRNA #5RV	AAACTCCGCTTTCAGCAGTGGTCTC	hsYBX1 gRNA#1 RV	AAACAGTTACCATCACACCCCGGGC
hsCPNE3 gRNA #3 RV	AAACGAAGCTCACCTGTAAGTTAC	hsGRIA3 gRNA #1FW	CACCGCGGGTTCATTGGCTGCAAGC	hsSEC63 gRNA #1FW	CACCGTGTTCCCACTGTCATCGTAC	hsYBX1 gRNA#2 FW	CACCGGGGGTGTGATGGTAACTAGGC
hsCREBBP gRNA #1 FW	CACCGTGGTGCTTGCACTCGTTGC	hsGRIA3 gRNA #1RV	AAACGCTTGCAGCCAATGAACCCGC	hsSEC63 gRNA #1RV	AAACGTACGATGACAGTGGGAACAC	hsYBX1 gRNA#2 RV	AAACGCCTAGTTACCATCACACCCC
hsCREBBP gRNA #1 RV	AAACGCAACGAGTGCAAGCACCAC	hsGRIA3 gRNA #2FW	CACCGAATGAACCCGCCTTCCAGAT	hsSEC63 gRNA #2FW	CACCGAGTTCCAGTACGATGACAGT	hsZBTB10 gRNA #1FW	CACCGTCGTAACCTCTTCGCGTGAA
hsCREBBP gRNA #2 FW	CACCGAGGGGGTCGGGGTCGACGAT	hsGRIA3 gRNA #2RV	AAACATCTGGAAGGCGGGTTCATTC	hsSEC63 gRNA #2RV	AAACACTGTCATCGTACTGGAACTC	hsZBTB10 gRNA #1RV	AAACTTCACGCGAAGAGGTTACGAC
hsCREBBP gRNA #2 RV	AAACATCGTCGACCCCGACCCCCTC	hsLGR4 gRNA #1FW	CACCGGGACAGGGAGACCGGTGCGA	hsSETD5 gRNA #1FW	CACCGCTTAGAAGATGTACTGCCA	hsZBTB10 gRNA #2FW	CACCGCTCTCGCCACGAGTTCACCT
hsCSNK1A1 gRNA #2FW	CACCGGGCCGCGACTCTCACGGATC	hsLGR4 gRNA #1RV	AAACTCGCACCGGTCTCCCTGTCCC	hsSETD5 gRNA #1RV	AAACTGGCAGTACATCTTCTAAGCC	hsZBTB10 gRNA #2RV	AAACAGGTGAACTCGTGGCGAGAGC
hsCSNK1A1 gRNA #2RV	AAACGATCCGTGAGAGTCGCGGCCC	hsLGR4 gRNA #3FW	CACCGGGGCTGCCTCTGCGCGTCCA	hsSETD5 gRNA #2FW	CACCGCTCTGTTTGGATATACTGTT	hsZNF217 gRNA #10FW	CACCGACCTTCTTCAGGATGGGTAG
hsCSNK1A1 gRNA #6FW	CACCGACAGGGTGACGCTCGGAGCG	hsLGR4 gRNA #3RV	AAACTGGACGCGCAGAGGCAGCCCC	hsSETD5 gRNA #2RV	AAACAACAGTATATCCAAACAGAGC	hsZNF217 gRNA #10RV	AAACCTACCCATCCTGAAGAAGGTC
hsCSNK1A1 gRNA #6RV	AAACCGCTCCGAGCGTCACCCTGTC	hsLGR5 gRNA #1FW	CACCGTCCTCCAGGAAGCGGAGACT	hsSETD5 gRNA #3FW	CACCGCATGAGCATTGCAATCCCTC	hsZNF217 gRNA #2FW	CACCGTTCCACCCAGCCGGGAAGCG
hsCTCF gRNA #1 FW	CACCGTGGAGCGATTAAACCGTGCG	hsLGR5 gRNA #1RV	AAACAGTCTCCGCTTCCTGGAGGAC	hsSETD5 gRNA #3RV	AAACGAGGGATTGCAATGCTCATGC	hsZNF217 gRNA #2RV	AAACCGCTTCCCGGCTGGGTGGAAC
hsCTCF gRNA #1 RV	AAACGCACGGTTTAATCGCTCCAC	hsLGR5 gRNA #2FW	CACCGGACTGATGTTGTTCATACTG	hsSHFM1 gRNA #1FW	CACCGCTCTATGGTAGCGTCAGCGT	hsZNF521 gRNA #1FW	CACCGAGCGAGTCCCTGCGGGTTA
hsCTCF gRNA #2 FW	CACCGCACGGTTTAATCGCTCCAC	hsLGR5 gRNA #2RV	AAACCAGTATGAACAACATCAGTCC	hsSHFM1 gRNA #1RV	AAACACGCTGACGCTACCATAGAGC	hsZNF521 gRNA #1RV	AAACTAACCCGCAGGGACTCGCTCC
hsCTCF gRNA #2 RV	AAACGTGGAGCGATTAAACCGTGC	hsLGR6 gRNA #1FW	CACCGCATCTCGGCGGTCGGGCTAC	hsSHFM1 gRNA #2FW	CACCGTGACGGTGGCGTTTCCTTG	hsZNF521 gRNA #3FW	CACCGCGCTCTGTACGTAATCACTG
hsCTNNB1_gRNA_FW	caccgttacctaaaggatgatttac	hsLGR6 gRNA #1RV	AAACGTAGCCCGACCGCGAGATGC	hsSHFM1 gRNA #2RV	AAACCAAGGAAACGCCACCGTCACC	hsZNF521 gRNA #3RV	AAACCAGTCATTCGTGAAGAAGGTC
hsCTNNB1_gRNA_RV	aaacgtaaatcatcctttaggtaac	hsLGR6 gRNA #2FW	CACCGTCGCGCCGTGCGTCCGCGCC	hsSMC1A gRNA #1FW	CACCGGCCTCTCGTGCATAGATAC	hsZSWIM6 gRNA #1FW	CACCGCAGCAAAGCCGTTTCGCGGG
hsddx3x gRNA #1 FW	CACCGTTTTCAGGCGTCTTAGCCGG	hsLGR6 gRNA #2RV	AAACGGCGCGGACGCACGGCGCGAC	hsSMC1A gRNA #1RV	AAACGTATCTATGCACGAGAGGCC	hsZSWIM6 gRNA #1RV	AAACCCGCGAAACGGCTTTGCTGC
hsddx3x gRNA #1 RV	AAACCGGCTAAGACGCCTGAAAAC	hsLRP5 gRNA #2FW	CACCGAGAGACCAACCGCATCGAGG	hsSMC1A gRNA #3FW	CACCGCCCTCATTGAGATTGACTA	hsZSWIM6 gRNA #5FW	CACCGCCGCGAAACGGCTTTGCTGC
hsddx3x gRNA #2 FW	CACCGGGGAGCGAATGCGTAAGGT	hsLRP5 gRNA #2RV	AAACCCTCGATGCGGTTGGTCTCTC	hsSMC1A gRNA #3RV	AAACTAGTCAATCTCAATGAGGGCC	hsZSWIM6 gRNA #5RV	AAACGCAGCAAAGCCGTTTCGCGGC
hsddx3x gRNA #2 RV	AAACCTTACGCATTCGCTCCCC	hsLRP5 gRNA #3FW	CACCGTTTCCAAGGGAGCCGTGTAC	hsSNTN gRNA #1FW	CACCGGGCATTTTCCTAGGTGCGC		
hsDIP2C gRNA #1 FW	CACCGTGCGGTCCGCCATGCTCCGC	hsLRP5 gRNA #3RV	AAACGTACACGGCTCCCTTGGAAAC	hsSNTN gRNA #1RV	AAACGCGCACCTAGGAAAATGCCC		
hsDIP2C gRNA #1 RV	AAACGCGGAGCATGGCGGACCGCAC	hsMARK2 gRNA #1FW	CACCGCCGAAGCGGCTAGAAACGGG	hsSNTN gRNA #3FW	CACCGTGGCTGTATGCACAGTACCC		
hsDIP2C gRNA #2 FW	CACCGCTGCGGTCCGCCATGCTCCG	hsMARK2 gRNA #1RV	AAACCCCGTTTCTAGCCGCTTCGGC	hsSNTN gRNA #3RV	AAACGGGTACTGTGCATACAGCCAC		
hsDIP2C gRNA #2 RV	AAACGGAGCATGGCGGACCGCAGC	hsMARK2 gRNA #4FW	CACCGCTAGCCGCTTCGGATGTTTC	hsSPAG9 gRNA #1FW	CACCGCGAGTTCGAGCGGCTTATC		
hsDIP2C gRNA #3 FW	CACCGCGGCGCCCGCGGAGCATGG	hsMARK2 gRNA #4RV	AAACGAAACATCCGAAGCGGCTAGC	hsSPAG9 gRNA #1RV	AACGATAAGCCGCTCGAACTCGCC		
hsDIP2C gRNA #3 RV	AAACCATGCTCCGCGGGCGCGC			hsSPAG9 gRNA #7FW	CACCGCTCCATGGTGGCAAGCGGAC		
				hsSPAG9 gRNA #7RV	AAACGTCCGCTTGCCACCATGGAGC		

Table 2: RT-qPCR Primer Sequences

Gene	Forward Sequence	Reverse Sequence
Human		
CTCF	CGCTAGTGGACAGATTGCTGA	AGGACGAGTACCTCTCCGTGG
ACTB	GCCGTCTTCCCCTCCATCGT	TGCTCTGGGCGTCGC
RSPO2	TTATTTAGGCCGTTGCTTT	GCTCCAATGACCAACTTCACATCCTT
Mouse		
Birc5	CTTCATCCACTGCCCTACCG	GCTCCTCTATCGGGTTGTCA
Bcl2l1	CGATGGAGGAACCAGGTTGT	GATAAGGTTCTGGTAGGCAGC
Ctgf	CTTCCCGAGAAGGGTCAAGC	TTCCAGTCGGTAGGCAGCTA
Wisp	TAGGAGTGTGTGCACAGGTGG	TACCTGCAGTTGGGTTGGAA
Wrch1	TACCCCACCGAGTACATCCC	GCTTGTCAAACTCATCCTGTCC
Axin2	AAATTCCATACCGGAGGATG	CCTCCCAGATCTCCTCAAAC
Actb	GCCGTCTTCCCCTCCATCGT	TGCTCTGGGCGTCGC

Table 3: Soft Agar Assay Results (Raw Mean Count/Quadrant)

Gene	HSC1L	N10	N5	S462	Gene	HSC1L	N10	N5	S462
APC	29	16	133	140	MARK2	0	-	31	17
ATL2	4	0	0	79	MYCN	0	0	0	83
AXIN2	49	-	102	9	NESD2	0	0	0	53
BAZ1B	16	0	52	71	NFAT5	0	0	0	38
BMPR2	0	46	0	100	NFATC1	4	104	0	58
CCM2	0	0	212	158	NOD2	5	5	1	43
CCNY	0	0	67	203	NPEPPS	0	0	95	3
CDC27	10	36	71	315	NRDC	9	0	0	9
CDK13	8	43	58	40	P4HB	0	0	0	59
CDKN2A	9	24	57	70	PABCL1	7	0	0	75
CNOT1	-	-	-	-	PCDH10	6	0	0	74
CNTFR	2	-	28	70	PICALM	2	0	0	56
COPG2	-	-	-	-	PLAA	0	4	43	0
CPNE3	30	57	38	49	PLEKHB2	0	0	0	16
CREBBP	0	67	52	53	PPP2CA	7	22	15	64
CSNK1A1	47	0	70	384	PPP2R2A	4	17	0	37
CTCF	18	0	42	285	PPP6R3	12	9	8	60
DDX3X	0	-	15	19	PRDX1	0	-	98	6
DIP2C	0	-	12	6	PTEN	8	3	0	66
DMD	0	-	27	20	PTPN14	2	5	36	115
DVL1	17	0	0	30	RAB12	0	1	36	9
DVL2	1	0	0	46	RAB2A	0	0	25	0
DYRK1A	15	0	0	57	RNF43	11	-	98	13
EED	4	0	0	41	SEC24A	8	3	-	-
EIF4ENIF	56	27	52	5	SEC63	0	0	30	6
EML4	3	13	20	197	SETD5	3	0	0	49
ERAS	0	0	7	23	SHFM1	12	-	24	3
FAF1	0	29	13	5	SMC1A	43	0	25	10
FAM168B	51	18	0	231	SNTN	30	1	22	8
FOXR2	0	0	3	211	SPAG9	0	1	17	11
GDI2	5	0	120	80	SPPL3	0	0	40	22
GFP	0	4	1	27	SRGAP2	0	0	10	3
GMDS	1	0	14	97	STAG2	0	1	83	14
GOSR1	0	0	4	65	STRN3	0	4	1	60
GRIA3	12	0	2	32	SUZ12	7	0	0	35
GSK3B	22	3	0	35	TAOK1	11	7	2	60
IFNG	8	47	0	52	TOP2B	9	1	47	72
IGSF8	22	0	0	61	TRIP10	0	1	0	37
JAK2	2	0	68	113	TRIP12	0	-	30	-
JMY	0	2	60	62	TXNDC11	0	3	4	-
KAT7	0	1	0	70	UBE2L3	2	2	0	11
KDM6A	0	1	0	117	WNT3a	8	0	24	32
KLF3	0	0	54	250	WNT5a	0	-	0	2
LGR4	0	0	0	51	WNT5b		-	61	-
LGR5	0	0	0	28	YAP1	1	0	0	109
LGR6	0	0	116	89	YBX1	0	0	0	-
LRP5	0	0	0	10	ZBTB10	0	1	0	-
MAEA	0	0	0	40	ZNF217	0	8	0	-
MANBAL	10	0	0	102	ZNF521	0	-	15	12
MAP3K4	11	0	3	51	ZNRF3	1	-	45	16
					ZSWIM6	0	2	0	27

Table 4: List of Antibodies

Name	Supplier, Cat#
APC	CST #2504
CTNNB1	CST #9582
TAOK1	Abcam #197891
ACTNB	CST #3700
YAP1	CST #14074
GDI2	CST #2564
VINCULIN	CST #13901
FAK	CST #71433
p-FAK	CST #8556
PTCH1	CST #2468
GLI1	CST #2463
RSPO2	sc-74883
TUBULIN	CST #2146
CTCF	CST #3417

Table 5: CTCF ChIP-PCR Primer Sequences and 3C Assay Primer Sequences

3PD_hnd3_Fw1 gca ctt ata aaa tag aag tta ccc	3PD_hnd3_Fw2 ttg gag gaa tgt aca ggt	3PD_hnd3_fw6 aca ctg tgt ttt aaa gta tcc t	3PD_hnd3_Fw7 ggt ctt ttc aac tat gtt
3PD_hnd3_Rv1 ctc tat atc gtc cct cta ca	3PD_hnd3_Rv2 ata aaa caa gaa ttc cta tct cc	3PD_hnd3_Rv6 caa ata ata tgc aca ctg ctc	3PD_hnd3_RV7 cac ttt ctt cat ttg tca cat
3PD_hnd3_Fw10 cat aag aaa acc caa atg aag at	3PD_bgl2_RV10 caa cct ata gta tga gaa act act	3PD_bgl2_Rv6 agt aga agt aga gcg gtt taa	3PD_bgl2_Rv5 atc atg tcc tcc ttc aca
3PD_hnd3_Rv10 tga cca gag aag atc ctg	3PD_bgl2_Fw10 caa tga atg aaa act tga aaa cc	3PD_bgl2_fw5 agg taa ctg gat cat ggg	3PD_bgl2_fw6 ctt gtt ttc ctt gga tgg g
3PD_bgl2_Rv2 gac aca gtg caa ttc tga a	3PD_bgl2_rv1 aac agg gga ggg act aa	3PD_ecoR1_Rv7 gat cag gaa cat cct tta gag	3PD_ecoR1_Rv6 gaa gca aac ttg gta gaa ga
3PD_bgl2_Fw2 tcc ctc ttc cct aaa act t	3PD_bgl2_fw1 ttc acagaa tgg cca gaa	3PD_ecoR1_Fw7 aaa gtg ctc agg ctc at	3PD_ecoR1_Fw6 aag tag aga tgg ggt ttc g
3PD_ecoR1_Rv3 cca cat cct caa aca aac a	3PD_ecoR1_Rv2 cca tgc cac ata cat att ttc	3C_RSPO2_ORF_bglll_Rv7 aat tct aaa atg tgc tga cac aga aac	3C_RSPO2_ORF_bglll_Rv6 aag aga ttc atc ata atg tag cca ctg ac
3PD_ecoR1_Fw3 tgt ata gtc ctt gct cct t	3PD_ecoR1_fw2 ctg ggc tca agg gtt ta	3C_RSPO2_ORF_bglll_Rv15 gag gga caa ttc aca caa ctt gag t	3C_RSPO2__ORF_bglll_Rv16 cag gtt agt tac ata tgt ata cat gtg cca tg
3C_RSPOS_ORF_bglll_Rv12 cag atg tgc ctt tgc acc aaa ata aaa	3C_RSPO2_ORF_bglll_Rv11 gcc act caa ata gta cag tgg tta gc	3c_RSPO2_ORF_bglll_Fw16 ctt ctt ttt ttt tct ttc agc ttc aga tta tcc tac	3C_RSPO2_ORF_bglll_Fw17 agg cag gca gat cac aaa gt
3C_RSPO2_ORF_bglll_Rv3 aca gac cag ctc aaa aga gaa aac tc	3C_RSPO2_ORF_bglll_Rv2 gtt gaa gat aaa gag aaa tta aat ttc aca ggc tct att aat c	3C_RSPO2_ORF_bglll_Fw8 ctc agg ccc gaa taa aag aaa aaa gc	3C_RSPO2_ORF_bglll_Fw7 cat tta gga tgt ggg atg act ggt tac
3C_RSPO2_ORF_bglll_Rv19 ctc gtc gca gtt tcc aga aaa aag	3C_RSPO2_ORF_bglll_Rv20 caa ccc agg cca aga aat att tat gtg	3PD_hnd3_Fw8 gtg ttt ata aat tgt tgc tga c	3PD_hnd3_Fw9 taa tg tac taa tgg ttg gaa
3C_RSPO2_ORF_bglll_Fw20 gct tac ata tgc ttt tcc att tag ttg ggt	3C_RSPO2_ORF_bglll_Fw12 cca ctt ttt ctt tat tca gtc tac cac tga t	3PD_hnd3_Rv8 gct tg tat tgg cac taa	3PD_hnd3_Rv9 cta tgt aat aat agg ct ac
3C_RSPO2_ORF_bglll_Fw4 tgt agt gtg ctc tta aag ctt taa ctt tc	3C_RSPO2_ORF_bglll_Fw3 aaa gtt taa agg gag tca tca gtc ctt c	3PD_bgl2_Rv4 gtt aag ggc aac cag aga	3PD_bgl2_Rv3 gtt gga aga agg gag aaa a
3C_RSPO2_ecoR1_Rv1 cca gga cca ttt act gaa tag gag aat t	3C_RSPO2_ecoR1_Rv6 gca gat ttg aag agg cat gtg gaa ttc	3PD_bgl2_fw4 tga aat tct ggg ttg aaa att c	3PD_bgl2_fw3 tca ttc aaa ctt acc ttt cac t
3C_RSPO2_ecoR` Fw3 gaa ttc cac atg cct ctt caa atc tg	3C_RSPO2_rv2 gga aga cgc tgt gtt gct cc	3PD_ecoR1_Rv5 cgg gac aga aca gaa tag t	3PD_ecoR1_Rv4 tca cac ata cga tgt cat tta
3C_RSPO2_rv3 ggg ccc ttt cta tca gct tcc	3C_RSPO2_rv1 gtt agc tct gtc tgt agc tag ga	3PD_ecoR1_fw5 ctc cca gag tgcaag at	3PD_ecoR1_fw4 ggg gaa aca gct aaa gaa
3PD_hnd3_Fw3 gag gcc agc tag ata ttc t	3PD_hnd3_Fw4 act gca atg gaa agt gc	3C_RSPO2_ORF_bglll_Rv5 aaa tca ggt aga atc agg tct aca ggg	3C_RSPO2_ORF_bglll_Rv4 gtg cca gta ctc cga att tca tat ctt c
3PD_hnd3_Rv3 tct tat tgt ata ctg cag caa	3PD_hnd3_Rv4 cct tta aaa gag agt tga att ca	3C_RSPO2_ORF_bglll_Rv17 gca gaa tca agt aca aac cct tga taa aat ac	3C_RSPO2_ORF_bglll_Rv18 gag gtt tag ggt tta tta gca gag aag taa tat gat c
3PD_bcl2_fw9 ctt taa ctt ctt ctg ggt att ac	3PD_bgl2_Rv7 aaa gag gtt aga cct aaa gc	3C_RSPO2_ORF_bglll_Fw18 agt tct ttt aat tgt cat gtt agg gtg tcg	3C_RSPO2_ORF_bglll_Fw19 atg tag tgt gct ctt aaa gct tta act ttc
3PD_bgl2_Rv9 aca gtc aag tga cta cca ta	3PD_bgl2_fw8 tga gat tta agg aaa caa gtt gt	3C_RSPO2_ORF_bglll_Fw6 gta atc agg ttg gga ata cag gca t	3C_RSPO2_ORF_bglll_Fw5 gag ata aaa gga tga att tct gtg act gcc
3PD_ecoR1_Rv10 cag aag cac ttt tac ata ata gt	3PD_ecoR1_Rv9 cat act agt tta aag tta aca gat gg	3PD_hnd3_FW5 tca agt gat cct cct atc tc	3C_proRSPO2_rv1 ccc acc ttt gaa aag tg
3PD_ecoR1_Fw10 tgt cac tta aac tat aca act ga	3PD_ecoR1_Fw9 ccc cta aca cat acg	3PD_hnd3_Rv5 cct ggg caa cat agt aag	3C_EIF3e_RSPO2_ecoR1 Fw7 gaa ttc ttt ttt cac taa caa aat caa gtg
3PD_ecoR1_Rv1atg ggg tca aag gga at	3C_RSPO2_ORF_bglll_Rv9 cct aag atg cat tcc cat ggg	3PD_bgl2_Rv8 agg ctt ttc atc tat gcg a	3C_EIF3e_fw3 ttt ggc aag atg gcg gag t
3PD_ecoR1_fw1 gct tat aga aac gtg tgg tt	3C_RSPO2_ORF_bglll_Rv13 aga aag cca gga aat taa ata tat gca gac tta g	3PD_bgl2_fw7 cca cac att ctt cgc tat t	
3C_RSPO2_ORF_bglll_Rv10 tcg gaa ctt tac ttc ctc agc tgt a	3C_RSPO2_ORF_bglll_Fw14 ctg tgg aaa atc tga aaa tgc aat agg tat aaa ac	3PD_ecoR1_Rv8 ttc tga aat tga ggc agt aa	
3C_RSPO2_ORF_bglll_Rv1 gtt ctt tta att gtg atg tta ggg tgt	3C_RSPO2_ORF_bglll_Fw10 ctc tgc tga ctt ata ggg cat ca	3PD_ecoR1_Fw8 gga gga gtc cct ctt tt	
3C_RSPO2_ORF_bglll_Fw13 gta ttt gac caa taa gag acg aat atc cag aat at	3C_RSPO2_ORF_bglll_Fw1 tct tct tct aag ggc act aat ccc att c	3C_RSPO2_ORF_bglll_Rv8 ccc tta aag ctt caa agt ata tcc ctc	
3C_RSPO2_ORF_bglll_Fw11 cct tgg cat tct tat atc acc att tga aag	3C_EIF3e_RSPO2_ecoR1 fw15 gaa ttc cac ttg agc att tga atg aag	3C_RSPO2_ORF_bglll_Rv14 caa aaa tcc att att cgt gtg cac aat tca c	
3C_RSPO2_ORF_bglll_Fw2 gtc ata tct gac ttc tct gag cag tgt	3C_proRSPO2_rv2 ggg ccc ttt gtt agc ac	3C_RSPO2_ORF_bglll_Fw15 ccc cat gct gtt ctc atg ata gtg	
3C_RSPO2_ecoR1_Rv9 ctt aag acg ttt ctt ctc aaa aac cgg	3C_EIF3e_fw1 cac aga ctc cct ttt ctt tgg c	3C_RSPO2_ORF_bglll_Fw9 aca acc aat tac gca cct ata ttt atc atg t	
3C_RSPO2_ecoR1_Rv19 gca gag ttt ttt ttt ttt tac cag gaa ttc	3C_EIF3e_Fw2 cct ttt ctt tgg caa gat ggc g	3C_EIF3e_RSPO2_ecoR1 Fw11 gaa ttc ttg att gga ttt ctg atc ctg ca	

Bibliography

1. Evans DG, Baser ME, McGaughran J, Sharif S, Howard E, Moran A (2002) Malignant peripheral nerve sheath tumors in neurofibromatosis 1. J Med Genet (5):311-314.
2. Katz D, Lazar A, Lev D (2009) Malignant peripheral nerve sheath tumour (MPNST): the clinical implications of cellular signalling pathways. Expert Rev Mol Med 11:e30.
3. Watson, AL, Rahrmann, EP, Moriarity B, Choi K, Conboy C, Greeley A, Halfond A, Anderson L, Wahl B, Keng, VW, Rizzardi A, Forser C, Collins MH, Sarver A, Wallace M, Schmechel S, Ratner N, Largaespada DA (2013) Canonical Wnt/β-catenin Signaling Drives Human Schwann Cell Transformation, Progression, and Tumor Maintenance. Cancer Discovery, Jun;3(6):674-89.
4. Goertz O, Langer S, Uthoff D, Ring A, Stricker I, Tannapfel A, Steinau H-U (2014) Diagnosis, treatment and survival of 65 patients with malignant peripheral nerve sheath tumors. Anticancer Research 34 (2): 777-783.
5. Kar M, Deo SV, Shukkla NK, Malik A, DattaGupta S, Mohanti BK, Thulkar S (2006) Malignant peripheral nerve sheath tumors (MPNST)- clinicopathological study and treatment outcome of twenty-four cases. World Journal of Surgical Oncology 4:55
6. Ferner RE, Gutmann DH (2002) International consensus statement on malignant peripheral nerve sheath tumors in neurofibromatosis. Cancer Res 62 (5):1573-1577.
7. Wong WW, Hirose T, Scheithauer BW, Schild SE, Gunderson LL (1998) Malignant peripheral nerve sheath tumor: analysis of treatment outcome. Int J Radiat Oncol Biol Phys 42 (2):351-360.
8. Jessen WJ, Miller SJ, Jousma E, Rizvi TA, Eaves D, Wu J, Widemann B, Kim MO, Dombi E, Dudley AH, Niwa-Kawakita M, Page GP, Giovannini M, Aronow BJ, Cripe TP, Ratner N (2013) MEK Inhibition Exhibits Efficacy in Human and Mouse Neurofibromatosis Tumors Despite Transcriptional Feedback onto ERK. J. Clinical Investigation, Jan 2;123(1):340-7.
9. Zou CY, Smith KD, Zhu QS, Liu J, McCutcheon IE, Slopis JM, Meric-Bernstam F, Peng Z, Bornmann WG, Mills GB, Lazar AJ, Pollock RE, Lev D (2009) Dual targeting of AKT and mammalian target of rapamycin: a potential therapeutic approach for malignant peripheral nerve sheath tumor. Mol Cancer Ther 8(5): 1157-1168.

10. Messiaen LM, Callens T, Mortier G, Beysen D, Vandenbroucke I, Van Roy N, Speleman F, Paepe AD (2000) Exhaustive mutation analysis of the NF1 gene allows identification of 95% of mutations and reveals a high frequency of unusual splicing defects. Hum Mutat 15 (6):541-555.
11. Ciriello G, Miller, ML, Aksoy BA, Senbabaoglu Y, Schultz Y, Sander C. (2013) Emerging landscape of oncogenic signatures across human cancers. Nature Genetics 45:1127–1133.
12. Cancer Genome Atlas Research Network (2017) Comprehensive and Integrative Genomic Characterization of Hepatocellular Carcinoma. Cell. 69(7):1327-1341.e23.
13. Altekruse SF, McGlynn KA, Reichman ME, Hepatocellular carcinoma incidence, mortality, and survival trends in the United States from 1975 to 2005 (2009) J Clin Oncol 27: 1584-1491.
14. Lachenmayer A, Alsinet C, Savic R, Cabellos L, Toffanin S, Hoshida Y, Villanueva A, Minguez B, Newell P, Tsai HW, Barretina J, Thung S, Ward SC, Bruix J, Mazzaferro V, Schwartz M, Friedman SL, Llovet JM (2012) Wnt-pathway activation in two molecular classes of hepatocellular carcinoma and experimental modulation by sorafenib. Clin Cancer Res. (18): 4997-5007. DOI: 10.1158/1078-0432.CCR-11-2322
15. Waller LP, Deshpande V, Pyrsopoulos N (2015) Hepatocellular carcinoma: A comprehensive review. World J Hepatol. Nov 18; 7(26): 2648–2663.
16. Lu L, Finegould MJ, Johnson RL (2018) Hippo pathway coactivators Yap and Taz are required to coordinate mammalian liver regeneration. Exp Mol Med. Jan 5;50(1):e423. doi: 10.1038/emm.2017.205.
17. Tschida BR, Temiz NA, Kuka TP, Lee LA, Riordan JD, Tierrablanca CA, Hullsiek R, Wagner S, Hudson WA, Linden MA, Amin K, Beckmann PJ, Heuer RA, Sarver AL, Yang JD, Roberts LR, Nadeau JH, Dupuy AJ, Keng VW, Largaespada DA (2017) Sleeping Beauty Insertional Mutagenesis in Mice Identifies Drivers of Steatosis-Associated Hepatic Tumors. Cancer Research. Dec 1;77(23):6576-6588.
18. Llovet JM, Montal R, Sia D, Finn RS. Molecular therapies and precision medicine in hepatocellular carcinoma (2018) Nature Reviews Clinical Oncology. 41571-018-0073-4
19. Lachenmayer A, Alsinet C, Savic R, Cabellos L, Toffanin S, Hoshida Y, Villanueva A, Mingues B, Newell P, Tsai HW, Barretina J, Thung S, Ward SC, Bruix J, Mazzaferri V,

Schwartz M, Friedman S, Llovet J (2012). Wnt-Pathway Activation in Two Molecular Classes of Hepatocellular Carcinoma and Experimental Modulation by Sorafenib. Clinical Cancer Research, 10.1158/1078-0432.CCR-11-2322.

20. Guichard C, Amaddeo G, Imbeaud S, Ladeiro Y, Pelletier L, Maad IB, Maad IB, Calderaro J, Bioulac-Sage P, Letexier M, Degos F, Clément B, Balabaud C, Chevet E, Laurent A, Couchy G, Letouzé E, Calvo F, Zucman-Rossi J (2012) Integrated analysis of somatic mutations and focal copy-number changes identifies key genes and pathways in hepatocellular carcinoma. Nat Genet. (44): 694-698. DOI: 10.1038/ng.2256
21. Kazazian HH (2004) Mobile elements: Drivers of genome evolution. Science (303) 1626–1632 doi:10.1126/science.1089670
22. Rahrmann, E., Watson, A., Keng, V.W., Choi, K., Moriarity, B.S., Beckmann, D.A., Wolf, N., Sarver, A., Collins, M.H., Moertel, C.L., Wallace, M., Gel, B., Serra, E., Ratner, N., and Largaespada, D.A. (2013) Forward genetic screen for Malignant Peripheral Nerve Sheath tumor formation identifies novel genes and genetic pathways driving tumorigenesis. Nature Genetics 45:7.
23. Keng Vw, Watson AL, Rahrmann EP, Li H, Tschida BR, Moriarity BS, Choi K, Rizvi TA, Collins MH, Wallace MR, Ratner N, Largaespada DA (2012) Conditional Inactivation of Pten with EGFR Overexpression in Schwann cells Models of Sporadic MPNST. Sarcoma 620834: 12.
24. Wodarz A, Nusse R (1998) Mechanisms of Wnt signaling in development. Ann Rev Cell Dev Biol. (14):59–88
25. Lowther W, Wiley K, Smith GH, Callahan R (2005) A new common integration site, Int7, for the mouse mammary tumor virus in mouse mammary tumors identifies a gene whose product has furin-like and thrombospondin-like sequences. J Virol. (79): 10093-10096. DOI: 10.1128/JVI.79.15.100093-100096.2005
26. Zhang L, Shay JW (2017) Multiple Roles of APC and its Therapeutic Implications in Colorectal Cancer. J nAtl Cancer Inst Aug 1;109(8). doi: 10.1093/jnci/djw332.
27. Ugolini F, Charafe-Jauffret E, Bardou VJ, Geneix J, Adelaide J, Labat-Moleur F, Penault-Llorca F, Longy M, Jacquemier J, Birnbaum D, Pébusque MJ (2001) WNT pathway and mammary carcinogenesis: loss of expression of candidate tumor suppressor

gene SFRP1 in most invasive carcinomas except of the medullary type. Oncogene. (20): 5810-5817. DOI: 10.1038/sj.onc.1204706

28. Barker N, Clevers H (2006) Mining the Wnt pathway for cancer therapeutics. Nature reviews. Drug discovery. (5): 997-1014. DOI: 10.1038/nrd2154
29. Kahn M (2014) Can we safely target the WNT pathway? Nature reviews. Drug discovery. (13): 513-532. DOI: 10.1038/nrd4233
30. Niehrs C (2012) The complex world of WNT receptor signalling. Molecular Cell Biology (13): 767-779.
31. Sharma AR, Chakraborty C, Lee SS, Sharma G, Yoon JK, Doss CGP, Song DK, Nam JS (2014) Computational Biophysical, Biochemical, and Evolutionary Signature of Human R-Spondin Family Proteins, the Member of Canonical Wnt/β-catenin Signaling Pathway. BioMed Research International, 974316:22.
32. Buske P, Przybilla J, Loeffler M, Sachs N, Sato T, Clevers H, Galle J (2012) On the biomechanics of stem cell niche formation in the gut: modeling growing organoids. FEBS Journal 279; 3475–3487.
33. Hankenson KD[1], Sweetwyne MT, Shitaye H, Posey KL. (2010) Thrombospondins and novel TSR-containing proteins, R-spondins, regulate bone formation and remodeling. Curr Osteoporos Rep. Jun;8(2):68-76. doi: 10.1007/s11914-010-0017-0.
34. Zhao B, Li L, Lei Q, Guan KL (2010) The Hippo-YAP pathway in organ size control and tumorigenesis: an updated version. Genes and Dev. 2010; 24:862-874.
35. Moon S, Park SY, Park HW (2018) Regulation of the Hippo pathway in cancer biology. Cell Mol Life Sci. 2018 Jul;75(13):2303-2319. doi: 10.1007/s00018-018-2804-1.
36. Chakraborty S, Njah K, Pobbati AV, Lim YB, Raju A, Lakshmanan M, Tergaonkar V, Lim CT, Hong W (2017) Agrin as a Mechanotransduction Signal Regulating YAP through the Hippo Pathway. Mar 7;18(10):2464-2479. doi: 10.1016/j.celrep.2017.02.041.
37. Wu LMN, Deng Y, Wang J, Zhao C, Wang J, Rao R, Xu L, Zhou W, Choi K, Rizvi TA, Remke M, Rubin JB, Johnson RL, Carroll TJ, Stemmer-Rachamimov AO, Wu J, Zheng Y, Xin M, Ratner N, Lu QR (2018) Programming of Schwann Cells by Lats1/2-TAZ/YAP Signaling Drives Malignant Peripheral Nerve Sheath Tumorigenesis. Feb 12;33(2):292-308.e7. doi: 10.1016/j.ccell.2018.01.005.

38. Wu MF, Wang SG (2008) Human TAO kinase 1 induces apoptosis in SH-Sy5Y cells. Cell Biol Int. Jan;32(1):151-6. Epub 2007 Aug 30.
39. Lee DH, Park JO, Kim TS, Kim SK, Kim TH, Kim MC, Park GS, Kim JH, Kuninaka S, Olson EN, Saya H, Kim SY, Lee H, Lim DS. (2016) LATS-YAP/TAZ controls lineage specification by regulating TGFβ signaling and Hnf4α expression during liver development. Nat Commun. 2016 Jun 30;7:11961. doi: 10.1038/ncomms11961.
40. Scholer-Dahirel A, Schlabach MR, Loo A, Bagdasarian L, Meyer R, Guo R, Woolfenden S, Yu KK, Markovits J, Killary K, Sonkin D, Yao YM, Warmuth M, Sellers WR, Schlegel R, Stegmeier F, Mosher RE, McLaughlin ME (2011) Maintenance of adenomatous polyposis coli (APC)-mutant colorectal cancer is dependent on Wnt/beta-catenin signaling. Proc Natl Acad Sci U S A.1 Oct 11;108(41):17135-40. doi: 10.1073/pnas.1104182108.
41. Mori M, Triboulet R, Mohseni M, Schlegelmilch K, Shrestha K, Camargo FD, Gregory RI (2014) Hippo signaling regulates microprocessor and links cell-density-dependent miRNA biogenesis to cancer. Cell. Feb 27;156(5):893-906. doi:10.1016/j.cell.2013.12.043.
42. Jaffe AB, Hall A (2005) Rho GTPases: Biochemistry and Biology. Annu Rev Cell Dev Biol 21:247-69
43. Porter AP, Papaioannou A, Malliri A (2016) Deregulation of Rho GTPases in cancer. Small GTPases (7) 3: 123-138.
44. Said N, Sanchez-Carbayo M, Smith SC, Theodorescu D (2012) RhoGDI2 suppresses lung metastasis in mice by reducing tumor versican expression and macrophage infiltration. J Clin Invest. 2012 Apr;122(4):1503-18. doi: 10.1172/JCI61392.
45. Seshagiri, S., E. W. Stawiski, S. Durinck, Z. Modrusan, E. E. Storm, C. B. Conboy, S. Chaudhuri, Y. Guan, V. Janakiraman, B. S. Jaiswal, J. Guillory, C. Ha, G. J. Dijkgraaf, J. Stinson, F. Gnad, M. A. Huntley, J. D. Degenhardt, P. M. Haverty, R. Bourgon, W. Wang, H. Koeppen, R. Gentleman, T. K. Starr, Z. Zhang, D. A. Largaespada, T. D. Wu and F. J. de Sauvage (2012) Recurrent R-spondin fusions in colon cancer. Nature 488(7413): 660-664.
46. Starr TK, Allaei R, Silverstein KAT, Staggs RA, Sarver AL, Bergemann TL, Gupta M, O'Sullivan MG, Matise I, Dupuy AJ, Collier LS, Powers S, Oberg AL, Asmann YW,

Thibodeau SN, Tessarollo L, Copeland NG, Jenkins NA, Cormier RT, Largaespada DA (2009) A transposon-based genetic screen in mice identifies genes altered in colorectal cancer. Science. Mar;323(5922):1747-1750.

47. Shinmura K, Kahyo T, Kato H, Igarashi H, Matsuura S, Nakamura S, Kurachi K, Nakamura T, Ogawa H, Funai K, Tanahashi M, Niwa H, Sugimura H (2014) RSPO fusion transcripts in colorectal cancer in Japanese population. Mol Biol Rep. 2014. DOI: 10.1007/s11033-014-3409-x
48. Takeda H, Wei Z, Koso H, Rust AG, Yew CC, Mann MB, Ward JM, Adams DJ, Copeland NG, Jenkins NA (2015) Transposon mutagenesis identifies genes and evolutionary forces driving gastrointestinal tract tumor progression. Nat Genet. DOI: 10.1038/ng.3175
49. March HN, Rust AG, Wright NA, ten Hoeve J, de Ridder H, Elridge M, van der Weyden L, Berns A, Gadiot J, Uren A, Kemp R, Arends MJ, Wessels LF, Winton DJ, Adams DJ (2011) Insertional mutagenesis identifies multiple networks of cooperating genes driving intestinal tumorigenesis. Nature genetics. DOI: 10.1038/ng.990
50. Starr TK, Scott PM, Marsh BM, Zhao L, Than BL, O'Sullivan MG, Sarver AL, Dupuy AJ, Largaespada DA, Cornier RT (2011) A Sleeping Beauty transposon-mediated screen identifies murine susceptibility genes for adenomatous polyposis coli (Apc)-dependent intestinal tumorigenesis. Proceedings of the National Academy of Sciences of the United States of America. (108): 5765-5770. DOI: 10.1073/pnas.1018012108
51. Conboy CB, Vélez-Reyes GL, Burns M, Alsinet C, Abrahante J, Rathe SK, Temiz NA, Linden M, Ahmed K, Kuka T, Keng VW, Harris R, Llovet J, Starr TK, Largaespada DA. R-spondin 2 is overexpressed in multiple cancers and drives Wnt signaling. Under Review, PlosOne.
52. Vélez-Reyes GL, Conboy CB, Tschida BR, Hu H, Burns M, Kaufmann G, Keller B, Alsinet C, Abrahante J, Rathe SK, Temiz NA, Linden M, Ahmed K, Kuka T, Keng VW, Harris R, Llovet J, Starr TK, Largaespada DA. RSPO2 Drives Hepatocellular Carcinoma Development in a YAP-dependent Manner. Accepted. Hepatology Communications.
53. Wu C, Qiu S, Lu L, Zou J, Li W, Wang O, Xhao H, Wang H, Tang J, Chen L, Xu T, Sun Z, Liao W, Luo G, Lu X (2014) RSPO2-LGR5 signaling has tumor-suppressive activity in colorectal cancer. Nature Communications 5:3149.

54. Ong CT, Corces VG. (2014). CTCF: an architectural protein bridging genome topology and function. Nature Genetics, 15: 234-246.
55. Gaydos L, Wang W, Strome S (2014) H3K27me and PRC2 transmit a memory of repression across generations and during development. Science 345(6203): 1515-1518.
56. Li T, Ju J-F, Qiu X, Ling J, Chen H, Wang S, Hou A, Vu TH, Hoffman AR (2008) CTCF regulates allelic expression of Igf2 by orchestrating a pormoter-polycomb repressive complex 2 intrachromosomal loop. Molecular and cellular biology 28 (2): 6473-6382.
57. Wang H, Ge S, Qian G, Li W, Cui J, Wang G, Hoffman A, Hu J-F (2015) Restoration of IGF2 imprinting by polycomb repressive complex 2 docking factor SUZ12 in colon cancer cells. Experimental Cell Research 338: 214-221.
58. Gaydos L, Wang W, Strome S (2014) H3K27me and PRC2 transmit a memory of repression across generations and during development. Science 345(6203): 1515-1518.
59. Wang K, Ubriaco G, Sutherland LC. (2007). RBM6-RBM5 transcription-induced chimeras are differentially expressed in tumors. BMC Genomics 2007, 8:348.
60. Akiva P, Toporik A, Edelheit S, Peretz Y, Diber A, Shemesh R, Novik A, Sorek R. (2006). Transcription-mediated gene fusion in the human genome. Cold Spring Harbor Laboratory Press Genome Research, 16: 30
61. Yoon JK, Lee JS (2012) Cellular signaling and biological functions of R-spondins. Cellular Signaling 24:369-377.
62. Hao H-X, Xie Y, Zhang Y, Charlat O, Oster E, Avello M, Lei H, Mickanin C, Liu D, Ruffner H, Mao X, Ma Q, Zamponi R, Bousmeester T, Finan PM, Kirshchner MW, Porter JA, Serluca FC, Cong F (2012) ZNRF3 pormotes Wnt receptor turnover in an R-spondin-sensitive manner. Nature 485:195-200.
63. Koo BK, Spit M, Jordens I, Low TY, Stange DE, Van de Wetering M, Van Es JH, Mohammed S, Heck AJ, Maurice MM, Clevers H (2012) Tumour suppressor RNF43 is a stem-cell E3 ligase that induces endocytosis of Wnt receptors. Nature. (488): 665-669. DOI: 10.1038/nature11308
64. Chartier C, Raval J, Axelrod F, Bond C, Cain J, Dee-Hoskins C, Ma S, Fischer MM, Shah J, Wei J, Ji M, Lam A, Stroud M, Yen WC, Yeung P, Cancilla B, O'Young G, Wang M, Kapoun AM, Lewicki J, Hoey T, Gurney A (2016) Therapeutic Targeting of Tumor-Derived R-Spondin Attenuates β-Catenin Signaling and Tumorigenesis in

Multiple Cancer Types. Cancer Research. (76): 713-723. DOI: 10.1158/0008-5472.CAN-15-0561

65. Li H, Chang Lj, Neubauer DR, Muir DF, Wallace MR (2016) Immortalization of human normal and NF1 neurofibroma Schwann cells. Lab Invest 96(10):1105-1115.
66. Liu J, Pan S, Hsieh MH, Ng N, Sun F, Wang T, Kasibhatla S, Schuller AG, Li AG, Cheng D, Li J, Tompkins C, Pferdekamper A, Steffy A, Cheng J, Kowal C, Phung V, Guo G, Wang Y, Graham MP, Flynn S, Brenner JC, Li C, Villarroel MC, Schultz PG, Wu X, McNamara P, Sellers WR, Petruzzelli L, Boral AL, Seidel HM, McLaughlin ME, Che J, Carey TE, Vanasse G, Harris JL. (2013) Targeting Wnt-driven cancer through the inhibition of Porcupine by LGK974. PNAS. (110) 50: 20224-20229.
67. Kamal A, Riyaz S, Srivastava AK, Rahim A. Tankyrase inhibitors as therapeutic targets for cancer. Curr Top Med Chem. 2014;14(17):1967-76.
68. Hong EL, Sloan CA, Chan ET, Davidson JM, Malladi VS, Strattan JS, Hitz BC, Gabdank I, Narayanan AK, Ho M, Lee BT, Rowe LD, Dreszer TR, Roe GR, Podduturi NR, Tanaka F, Hilton JA, Cherry JM (2016) Principles of metadata organization at the ENCODE data coordination center. Database (Oxford). Mar 15;2016. pii: baw001. doi: 10.1093/database/baw001
69. Ziebarth JD, Bhattacharya A, Cui Y (2013) CTCFBSDB 2.0: a database for CTCF-binding sited and genome organization. Nucleic Acids Research. 41 (D1):D188-D194
70. Han J, Zhang Z, Wang K (2018) 3C and 3C-based techniques: the powerful tools for spatial genome organization deciphering. Mol Cytogenet. (11): 21. doi: 10.1186/s13039-018-0368-2.
71. Ferent J1, Zimmer C, Durbec P, Ruat M, Traiffort E (2013) Sonic Hedgehog signaling is a positive oligodendrocyte regulator during demyelination. J Neurosci. Jan 30;33(5):1759-72. doi: 10.1523/JNEUROSCI.3334-12.2013.
72. Clayton RF, Rinaldi A, Kandyba EE, Edward M, Willberg C, Klenerman P, Patel AH (2005) Liver cell lines for the study of hepatocyte function and immunological response. Liver International. (25): 389-402. DOI: 10.1111/j.1478-3231.2005. 01017.x
73. Rosenbluh J, Nijhawan D, Cox AG, Li X, Neal JT, Schafer EJ, Zack TI, Wang X, Tsherniak A, Schinzel AC, Shao DD, Schumacher SE, Weir BA, Vazquez F, Cowley GS, Root DE, Mesirov JP, Beroukhim R, Kuo CJ, Goessling W, Hahn WC. (2012) β-

catenin driven cancers require a YAP1 transcriptional complex for survival and tumorgenesis. Cell. (151):1457-1473. DOI: 10.1016/j.cell.2012.11.026

74. Azzolin L, Panciera T, Soligo S, Enzo E, Bicciato S, Dupont S, Bresolin S, Frasson C, Basso G, Guzzardo V, Fassina A, Cordenonsi M, Piccolo S (2014) YAP/TAZ incorporation in the β-catenin destruction complex orchestrates the Wnt response. Cell. (158): 1-14. DOI: 10.1016/j.cell.2014.06.013
75. Fitamant J, Kottakis F, Benhamouche S, Tian HS, Chuvin N, Parachoniak CA, Nagle JM, Perera RM, Lapouge M, Deshpande V, Zhu AX, Lai A, Min B, Hoshida Y, Avruch J, Sia D, Campreciós G, McClatchey AI, Llovet JM, Morrissey D, Raj L, Bardeesy N (2015) YAP inhibition restores hepatocyte differentiation in advanced HCC, leading to tumor regression. Cell Reports. 2015; S2211-1247(15)00173-4. DOI: 10.1016/j.celrep.2015.02.027
76. Flavahan WA, Drier Y, Liau BB, Gillespie SM, Venteicher AS, Stemmer-Rachamimov AO, Suvá ML, Bernstein BE (2016) Insulator dysfunction and oncogene activation in IDH mutant gliomas. Nature 529: 110-114.
77. Gibault F, Bailly F, Corvaisier M, Coevoet M, Huet G, Menyl P, Cotelle P (2017) Molecular Features of the YAP Inhibitor Verteporfin: Synthesis of Hexasubstituted Dipyrrins as Potential Inhibitors of YAP/TAZ, the Downstream Effectors of the Hippo Pathway. Jun 21;12(12):954-961. doi: 10.1002/cmdc.201700063.
78. Tanaka K, Osada H, Murakami-Tonami Y, Horio Y, Hida T, Sekido Y (2017) Statin suppresses Hippo pathway inactivated malignant mesothelioma cells and blocks the YAP/CD44 growth stimulatory axis. Cancer Letter. (385):215-224.
79. Yin X, Yi H, Wang L, Wu W, Wu X, Yu L (2107) R-spondin 2 promotes proliferation and migration via the Wnt/β-catenin pathway in human hepatocellular carcinoma. Oncology Letters. 14(2): 1757-1765. DOI: 10.3892/ol.2017.6339.